A defence pathway linking plasma membrane and chloroplasts and co-opted by pathogens

Laura Medina-Puche[1], Huang Tan[1,2], Vivek Dogra[1,3], Mengshi Wu[1,2], Tabata Rosas-Diaz[1,4], Liping Wang[1,2], Xue Ding[1,2], Dan Zhang[1,2,5], Xing Fu[1], Chanhong Kim[1], Rosa Lozano-Duran[1]*

[1]Shanghai Center for Plant Stress Biology, CAS Center for Excellence in Molecular Plant Sciences, Chinese Academy of Sciences, Shanghai 201602, China. [2]University of the Chinese Academy of Sciences, Beijing 100049, China. [3]Present address: Biotechnology Division, CSIR-Institute of Himalayan Bioresource Technology, 176061 Palampur, India. [4]Present address: Instituto de Hortofruticultura Subtropical y Mediterránea "La Mayora" (IHSM-UMA-CSIC), Area de Genética, Facultad de Ciencias, Universidad de Málaga, Campus de Teatinos s/n, E-29071 Málaga, Spain. [5]Present address: Department of Cell Biology, Centre for Organismal Studies Heidelberg, Heidelberg University, 69120 Heidelberg, Germany.

*Lead contact

Corresponding author: lozano-duran@sibs.ac.cn

Authors' email addresses:

Laura Medina-Puche: laura@sibs.ac.cn

Huang Tan: tanhuang@sibs.ac.cn

Vivek Dogra: dogra@sibs.ac.cn

Mengshi Wu: mswu@psc.ac.cn

Tabata Rosas-Diaz: tabatarosas@uma.es

Liping Wang: wlp@sibs.ac.cn

Xue Ding: dingxue@sibs.ac.cn

Dan Zhang: zhangdan@sibs.ac.cn

Xing Fu: xfu@sibcb.ac.cn

Chanhong Kim: chanhongkim@sibs.ac.cn

Rosa Lozano-Duran: lozano-duran@sibs.ac.cn

SUMMARY

Chloroplasts are crucial players in the activation of defensive hormonal responses during plant-pathogen interactions. Here, we show that a plant virus-encoded protein re-localizes from the plasma membrane to chloroplasts upon activation of plant defence, interfering with the chloroplast-dependent anti-viral salicylic acid (SA) biosynthesis. Strikingly, we have found that

plant pathogens from different kingdoms seem to have convergently evolved to target chloroplasts and impair SA-dependent defences following an association with membranes, which relies on the co-existence of two subcellular targeting signals, an N-myristoylation site and a chloroplast transit peptide. This pattern is also present in plant proteins, at least one of which conversely activates SA defences from the chloroplast. Taken together, our results suggest that a pathway linking plasma membrane to chloroplasts and activating defence exists in plants, and that such pathway has been co-opted by plant pathogens during host-pathogen co-evolution to promote virulence through suppression of SA responses.

KEYWORDS

Plasma membrane, chloroplast, retrograde signalling, salicylic acid, defence, geminivirus, effector, pathogen, plant

INTRODUCTION

Beyond their role as photosynthetic organelles enabling photoautotrophy, chloroplasts are emerging as hubs in the integration of environmental stimuli and determinants of downstream responses (Chan et al., 2016, de Souza et al., 2017, Zhu, 2016, de Torres Zabala et al., 2015, Xiao et al., 2013, Zhao et al., 2016). A growing body of evidence substantiates the fundamental function of chloroplasts in orchestrating defence responses: upon perception of a biotic threat, this organelle acts as the source of calcium and reactive oxygen species (ROS) bursts and communicates with the nucleus through retrograde signalling (Chan et al., 2016), initiating a signalling cascade that leads to the expression of defence-related genes, including those responsible for the biosynthesis of the defence hormone salicylic acid (SA), subsequently produced in the chloroplast stroma (Serrano et al., 2016; Nomura et al., 2012). The chloroplast-nucleus communication following perception of a biotic threat at the cell surface, which leads to the activation of Pattern-Triggered Immunity (PTI), involves the thylakoid membrane-associated Calcium Sensing Receptor (CAS); although the exact molecular function of CAS in unclear, this protein is required for PTI-induced transcriptional reprograming, SA biosynthesis, callose deposition, and anti-bacterial and anti-fungal resistance (Nomura et al., 2012; Tang et al., 2020). How the information of pathogen attack is relayed from the cell periphery (e.g. during a bacterial infection) or possibly other subcellular compartments (e.g. during viral infections) to chloroplasts, however, remains elusive, while the molecular bases of retrograde signalling during defence responses are largely unexplored.

In agreement with a prominent role of chloroplast function in defence and in the context of the arms race between pathogens and hosts, a number of virulence factors from pathogens belonging to different kingdoms of life, including bacteria, viruses, fungi, and oomycetes, have been described to target this organelle (e.g. de Torres Zabala et al., 2015, Fondong et al., 2007, Rodriguez-Herva et al., 2012, Rosas-Diaz et al., 2018, Jelenska et al., 2007, Jelenska et al., 2010, Li et al., 2014, Liu et al., 2018, Petre et al., 2016; Xu et al., 2019; Tang et al., 2020; Gao et al., 2020). In a few cases, it has been demonstrated or suggested that chloroplast-localized viral proteins can promote viral pathogenesis (Gnanasekaran et al., 2019; Bhattacharyya et al., 2015; Krenz et al., 2010). We recently showed that the C4 protein from the geminivirus *Tomato yellow leaf curl virus* (TYLCV) contains two overlapping localization signals, namely an N-myristoylation site for plasma membrane (PM) tethering and a chloroplast transit peptide (cTP) for chloroplast targeting (Rosas-Diaz et al., 2018). While at least one of the roles of C4 at the PM is to suppress

the cell-to-cell movement of RNA interference (RNAi) (Rosas-Diaz et al., 2018; Fan et al., 2019), the function of C4 in the chloroplast remained enigmatic.

Here, we show that C4 shifts its localization from the PM to chloroplasts upon activation of defence by the replication-associated viral protein (Rep) or by exogenous treatments with the bacterial elicitor peptide flg22 or the plant peptide Pep1. Once inside the organelle, C4 associates with the thylakoid transmembrane protein CAS. The effect of C4 in the chloroplast is consistent with a suppression of CAS function in retrograde signalling, as expression of this viral protein leads to decreased CAS-dependent immune responses. The C4-facilitated manipulation of chloroplast-mediated defences is biologically relevant, since knocking down *CAS* or depleting downstream SA promotes viral accumulation and partially complements a C4 null mutation in the virus, pointing at the suppression of SA responses as one of the main roles of this virus-encoded protein.

Strikingly, we have found the coexistence of the overlapping targeting signals contained in C4, the N-myristoylation site and the cTP, in a number of evolutionarily unrelated plant pathogen-encoded effector proteins from DNA viruses, RNA viruses, and bacteria. Importantly, some of these effectors show dual membrane/chloroplast localization and suppress chloroplast-dependent defences when targeted to this organelle. Moreover, co-occurrence of these two targeting signals can also be found in a conserved set of plant proteins, many of which have a described role in the regulation of defence responses. We demonstrate that one of these proteins, the Arabidopsis Calcium Protein Kinase 16 (CPK16), re-localizes from the PM to chloroplasts upon flg22 treatment to promote chloroplast-dependent defences. Based on the results presented here, we propose that a protein re-localization-dependent pathway physically linking PM and chloroplasts and regulating defence exists in plants, and that this pathway has been co-opted by pathogens during evolution to suppress defence responses and promote virulence.

RESULTS

The C4 protein from the geminivirus *Tomato yellow leaf curl virus* shifts its localization from the plasma membrane to chloroplasts upon activation of defence

When expressed in plant cells, the C4 protein from TYLCV fused to GFP at its C-terminus localizes preferentially at the PM, with a minor fraction visible in chloroplasts (Figure 1A, B; Rosas-Diaz et al., 2018). The PM localization of C4 depends on an intact N-myristoylation motif (Figure 1A; Rosas-Diaz et al., 2018); C4 is myristoylated on the glycine in position 2 (G2), as detected by

mass spectrometry analysis following immunoprecipitation (IP) of transiently expressed C4-GFP in *Nicotiana benthamiana* (Figures S1A and S1B). Consistent with this, silencing of the *N. benthamiana* N-myristoyl transferase *NMT* genes by virus-induced gene silencing (VIGS) (Figure 1C, S1C-S1E) or treatment with the myristoylation inhibitor benzothiazole (BT) abolish the PM localization of C4-GFP (Figure S1F). Strikingly, when co-expressed with a TYLCV infectious clone, C4-GFP is depleted from the PM and accumulates in chloroplasts (Figure 1D); co-expression with the viral Replication-associated protein (Rep) alone is sufficient to trigger this shift in localization (Figure 1E). Expression of Rep in *N. benthamiana* leads to the activation of defence responses, probably owing to the recognition of the protein or its activity (Ding et al., 2019); in order to test whether activation of defence could lead to the re-localization of C4 from the PM to chloroplasts, we treated *N. benthamiana* leaves transiently expressing C4-GFP with the bacterial elicitor peptide flg22, which is recognized by a receptor complex at the cell surface and activates PTI (Felix et al., 1999; Gomez-Gomez and Boller, 2000). As shown in Figures 1F and S1G, flg22 treatment results in a clear accumulation of C4-GFP in chloroplasts, at the expense of the PM pool; treatment with the translation inhibitor cycloheximide (CHX) supports the idea that the shift in PM/chloroplast C4-GFP accumulation ratio is due to physical re-localization of the protein, and not to differential targeting following synthesis *de novo*. The plant immunogenic peptide Pep1 similarly triggers the chloroplast re-localization of C4 in *N. benthamiana*, while treatment with the bacterial derived peptide elf18, for which *N. benthamiana* lacks a receptor, has no noticeable effect on the subcellular distribution of the protein (Figure S1H-J). The increase in chloroplast-localized C4-GFP after flg22 treatment can also be detected by organelle purification and western blot (Figure 1G); additionally, a 33 KDa variant of C4, corresponding to C4-GFP after the chloroplast import-coupled cleavage of the cTP (mature chloroplast form), accumulates at the expense of the full-length version of the fusion protein (Figure 1G and S1K). The accumulation of C4-GFP in the chloroplast following flg22 treatment is concomitant to its depletion from the PM, as observed in the total protein fraction (Figure 1G); additional bands, potential degradation products from the PM-pool of C4-GFP, can also be detected prior to fractionation. Chloroplast fractionation indicates that C4 is a peripheral thylakoid membrane (Figure 1H, 1I, and S1L). Phosphorylation, an essential post-translational modification in the signal relay following PAMP perception, is required for the PM-to-chloroplast re-localization of C4, since more C4-GFP is retained at the PM following flg22 treatment in the presence of the phosphorylation inhibitor K525a (Figures S1M and N). Chloroplast import of C4 depends on a functional protein import TOC/TIC (Translocon of the Outer/Inner membrane of the Chloroplast) complex: silencing of the genes encoding TOC75III, an essential component of this import complex, markedly reduces the

accumulation of C4 in the chloroplast following flg22 treatment (Figures S1O-S1Q). Notably, accumulation of C4 in the chloroplast in transgenic Arabidopsis lines expressing the non-myristoylable $C4_{G2A}$ does not affect photosynthetic efficiency, chloroplast ultrastructure, or general plant development (Figure 1J-N).

C4 interacts with Calcium Sensing Receptor in chloroplasts and suppresses downstream defence responses

Following activation of PTI, retrograde signalling allows communication of chloroplasts with the nucleus, activating expression of genes required for the biosynthesis of the defense hormone salicylic acid (SA) (Qi et al., 2018; Zhang and Li, 2019; Nomura et al., 2012). Since activation of PTI by flg22 or Pep1 treatments leads to the re-localization of C4 from the PM to the chloroplast, we measured the expression of SA biosynthetic and responsive genes (*ICS1* and *PR1*, respectively) as well as the accumulation of SA after treatment with flg22 in transgenic Arabidopsis plants expressing $C4_{G2A}$ (Figures 2A, B, and S2A), with the aim to detect a potential interference of C4 with this signalling cascade. As shown in Figure 2A and B, the presence of C4 in the chloroplast results in lower expression of SA-related genes and SA content after flg22 treatment; C4, however, does not impair SA perception or downstream responses, as demonstrated by exogenous SA treatments (Figure S2B). Importantly, the suppression of SA biosynthesis seems to be relevant for the viral infection, in agreement with previous observations (Li et al., 2019), since transgenic Arabidopsis or tomato plants depleted in SA (*NahG* or *sid2*/*NahG* transgenic plants) support higher viral accumulation. In addition, SA depletion in Arabidopsis can partially complement a null mutation in C4, suggesting that the suppression of SA responses is one of the main functions of C4 in the context of the infection (Figures 2C and S2C). The observation that Arabidopsis *sid2/NahG* plants, which accumulate very low levels of the SA degradation product catechol (Heck et al., 2003), support higher accumulation of TYLCV to a similar extent than *NahG* plants (Figure 2C), suggests that it is indeed the lack of SA, and not the increase in catechol, what improves viral performance. An *eds5* mutant, deficient in isochorismate-derived SA (Rekhter et al., 2019), is also more susceptible to TYLCV infection (Figure S2D). Affinity purification followed by mass spectrometry analysis (AP-MS) upon transient expression of $C4_{G2A}$ in *N. benthamiana* identified the plant-specific Calcium Sensing Receptor (CAS) as a putative interactor of C4 in the chloroplast (Figure 2D); this protein-protein interaction was subsequently confirmed by bimolecular fluorescent complementation (BiFC) and co-IP analyses (Figures 2E, F, and S2F, G). CAS is described as a thylakoid membrane-spanning

protein (Nomura et al., 2012; Cutolo et al., 2019); topology analyses demonstrate that the C-terminus of CAS faces the stroma and interacts with C4, itself associated to the thylakoid membrane as peripheral protein (Figures 2G and S2E-S2G). As expected, the interaction between C4 and CAS is increased following flg22 treatment (Figures S2H-K). Interestingly, CAS has been previously demonstrated to be required for retrograde signalling in PTI and the ensuing activation of SA biosynthesis and signalling (Nomura et al., 2012; Tang et al., 2020). Therefore, we next tested known CAS-dependent responses to flg22 in our transgenic Arabidopsis lines expressing chloroplast-localized C4. As shown in Figures 2H-K, plants expressing $C4_{G2A}$ display immune defects at different levels, including reduced cytoplasmic calcium burst (Figures 2H and S2L), lower callose deposition (Figure 2I), defective transcriptional reprogramming (Figures 2J and S2M), and increased susceptibility to *Pseudomonas syringae* pv. *tomato* DC3000 (Figures 2K and S2N), all of them phenocopying a *cas* mutant and hence consistent with an inhibition of this protein. Of note, and as expected, flg22 perception is not affected in $C4_{G2A}$ transgenic lines or in a *cas* mutant, since the early apoplastic ROS burst as well as the late seedling growth inhibition occur normally in these plants in response to flg22 treatment (Figures S2O and P; Nomura et al., 2012). The biological relevance of the potential C4-mediated inhibition of CAS is illustrated by the fact that a *cas* Arabidopsis mutant as well as *N. benthamiana* or tomato plants in which *CAS* has been knocked down by virus-induced gene silencing (VIGS) are all more susceptible to TYLCV infection, indicating that suppression of CAS function has a positive impact on the virus' performance (Figures 2L and S2Q).

Proteins encoded by evolutionarily unrelated pathogens contain overlapping membrane- and chloroplast-targeting signals and suppress chloroplast-mediated defences

Our results show that TYLCV has evolved a strategy, through the action of the virus-encoded C4 protein and its shuttling from the PM to the chloroplast, to interfere with chloroplast-mediated SA-dependent defence responses and promote viral performance. Since SA has been shown to counter virus infection in different plant-virus interactions (e.g. Chen et al., 2010; Ji et al., 2001; Kachroo et al., 2000; Malamy et al., 1990) and chloroplasts are crucial players in this pathway, we hypothesized that other plant viruses might have independently evolved similar strategies to target this organelle when they are perceived by the plant. In an attempt to identify such hypothetical proteins, we searched public databases for proteins encoded by plant viruses containing both an N-myristoylation motif and a cTP. Surprisingly, we found ~400 viral proteins in which these two localization signals co-exist, encoded by viral species belonging to four different

families (Figures 3A and S3A); most of these proteins are encoded by geminiviruses and are positional homologues of C4 (Figure S3A). From this set of proteins, we selected four to test the functionality of their predicted localization signals as well as their biological effect following chloroplast localization: C4 from the curtovirus *Beet curly top virus* (BCTV) (Fam. *Geminiviridae*); AC4 from the bipartite begomovirus *East African cassava mosaic virus* (EACMV) (Fam. *Geminiviridae*); the capsid protein (CP) from the cucumovirus *Cucumber mosaic virus* (CMV) (Fam. *Bromoviridae*); and the P3 protein from the nepovirus *Grapevine fanleaf virus* (GFLV) (Fam. *Secoviridae*) (Figure S3B). Curiously, although the CP protein from multiple CMV isolates contains a predicted cTP, this protein possesses a predicted N-terminal myristoylation site in one isolate only (Figure S3C and D). In all cases, the wild-type version of these viral proteins fused to GFP transiently expressed in *N. benthamiana* appeared as associated to membranes, while the non-myristoylable (G2A) mutant versions accumulated in the chloroplast (Figure 3B). As previously described for C4 from TYLCV, PM localization of the C4 proteins encoded by EACMV and BCTV required a functional NMT (Figure S3E and F). Treatment with flg22 triggered the re-localization of C4 from BCTV and AC4 from EACMV to chloroplasts; this effect could not be clearly observed for CP and P3, suggesting that a different signal might be required in these two cases (Figure 3C). We next tested immune readouts in *N. benthamiana* leaves transiently expressing the chloroplast-localized (G2A) version of these proteins. Strikingly, the chloroplastic versions of all four viral proteins reduced the expression of *NbICS1*, *NbPR1*, and other defence-related genes, as well as the cytosolic calcium burst, in response to flg22, while all but P3 enhanced susceptibility against the pathogenic bacteria *Pto* DC3000 *ΔhopQ1* (Figures 3D, 3F, and S3H-J), indicating that these phylogenetically unrelated viral effectors are capable of interfering with SA-mediated defence from the chloroplast. Expression of these proteins does not interfere with the apoplastic ROS burst that follows flg22 treatment, indicating that perception of flg22 occurs normally (Figures 3G and S3K).

Given that viral proteins from independent origins show a similar coexistence of targeting signals and share the capacity to interfere with SA-dependent defences from the chloroplast, and considering the general role of SA on different plant-pathogen interactions, we next sought to answer the question of whether unrelated plant pathogens such as bacteria can encode effector proteins with a similar localization pattern and effect. With this purpose, we screened the predicted proteome of the plant pathogenic bacterium *Ralstonia solanacearum* GMI1000 for proteins containing both an N-myristoylation motif and a cTP. This search yielded 2 proteins (GALA1 and GALA3) (Figures 4A and S4A). Interestingly, both proteins have been described as effector proteins secreted inside plant cells during bacterial infection (Mukaihara et al, 2010).

For subsequent functional characterization, we selected *R. solanacearum* GALA1, since GALA3 could not be detected by confocal microscopy upon transient expression in *N. benthamiana* leaves. GALA1-GFP showed the predicted dual PM/chloroplast localization, and its accumulation in the chloroplast increased upon treatment with flg22 (Figures 4B, C and S4B). Both bacterial effectors, GALA1 and GALA3, could be detected in chloroplasts upon expression of their G2A version fused to GFP following organelle purification and IP (Figure S4C). Importantly, chloroplast accumulation of either of these effectors led to a reduction in the cytoplasmic calcium burst in response to flg22 treatment (Figures 4D and S4D). Since *R. solanacearum* is capable of efficiently infecting Arabidopsis, we generated stable transgenic Arabidopsis plants expressing $GALA1_{G2A}$ or $GALA3_{G2A}$ fused to GFP, which showed the expected chloroplast localization (Figures S4E and F). These plants display altered expression of SA-responsive genes following flg22 treatment, and are more susceptible to *Pto* DC3000 (Figures 4E-G and S4G), indicating that these bacterial effector proteins can disturb SA-dependent defences when localized in the chloroplast. Nevertheless, perception of flg22 is not affected in these plants, since production of apoplastic ROS upon elicitation with the peptide occurs normally (Figures 4H and S4H).

The plant-encoded CPK16 contains overlapping targeting signals and re-localizes from PM to chloroplasts to promote chloroplast-mediated defence responses

The finding that pathogens from different kingdoms of life seem to have convergently evolved to target chloroplasts and impair SA-dependent defences following a previous association with membranes raises the idea that a pathway linking PM to chloroplasts might exist in plants, and that such pathway might have been co-opted by different plant pathogens during host-pathogen co-evolution. Following this rationale, we decided to screen the predicted Arabidopsis proteome to identify proteins containing both an N-myristoylation motif and a cTP, and found 78 proteins fulfilling this criterion (Figure 5A and Table S1). Interestingly, functional enrichment analysis of this subset of proteins unveiled an over-representation of defence regulators and protein kinases (Figure S5A). We next performed a similar screen using the predicted tomato and rice proteomes, and found 68 and 107 proteins containing both localization signals, respectively (Figures S5B, C and Tables S3 and S4), among which defence regulators and protein kinases are also over-represented (Figures S5D-E). Strikingly, comparison of the identified proteins in Arabidopsis, tomato, and rice yielded a core of 26 homologous proteins common to all three species and containing an N-myristoylation site and a cTP (Table S2 and Figure 5B), which shows an over-representation of proteins described as involved in SA signalling and systemic acquired

resistance as well as protein kinases (Figure 5C). Of note, the green alga *Chlamydomonas reinhardtii*, the liverwort *Marchantia polymorpha*, and the moss *Physcomitrella patens* also encode proteins containing the N-myristoylation motif and the cTP (19, 30, and 21, respectively; Figure 5D and Tables S5, 6, and 7), with a significant over-representation of protein kinases (Figures S5F-H).

Among the proteins identified in Arabidopsis, one of them, Calcium-Dependent Kinase 16 (CPK16), had already been shown to associate to the PM in an N-myristoylation motif-dependent manner and to harbour a functional cTP (Stael et al., 2011); however, chloroplast localization could be observed only upon mutation of the myristoylation site, and hence its biological significance was unclear. Following transient expression in *N. benthamiana*, CPK16-GFP could be observed mostly at the PM, while, as previously described, a $CPK16_{G2A}$ mutant version was detected in chloroplasts (Figure 6A); stable expression in Arabidopsis yielded similar results (Figure 6B). PM localization of CPK16 requires an active NMT (Figures 6C and S6A). Interestingly, after flg22 treatment, CPK16-GFP accumulated in chloroplasts, similarly to C4-GFP (Figures 6D and S6B); chloroplast localization could still be detected after CHX treatments (Figures 6D and E). The accumulation of CPK16 in the chloroplast can also be detected following chloroplast purification, and is concomitant to its depletion from the PM, as observed in the total protein fraction (Figure 6E); chloroplast-localized CPK16-GFP cannot be detected in the total protein fraction, possibly due to dilution issues in the absence of enrichment. As proof-of-concept, we decided to investigate whether CPK16 plays a role in defence responses when localized in the chloroplast. For this purpose, we generated transgenic Arabidopsis lines expressing wild-type CPK16 or its chloroplast-localized $CPK16_{G2A}$ version under the 35S promoter (Figure S6C); these transgenic lines had no obvious developmental phenotype (Figure S6D). Following flg22 treatment, both CPK16 and $CPK16_{G2A}$ plants displayed normal ROS burst but enhanced expression of SA marker genes (*ICS1*, *PAD4*, and *PR1*) (Figures 6F, G, and S6E). Although a moderate increase in the amplitude of the flg22-triggered cytoplasmic calcium burst could be detected in *N. benthamiana* as the result of CPK16 overexpression, $CPK16_{G2A}$ had no evident effect on this readout (Figures 6H and S6F). Importantly, both CPK16- and $CPK16_{G2A}$-overexpressing lines are more resistant to *Pto* DC3000 (Figures 6I and S6G) and to TYLCV (Figure 6J), indicating that CPK16 contributes to anti-bacterial and anti-viral defences from the chloroplast.

DISCUSSION

In addition to their function as energy providers, chloroplasts play an essential role in different aspects of plant biology as stress sensors and signal integrators; however, how these organelles, which reside inside the cell separated from the cytosol by a double membrane, can sense external cues is a long-standing question.

Taken together, the results presented here suggest the existence of a conserved pathway in plants that physically connects the PM and chloroplasts through protein re-localization upon a specific trigger, namely the perception of a biotic threat (Figure 7). This pathway, exemplified by CPK16, would involve proteins harbouring two overlapping and conflicting targeting signals: an N-myristoylation site, tethering the protein to the PM, and a cTP, targeting the protein to the chloroplast following release from the PM. N-myristoylation occurs co-translationally, which could account for the default PM localization of these proteins in basal conditions. Remarkably, the Arabidopsis N-myristoylome is enriched in defence-related proteins (Boisson et al., 2003). Our results show that CPK16 localizes to the PM in basal conditions, as previously observed (Stael et al., 2011), but can re-localize to chloroplasts following flg22 treatment; chloroplast-localized CPK16 enhances chloroplast-dependent defence responses, indicating that this protein can act as a modulator of defence through its function in the chloroplast. Many other Arabidopsis proteins containing both targeting signals are known defence regulators (e.g. BIK1, BSK1, AGI1, CPK28); whether these and the other proteins in this subset localize in the chloroplast under specific conditions and, if so, what their function in the organelle and their contribution to defence responses are remains to be investigated. Of note, the subsets of proteins containing these two targeting signals present an over-representation of protein kinases in all species analysed (*C. reinhardtii*, *M. polymorpha*, *P. patens*, *A. thaliana*, *O. sativa*, and *S. lycopersicum*), suggesting that kinases that work in other subcellular compartments can function in the chloroplast upon perception of certain stimuli, and underscoring the potential relevance of protein phosphorylation for signalling relay in this putative pathway.

Strongly supporting the notion of this pathway having a central function in plant defence is the finding that its co-option and potential disruption by pathogens has evolved multiple times independently: effectors containing an N-myristoylation motif and a cTP and suppressing chloroplast-dependent defences from this organelle have been identified as encoded by DNA viruses, RNA viruses, and bacteria. Future work will unveil how prevalent the coexistence of these two signals is among pathogen effectors, including those belonging to other kingdoms of life.

The pathway proposed here would allow for timely, rapid, and precise information relay from the PM to the chloroplast, fine-tuning retrograde signalling to orchestrate appropriate responses upon

signal integration in the plastid, avoiding negative consequences of activating defence and shutting down photosynthesis in the absence of a threat. Additionally, it could allow for dual functions of the participating proteins, since they could exert a given role in basal conditions, at the PM, and a different one once a biotic threat is perceived and they are translocated into the chloroplast – for instance, by keeping signalling in an off state in the absence of stimulus, but promoting downstream responses upon pathogen perception.

One example of how the subcellular compartmentalization enabled by protein re-localization can give rise to multifunctionality is illustrated by the C4 protein encoded by TYLCV. At the PM, C4 interacts with the receptor-like kinases BAM1 and BAM2 and hinders the intercellular spread of RNAi (Rosas-Diaz et al., 2018; Fan et al., 2019); following activation of defence, which is triggered by the presence or activity of the virus-encoded Rep protein, C4 is translocated to the chloroplast, where it interacts with CAS and interferes with the CAS-dependent defence responses, including SA biosynthesis. Interestingly, C4 seems to be retained at plasmodesmata, where it interacts with BAM1/2 (Rosas-Diaz et al., 2018), even after being generally depleted from the PM following activation of defence (Supplemental figure 1R); this potential selectivity of the C4 pool undergoing re-localization could ensure that both functions of C4 are maintained throughout the different stages of the infection. This model could also apply to other pathogen effectors, which could have additional virulence-promoting roles at the PM in the absence of a defensive trigger. The identification of the targets of independently evolved effectors following chloroplast translocation could make a powerful contribution to elucidating the molecular mechanisms involved in chloroplast-nucleus communication during plant-pathogen interactions.

An intriguing question is how these myristoylated, PM-localized proteins get released in order to be translocated to the chloroplast. Since myristoylation is an irreversible covalent lipidation, an additional post-translational modification would be required for the release to occur. In animals, phosphorylation-dependent PM detachment of a N-myristoylated protein has been demonstrated (Thelen et al., 1991); since phosphorylation is a prevalent event during activation of defence signalling at the PM, this modification might be a plausible candidate to modulate the localization of plant defence regulators or mimicking pathogen effectors. As the results with the non-myristoylable versions of these plant- or pathogen-encoded proteins indicate, PM release would be sufficient to guarantee immediate chloroplast localization.

Multiple environmental and developmental cues are perceived at the PM. Considering their central role in plant biology, it would be conceivable that some of these signals get relayed to chloroplasts in order to coordinate appropriate downstream physiological responses. In this

scenario, whether a similar, post-translational modification-based mechanism operates to enable communication between the PM and chloroplasts following perception of non-defence related cues is a question worth exploring.

ACKNOWLEDGEMENTS

The authors thank Xinyu Jian, Aurora Luque, Tamara Jimenez-Gongora, Yujing (Ada) Liu, Rahoul Mohan Singh, and the PSC Proteomics and Metabolomics Core Facility, the PSC Cell Biology Core Facility, and the PSC Genomics Core Facility for technical assistance, Jose Rufian, Yuzhen Mei, and Xueping Zhou for experimental advice, and Simon Stael, Marc Somssich, and all members in Rosa Lozano-Duran's and Alberto Macho's groups for stimulating discussions and helpful suggestions. The authors thank Jiamin Luo and Alberto Macho for sharing the construct 35S:*GUS-3xHA*, and are grateful to Alberto Macho, Tamara Jimenez-Gongora, and Sebastian Wolf for critical reading of the manuscript. This research was supported by the the National Natural Science Foundation of China (NSFC) (grant numbers 31671994 and 31870250 to RL-D), the 100 Talents Program from the Chinese Academy of Sciences (CAS) (to RL-D), the Shanghai Center for Plant Stress Biology, and a Young Investigator Grant from the NSFC to LM-P (grant number 31850410467). LM-P is the recipient of a President's International Fellowship Initiative (PIFI) postdoctoral fellowship (No. 2018PB058) from CAS.

AUTHOR CONTRIBUTIONS

RL-D conceived the project; LM-P, HT, VD, MW, TR-D, LW, XD, and DZ performed experiments; LM-P, VD, FX, CK and RL-D analysed data. RL-D wrote the manuscript with input from all authors.

DECLARATION OF INTERESTS

The authors declare no competing interests.

FIGURE LEGENDS

Figure 1. The C4 protein from TYLCV shifts its localization from plasma membrane to chloroplasts upon activation of defence.

(**A, B**) Localization of the WT and the non-myristoylable ($C4_{G2A}$) C4 versions fused to GFP in *N. benthamiana* (A) or cotyledons of Arabidopsis seedlings (B). Scale bar = 25 µm.

(**C**) Localization of the WT C4 fused to GFP in *NbNMT*-silenced *N. benthamiana* plants. Scale bar = 10 µm.

(**D**) Localization of C4-GFP in TYLCV-infected cells (D) or when co-expressed with other TYLCV-encoded proteins in *N. benthamiana* (E). Scale bar = 25 µm (D); 50 µm (E).

(**F**) Localization of C4-GFP following treatment with 1 µM flg22 (1 h and 24 h post-treatment) in the presence of CHX (50 µg/ml, 2 h). Scale bar = 25 µm.

(**G**) Western blot of total and chloroplast-localized C4 protein transiently expressed in *N. benthamiana* with or without flg22 treatment (flg22 1 µM, 6 h) in the presence of CHX (50 µg/ml, 2 h prior to flg22 treatment). Total: total protein. Chloroplast: protein from the isolated chloroplasts fraction. Numbers below blots indicate relative intensity. "C4-GFP" indicates the full-length, PM-localized C4-GFP; "cpC4-GFP" indicates the mature chloroplast form of C4-GFP. Asterisks indicate unidentified bands, potential degradation products of the PM C4-GFP pool.

(**H, I**) $C4_{G2A}$-RFP transiently expressed in *N. benthamiana* (H) or stably expressed in Arabidopsis (I) is associated to the chloroplast thylakoid membrane. C: total chloroplast; T: thylakoid; S: stroma; LhcB1: light harvesting complex protein B1 (25 kDa) (thylakoid marker); RbcL: rubisco large subunit (52.7 kDa) (stromal marker). "*" marks the $C4_{G2A}$-RFP band. "#" marks the free RFP band.

(**J, K**) Chloroplast-localized C4 does not affect photosynthetic efficiency (J) or chloroplast ultrastructure (K). See Methods for details. Images in (K) are from ten-day-old seedlings grown in long day.

(**L, M, N**) Expression of chloroplast-localized C4 does not visibly affect development in transgenic Arabidopsis lines (Bar = 1 cm (L); 7 cm (M)). w-o: week-old. In (N), Bars represent SE of n = 3; asterisks indicate a statistically significant difference (*P < 0.05, **P < 0.01, ***P < 0.001) according to a one-way ANOVA with post-hoc Dunnett's multiple comparisons test.

AF: Autofluorescence; CBB: Coomassie brilliant blue; EV: empty vector. See also Figure S1.

Figure 2. Chloroplast-localized C4 interacts with Calcium Sensing Receptor and suppresses downstream defence responses.

(**A**) Flg22-induced *ICS1* and *PR1* expression in ten-day-old WT or transgenic Arabidopsis lines expressing $C4_{G2A}$. *ACT2* was used as the normalizer. Data are mean ± SE of three independent biological replicates.

(**B**) Total SA content quantified in ten-day-old WT or transgenic Arabidopsis lines expressing $C4_{G2A}$ following elicitation with flg22 (1 µM, 12 h). Data are mean ± SE of three independent biological replicates. Lowercase letters indicate statistically significant differences between mean values (P <0.001), according to a one-way ANOVA with post-hoc Tukey's multiple comparisons test.

(**C**) Relative viral accumulation in Arabidopsis *NahG* and *sid2/NahG* plants infected with TYLCV wild type (TYCLV) or a C4 null mutant version (TYLCV_$C4_{1-8}$) at 21 days post-inoculation (dpi). Values represent the average of eight plants. Error bars represent SE. ND: not detected. "%" indicates the percentage of TYLCV_$C4_{1-8}$ accumulation compared to TYLCV (100%). Experiments were repeated three times with similar results.

(**D**) CAS peptides identified in AP-MS analysis after purification of $C4_{G2A}$-GFP from *N. benthamiana* leaves (two independent experiments). "-" indicates no peptide was detected.

(**E**) Bimolecular fluorescence complementation (BiFC) assay with $C4_{G2A}$ and CAS in *N. benthamiana*. Scale bar = 25 µm.

(**F**) $C4_{G2A}$ interacts with the C-terminal part of CAS by co-immunoprecipitation upon transient co-expression in *N. benthamiana* leaves.

(**G**) Topology analysis of chloroplast-localized C4 and CAS proteins. P: thylakoid pellet; S: supernatant; POR: protochlorophyllide oxidoreductase (37 kDa) (a thylakoid peripheral protein facing stroma); PsbO: photosystem II subunit O (33 kDa) (a lumen-localized protein).

(**H**) Chloroplast-localized C4 interferes with the cytoplasmic calcium transient in response to flg22. The calcium sensor aequorin (AEQ) was transiently co-expressed with $C4_{G2A}$ or GUS (as negative control) in *N. benthamiana* leaves. The vertical dashed lines indicate flg22 (1 µM) application. Values represent the average of six plants. Error bars represent SE. Asterisks indicate a statistically significant difference (****P < 0.0001) according to a two-tailed comparisons *t*-test. This experiment was repeated three times with similar results. See also Figure S2L.

(**I**) Chloroplast-localized C4 impairs flg22-induced callose deposition. Average numbers of callose deposits per 2.5 mm^2 ± SE (n=10) are shown. This experiment was repeated three times with similar results.

(**J**) Transcriptional overlap between transgenic Arabidopsis seedlings expressing $C4_{G2A}$ and a *cas-1* mutant upon flg22 treatment (1 µM, 12 h). UR: up-regulated; DR: down-regulated. Comparisons are made with treated WT plants.

(**K**) Transgenic Arabidopsis plants expressing $C4_{G2A}$ display increased susceptibility to *Pto* DC3000. Data are mean ± SE of n = 4. This experiment was repeated three times with similar results. Asterisks indicate a statistically significant difference (***P* < 0.01, ****P* < 0.001) according to a one-way ANOVA with post-hoc Dunnett's multiple comparisons test. See also Figure S2N.
(**L**) Relative accumulation of TYLCV or TYLCV_$C4_{1-8}$ in *cas-1* Arabidopsis plants and *N. benthamiana* and tomato plants in which *CAS* has been silenced by VIGS at 21 dpi. Values represent the average of six plants. Error bars represent SE. ND: not detected. Experiments were repeated three times with similar results.

AF: Autofluorescence; CBB: Coomassie brilliant blue; EV: empty vector. See also Figure S2.

Figure 3. Proteins encoded by plant viruses contain overlapping membrane- and chloroplast-targeting signals and suppress chloroplast-mediated defences.
(**A**) Flow diagram illustrating the number of proteins encoded by plant viruses and containing an N-myristoylation motif, a chloroplast transit peptide, or both, and the families they belong to.
(**B**) Localization of selected viral proteins in *N. benthamiana*. Scale bar = 25 µm. Arrowheads indicate chloroplasts.
(**C**) Localization of selected geminiviral proteins following treatment with 1 µM flg22 (1h and 24h) in the presence of CHX (50 µg/ml, 2 h prior to PAMP treatment) in *N. benthamiana*. Scale bar = 25 µm. Arrowheads indicate chloroplasts.
(**D, E**) Chloroplast-localized viral proteins suppress expression of SA-related genes (D) and interfere with the cytoplasmic calcium transient (E) upon flg22 treatment in *N. benthamiana* leaves. In (D), *NbEF1α* was used as an internal standard; values represent the average of four independent experiments with three plants each; data are mean ± SE of three independent experiments. In (E), error bars represent SE. Asterisks indicate a statistically significant difference (***P* < 0.01, *****P* < 0.0001) according to a two-tailed comparisons *t*-test; experiments were repeated three times with similar results. See Figure 2H for details. See also Figure S3H.
(**F**) Chloroplast-localized viral proteins increase susceptibility to *Pto* DC3000 Δ*hopQ1-1*. Data are mean ± SE. Asterisks indicate a statistically significant difference (****P* < 0.001) according to a two-tailed comparisons *t*-test. Experiments were repeated three times with similar results. See also Figure S3I.
(**G**) Total apoplastic ROS production in the 60 min following flg22 treatment in *N. benthamiana* leaves expressing chloroplast-localized viral proteins. Error bars indicate SE (n = 24). Asterisks

indicate a statistically significant difference (**P < 0.01, ****P < 0.0001) according to a two-tailed comparisons *t*-test. Experiments were repeated three times with similar results.

AF: Autofluorescence; EV: empty vector. See also Figure S3.

Figure 4. Effector proteins from plant pathogenic bacteria contain overlapping membrane- and chloroplast-targeting signals and suppress chloroplast-mediated defences.

(**A**) Flow diagram illustrating the number of proteins encoded by the plant pathogenic bacterial strain *Ralstonia solanacearum* (GMI1000) and containing an N-myristoylation motif, a chloroplast transit peptide, or both.

(**B**) Localization of WT GALA1 from *R. solanacearum* (GALA1) and the non-myristoylable ($GALA1_{G2A}$) version fused to GFP in *N. benthamiana*. Scale bar = 25 µm. Arrowheads indicate chloroplasts.

(**C**) Localization of GALA1-GFP following treatment with flg22 (1 µM, 24 h) in the presence of CHX (50 µg/ml, 2 h prior to PAMP treatment) in *N. benthamiana.* Scale bar = 25 µm. Arrowheads indicate chloroplasts.

(**D**) Chloroplast-localized GALA1 and GALA3 interfere with the cytoplasmic calcium transient in response to flg22. See Figure 2H for details. Values represent the average of six plants. Error bars represent SE. Asterisks indicate a statistically significant difference (****P < 0.0001) according to a two-tailed comparisons *t*-test. Experiments were repeated three times with similar results. See also Figure S4D.

(**E, F**) Chloroplast-localized GALA1 (E) and GALA3 (F) hampers expression of SA biosynthetic and differentially affect expression of CAS-dependent genes upon flg22 treatment (1 µM, 24 h). *ACT2* was used as the normalizer. Data are mean ± SE of three independent biological replicates with three technical replicates each.

(**G**) Transgenic Arabidopsis plants expressing chloroplast-localized GALA1 or GALA3 ($GALA1_{G2A}$ and $GALA3_{G2A}$ plants) display increased susceptibility to *Pto* DC3000. Data are mean ± SE of n = 4. This experiment was repeated four times with similar results. Asterisks indicate a statistically significant difference (*P < 0.05, **P < 0.01) according to a one-way ANOVA with post-hoc Dunnett's multiple comparisons test. See also Figure S4G.

(**H**) Total apoplastic ROS production in the 60 min following flg22 treatment in *N. benthamiana* leaves 48 h after transient transformation. Error bars indicate SE (n = 24). Asterisks indicate a statistically significant difference (****P < 0.0001) according to a two-tailed comparisons *t*-test. Experiments were repeated three times with similar results.

AF: Autofluorescence; EV: empty vector. See also Figure S4.

Figure 5. A core of conserved plant defence-related proteins contain overlapping N-myristoylation motifs and cTPs.

(**A**) Flow diagram illustrating the number of proteins encoded by *Arabidopsis thaliana* containing an N-myristoylation motif, a chloroplast transit peptide, or both.

(**B**) Venn diagram of proteins with overlapping N-myristoylation motifs and cTPs in the predicted proteomes of Arabidopsis, tomato, and rice.

(**C**) The subset of 26 common proteins containing overlapping N-myristoylation motifs and cTPs in the predicted proteomes of Arabidopsis, tomato, and rice is enriched in defence-related GO terms. BP: biological process ontology; MF: molecular function ontology; CC: cellular component ontology.

(**D**) Plant phylogenetic tree indicating the relationship between the species analyzed, the number of proteins containing an N-myristoylation motif and a cTP in their predicted proteomes, and the prevalence of the coexistence of these two targeting signals.

See also Figure S5 and Tables S1-S7.

Figure 6. The plant Calcium protein kinase 16 (CPK16) contains overlapping plasma membrane- and chloroplast-targeting signals, shifts its localization from plasma membrane to chloroplasts upon activation of defence, and activates chloroplast-mediated defences.

(**A, B**) Localization of the WT (CPK16) and the non-myristoylable ($CPK16_{G2A}$) versions fused to GFP transiently expressed in *N. benthamiana* (A) or stably expressed in *A. thaliana* (B). Scale bar = 25 µm. Dashed squares indicate zoom-in panels. Arrowheads indicate chloroplasts.

(**C**) Localization of CPK16-GFP n *NbNMT*-silenced *N. benthamiana* plants. Scale bar = 10 µm.

(**D**) Localization of CPK16-GFP following treatment with flg22 (1 µM, 12 h) in the presence of CHX (50 µg/ml, 2 h prior to flg22 treatment). Scale bar = 25 µm.

(**E**) Western blot of total and chloroplast-localized CPK16 protein transiently expressed in *N. benthamiana* leaves with or without flg22 treatment in the presence of CHX (50 µg/ml, 2 h prior to flg22 treatment). Total: total protein. Chloroplast: chloroplast protein from an isolated chloroplasts fraction. Numbers below blots indicate relative intensity. “CPK16-Myc” indicates the full-length, PM-localized CPK16-GFP; “cpCPK16-Myc” indicates the mature chloroplast form of

CPK16-Myc. The asterisk indicates unidentified bands, potential degradation product of the PM CPK16-Myc pool.

(**F**) Total apoplastic ROS production in the 60 min following flg22 treatment in transgenic Arabidopsis plants overexpressing CPK16 or $CPK16_{G2A}$. Error bars indicate SE (n = 16). (*P* = 0.666, according to a one-way ANOVA). Experiments were repeated three times with similar results.

(**G**) Constitutive chloroplast localization of CPK16 in transgenic $CPK16_{G2A}$ *A. thaliana* plants promotes expression of defence-related marker genes upon activation of defence. *ACT2* was used as the normalizer. Data are mean ± SE of three independent biological replicates with three technical replicates each.

(**H**) CPK16 modulates the cytoplasmic calcium-burst in response to flg22. See Figure 2H for details. Values represent the average of six plants. Error bars represent SE. Asterisks indicate a statistically significant difference (****$P < 0.0001$) according to a two-tailed comparisons *t*-test. Experiments were repeated three times. See also Figure S6F.

(**I**) Transgenic Arabidopsis plants overexpressing CPK16 or $CPK16_{G2A}$ display increased resistance against *Pto* DC3000. Data are mean ± SE of n = 4. This experiment was repeated four times with similar results. Asterisks indicate a statistically significant difference (*$P < 0.05$, **$P < 0.01$, ***$P < 0.001$) according to a one-way ANOVA with post-hoc Dunnett's multiple comparisons test. See also Figure S6G.

(**J**) Relative viral accumulation in transgenic Arabidopsis plants overexpressing *CPK16* or $CPK16_{G2A}$ inoculated with TYCLV or $TYLCV\_C4_{1-8}$ at 21 dpi. Values represent the average of ≥6 plants. Error bars represent SE. ND: not detected. Experiments were repeated three times with similar results.

AF: Autofluorescence; CBB: Coomassie brilliant blue; EV: empty vector. See also Figure S6.

Figure 7. Model of the proposed pathway linking plasma membrane to chloroplasts and activating defence in plants and its co-option by plant pathogens to promote virulence through suppression of SA responses. Activation of defence following perception of a biotic threat at the plasma membrane would trigger release of the indicated proteins and their subsequent re-localization to chloroplasts, where they would activate (green arrow) or repress (red arrows) downstream SA-dependent defence responses.

SUPPLEMENTAL INFORMATION

SUPPLEMENTAL FIGURES

Figure S1. C4 shifts its localization from the plasma membrane to the chloroplast following activation of PTI, Related to Figure 1.

(**A**) MS spectrum of the myristoylated Nt-peptide ^{2}GNHISMCLSNSK^{13} of the C4 protein. MS spectrum represents the results obtained in one replicate. Similar results were obtained in a second replicate.

(**B**) Modifications detected by IP-MS in the Nt-peptide ^{2}GNHISMCLSNSK^{13} of C4 in two independent replicates.

(**C**) *NbNMT* silencing in TRV2-*NbNMT*-infected *N. benthamiana* produces a visible phenotype. Pictures show plants at 14 dpi. Experiments were repeated at least three times with similar results; results from one experiment are shown. Scale bar = 2 cm.

(**D**) *NbNMT* silencing in TRV2-*NbNMT*-infected *N. benthamiana* plants as quantified by qRT-PCR. RNA was extracted from the three most apical leaves at 14 dpi. Values represent the average of three plants. *NbEF1α* was used as internal standard for *N. benthamiana*. Error bars represent SE. Experiments were repeated three times with similar results; results from one experiment are shown.

(**E**) Confocal images from TRV2- and TRV2-*NbNMT*-infected plants as a negative control of background autofluorescence (to Figure 1C, Supplemental figure 3E, and Figure 6C). Scale bar = 10 µm.

(**F**) Pretreatment with benzothiazole, an inhibitor of NMTs (100 µM, 18 h and 6 h prior to visualization), impairs the PM accumulation of C4 upon transient expression in *N. benthamiana* leaves. Dimethyl sulfoxide (DMSO) was used as a mock solvent control. Scale bar = 10 µm. BT: Benzothiazole.

(**G**) C4-GFP PM/chloroplasts intensity ratio upon flg22 (1 h) or mock treatment (from Figure 1F), quantified using ImageJ. Bars represent SE of n = 6. Asterisks indicate a statistically significant difference (***P value = 0.0004) according to a two-tailed comparisons t-test.

(**H**) C4 re-localizes from PM to chloroplasts in response to treatment with the damage-associated molecular pattern Pep1 upon transient expression in *N. benthamiana* leaves. Localization of the wild-type C4 version fused to GFP was compared following treatment with 1 µM Pep1 or mock treatment (24 h post-treatment) in the presence of CHX (50 µg/ml, 2 h). Scale bar = 25 µm.

(**I**) C4-GFP PM/chloroplasts intensity ratio upon Pep1 (1 h) or mock treatment (from Supplemental figure 1H), quantified using ImageJ. Bars represent SE of n = 6. Asterisks indicate a statistically significant difference (***P value = 0.0002) according to a two-tailed comparisons t-test.

(**J**) C4 does not re-localize from PM to chloroplasts in response to elf18 peptide in *N. benthamiana*. Localization of the wild-type C4 version fused to GFP was compared following treatment with 1 µM elf18 or mock treatment (1 h and 24 h post-treatment). Scale bar = 25 µm.

(**K**) Western blot of C4-GFP and $C4_{G2A}$-GFP transiently expressed in *N. benthamiana* with or without flg22 treatment. Leaves were incubated 2h with CHX (50 µg/ml) prior to PAMP treatment (flg22 1 µM, 1 h and 24 h).

(**L**) Chloroplast fractionation of a *35S:RFP* Arabidopsis transgenic line (as a negative control to Figure 1I). Isolated chloroplasts from three-week-old Arabidopsis transgenic lines expressing free RFP were separated into membrane and stroma fractions. (C: total chloroplast; T: thylakoid; S: stroma; LhcB1: light harvesting complex protein B1 (25 kDa), a thylakoid membrane protein; RbcL: rubisco large subunit (52.7 kDa), a stromal protein).

(**M**) Pretreatment with K252a, an inhibitor of serine/threonine protein kinases (2 µM, 12 h and 1 h prior to PAMP treatment), impaired the re-localization of C4-GFP from PM to chloroplasts in response to treatment with the bacterial peptide elicitor flg22 (1 µM, 12 h) in *N. benthamiana*. Localization of C4-GFP was compared upon treatment with flg22 or mock treatment in the presence of CHX (50 µg/ml, 2 h). Dimethyl sulfoxide (DMSO) was used as a mock solvent control. Scale bar = 50 µm.

(**N**) C4-GFP PM/chloroplasts intensity ratio upon flg22 or mock treatment in plants pre-treated with K252a (from Supplemental figure 1M), quantified using ImageJ. Data are mean ± SE of n = 4. This experiment was repeated four times with similar results; results from one experiment are shown. Asterisks indicate a statistically significant difference (***P* < 0.01) according to a one-way ANOVA with post-hoc Dunnett's multiple comparisons test.

(**O**) *NbTOC75III* silencing in TRV-NbTOC75III-infected *N. benthamiana* plants produces a visible phenotype. Pictures show plants at 21 dpi. Experiments were repeated at least three times with similar results; results from one experiment are shown. Scale bar = 2 cm.

(**P**) *NbTOC75III* silencing in TRV-*NbTOC75III*-infected *N. benthamiana* plants quantified by qRT-PCR. RNA was extracted from the three most apical leaves at 21 dpi. Values represent the average of six plants. *NbEF1α* was used as internal standard for *N. benthamiana*. Error bars represent SE. Experiments were repeated three times with similar results; results from one experiment are shown.

(**Q**) C4-GFP import into chloroplasts in response to treatment with the bacterial peptide elicitor flg22 is reduced in *NbTOC75III*-silenced *N. benthamiana*. Localization of C4-GFP was compared upon treatment with 1 µM flg22 or mock treatment (12 h post-treatment) in the presence of CHX (50 µg/ml, 2 h). Scale bar = 25 µm.

(**R**) C4 re-localizes from PM to chloroplasts but is retained at plasmodesmata in response to flg22 or Pep1 treatments in *N. benthamiana* leaves. Localization of the wild-type C4 version fused to GFP was compared following treatment with 1 µM flg22, 1 µM Pep1 or mock treatment (24 h post-treatment) in the presence of CHX (50 µg/ml, 2 h). Scale bar = 25 µm. Arrowheads indicate plasmodesmata.

AF: Autofluorescence; CBB: Coomassie brilliant blue

Figure S2. C4 interacts with CAS in the chloroplast and suppresses SA-dependent defences, Related to Figure 2.

(**A**) Expression of the C4 transgene detected by qRT-PCR in 35S:$C4_{G2A}$ transgenic Arabidopsis plants. Data are mean ± SE of n= 6.

(**B**) Transgenic Arabidopsis plants expressing $C4_{G2A}$ respond normally to exogenous SA treatments. SA-induced gene expression was analysed at the indicated time points by qRT–PCR. *ACT2* was used as an internal standard. Data are mean ± SE of three experiments.

(**C**) Viral accumulation in SA-depleted transgenic tomato lines. Three-week-old transgenic *NahG* tomato plants were inoculated with TYLCV wild type or a C4 null mutant (TYLCV_$C4_{1-8}$). The relative viral DNA accumulation in plants was determined by qPCR of total DNA extracted from the six most apical leaves at 21 dpi. Values represent the average of eight plants. Error bars represent SE. ND: not detectable. "%" indicates the percentage of TYLCV_$C4_{1-8}$ accumulation compared to TYLCV (100%). Experiments were repeated three times; results from one representative experiment are shown.

(**D**) Viral accumulation in SA-depleted *eds5* Arabidopsis mutant. Three-week-old *eds5* plants were inoculated with TYLCV wild type or a C4 null mutant (TYLCV_$C4_{1-8}$). The relative viral DNA accumulation in plants was determined by qPCR of total DNA extracted from the six most apical leaves at 21 dpi. Values represent the average of ≥6 plants. Error bars represent SE. ND: not detectable. "%" indicates the percentage of TYLCV_$C4_{1-8}$ accumulation compared to TYLCV (100%). Experiments were repeated three times; results from one representative experiment are shown.

(**E**) Schematic representation of CAS and $CAS_{\Delta 230}$.

(**F**) Subcellular localization of CAS and $CAS_{\Delta 230.}$ GFP and RFP tags were fused to the Ct of the proteins. Scale bar = 25 µm.

(**G**) $C4_{G2A}$ interacts with CAS by bimolecular fluorescence complementation (BiFC). YFP fluorescence was observed in the chloroplasts upon transient coexpression in *N. benthamiana*

leaves. Scale bar = 25 µm. Experiments were repeated three times; results from one representative experiment are shown.

(**H, I**) Flg22 treatment enhances C4-CAS interaction in chloroplasts, measured by BiFC. YFP fluorescence was observed in the chloroplasts upon transient coexpression in *N. benthamiana* leaves following treatment with 1 µM flg22 or mock treatment (6 h) in the presence of CHX (50 µg/ml, 2 h). Scale bar = 25 µm. Experiments were repeated three times; results from one representative experiment are shown.

(**J, K**) YFP relative intensity in chloroplasts from H and I quantified using ImageJ. Data are mean ± SE of three experiments. Asterisks indicate a statistically significant difference (****$P < 0.0001$) according to a two-tailed comparisons *t*-test.

(**L**) Total luminescence from calcium burst assays after elicitation with 1 µM flg22 in *N. benthamiana* leaves in three independent replicates (from Figure 2H). Asterisks indicate a statistically significant difference (***$P < 0.001$, ****$P < 0.0001$) according to a two-tailed comparisons *t*-test.

(**M**) Chloroplast-localized C4 triggers transcriptional changes consistent with loss of function of CAS. qRT-PCR validation of RNA-seq data. *ACT2* was used as the normalizer. Data are mean ± SE of four independent biological replicates.

(**N**) *Pto* DC3000 growth in transgenic Arabidopsis plants expressing $C4_{G2A}$ o in the *cas-1* mutant in three independent replicates (from Figure 2K). Asterisks indicate a statistically significant difference (*$P < 0.05$, ***$P < 0.001$) according to a one-way ANOVA with post-hoc Dunnett's multiple comparisons test.

(**O**, **P**) Transgenic Arabidopsis plants expressing $C4_{G2A}$ are not affected in flg22 perception. (**O**) ROS burst as relative luminescence units (RLU) during 60 min and as total RLU after flg22 treatment. Error bars indicate SE (n = 8) ($P = 0.7276$, considered not significant, one-way ANOVA).

(**P**) Seedling growth inhibition (SGI) assay after flg22 treatment. Error bars indicate SE (n = 12). Lowercase letters indicate statistically significant differences between mean values ($P < 0.0001$), according to a one-way ANOVA with post-hoc Student's test.

(**Q**) *CAS* silencing in TRV2-CAS-infected *N. benthamiana* and tomato. Gene silencing was quantified by qRT-PCR. RNA was extracted from the three most apical leaves at 21 dpi. Values represent the average of six plants. *NbEF1α* and *SlActin* were used as internal standards for *N. benthamiana* and tomato, respectively. Error bars represent SE. Experiments were repeated three times with similar results; results from one experiment are shown.

AF: Autofluorescence; EV: empty vector.

Figure S3. Proteins encoded by plant viruses and containing overlapping N-myristoylation motifs and cTPs suppress defence responses from the chloroplast, Related to Figure 3.

(**A**) Plant virus species encoding proteins with overlapping N-myristoylation motifs and cTPs.

(**B**) Selected protein sequences from phylogenetically unrelated viral proteins with overlapping N-myristoylation motif and cTP.

(**C**) Phylogenetic analysis of *Cucumber mosaic virus* CP sequences from subgroup IA, IB and II. CP sequences are named according to their strain and accession numbers, taken from Roossinck (2002) and Moury (2004). The CP used for further experiments in this publication is contained in the blue box. Amino acid substitutions are indicated at the bottom of the tree. The phylogenetic tree was performed with MegAlign (DNASTAR Lasergene software).

(**D**) Aligned amino acid CP sequences used in C. Only the Nt containing the targeting signals of interest is shown. CP sequences are named according to their strain and accession numbers, taken from Roossinck (2002) and Moury (2004). Chloroplast transit peptides are highlighted in green, predicted myristoylated glycine residues are highlighted in red, QQ signal for proteolytic maturation upon import into chloroplasts is highlighted in yellow, and the CP used for further experiments in this publication is contained in a blue box. The protein sequences alignment was performed with MegAlign (DNASTAR Lasergene software).

(**E**) PM localization of C4 from the curtovirus *Beet curly top virus* (BCTV) (Fam. *Geminiviridae*) and AC4 from the bipartite begomovirus *East African cassava mosaic virus* (EACMV) (Fam. *Geminiviridae*) is impaired in *NbNMT*-silenced *N. benthamiana* plants. Scale bar = 10 µm.

(**F**) Pretreatment with benzothiazole, an inhibitor of NMTs (100 µM, 18 h and 6 h prior to visualization), impairs the PM accumulation of the C4 protein from BCTV and the AC4 protein from EACMV in *N. benthamiana* leaves. Dimethyl sulfoxide (DMSO) was used as a mock solvent control. Scale bar = 10 µm. BT: Benzothiazole.

(**G**) Viral proteins with the overlapping N-myristoylation motif and cTP suppress expression of SA-related genes upon activation of plant immunity in *N. benthamiana* leaves. Flg22 treatment (1 µM) was performed 48 h after transient transformation. Leaf discs from three plants were collected separately nine hours after treatment. Gene expression was analysed by qRT–PCR. *NbEF1α* was used as an internal standard. Values represent the average of four independent experiments with three plants used in each replicate. Data are mean ± SE of three independent experiments.

(**H**) Total luminescence from calcium burst after elicitation with 1 µM flg22 in *N. benthamiana* leaves in three independent replicates (from Figure 3E). Asterisks indicate a statistically

significant difference (*P < 0.05, **P < 0.01, ***P < 0.001, ****P < 0.0001) according to a two-tailed comparisons *t*-test. EV: empty vector.

(**I**) *Pto* DC3000 growth in *N. benthamiana* leaves transiently expressing selected chloroplast-localized viral proteins in three independent replicates (from Figure 3F). Asterisks indicate a statistically significant difference (***P < 0,001) according to a two-tailed comparisons *t*-test.

(**J**) Kinetics of ROS production as relative luminescence units (RLU) during 60 min in response to the elicitor flg22 in *N. benthamiana* leaves transiently expressing chloroplast-localized proteins (from Figure 3G). Error bars indicate SE (n = 24). Experiments were repeated three times with similar results; results from one experiment are shown.

AF: Autofluorescence.

Figure S4. Proteins encoded by the plant pathogenic bacterium *Ralstonia solanacearum* and containing overlapping N-myristoylation motifs and cTPs suppress defence responses from the chloroplast, Related to Figure 4.

(**A**) Proteins encoded by *Ralstonia solanacearum* GMI1000 containing an N-myristoylation motif and a cTP.

(**B**) GALA1-GFP PM/chloroplasts intensity ratio upon flg22 or mock treatment (from Figure 4C) quantified using ImageJ. Bars represent SE of n = 6. Asterisks indicate a statistically significant difference (***P value = 0.0003) according to a two-tailed comparisons *t*-test.

(**C**) $GALA1_{G2A}$ and $GALA3_{G2A}$ accumulate in chloroplasts upon transient expression in *N. benthamiana* leaves. $GALA_{G2A}$-GFP proteins were detected in chloroplasts isolated from *N. benthamiana* leaves (2 dpi) after immunoprecipitation with GFP-Trap beads. "-" indicates samples infiltrated with empty vector. "+" indicates samples expressing $GALA1_{G2A}$ or $GALA3_{G2A}$. "*" marks the expected bands.

(**D**) Total luminescence from calcium burst after elicitation with 1 µM flg22 in *N. benthamiana* leaves transiently expressing $GALA1_{G2A}$ or $GALA3_{G2A}$ in three independent replicates (from Figure 4D). Asterisks indicate a statistically significant difference (***P < 0.001, ****P < 0.0001) according to a two-tailed comparisons *t*-test.

(**E**) Expression of *GALA1* and *GALA3* transgenes detected by qRT-PCR in ten-day-old transgenic Arabidopsis seedlings. Data are mean ± SE of n= 6.

(**F**) Localization of the wild-type (GALA1) and the non-myristoylable ($GALA1_{G2A}$) versions of GALA1 fused to GFP in three-day-old transgenic Arabidopsis lines. Scale bar = 25 µm. AF: autofluorescence.

(**G**) *Pto* DC3000 growth in transgenic Arabidopsis plants expressing chloroplast-localized GALA1 or GALA3 ($GALA1_{G2A}$ and $GALA3_{G2A}$ plants) (from Figure 4G). Values represent the average of four independent replicates. Values of each replicate were calculated from four independent plants. Data are mean ± SE. Asterisks indicate a statistically significant difference (*P < 0.05, **P < 0.01, ***P < 0.001) according to a one-way ANOVA with post-hoc Dunnett's multiple comparisons test.

(**H**) Kinetics of ROS production as relative luminescence units (RLU) during 60 min in response to the elicitor flg22 in *N. benthamiana* leaves transiently expressing $GALA1_{G2A}$ or $GALA3_{G2A}$ (from Figure 4H). Error bars indicate SE (n = 24). Experiments were repeated three times with similar results; results from one experiment are shown.

EV: empty vector.

Figure S5. A core of conserved plant defence-related proteins contain overlapping N-myristoylation motifs and cTPs, Related to Figure 5.

(**A**) Functional enrichment analysis of the 78 proteins in the *Arabidopsis thaliana* proteome containing overlapping N-myristoylation motifs and cTPs. BP: biological process ontology; MF: molecular function ontology; CC: cellular component ontology.

(**B**) Flow diagram illustrating the number of proteins encoded by tomato (*Solanum lycopersium*) containing an N-myristoylation motif, a chloroplast transit peptide, or both.

(**C**) Flow diagram illustrating the number of proteins encoded by rice (*Oriza sativa* subsp. *japonica*) containing an N-myristoylation motif, a chloroplast transit peptide, or both.

(**D**) Functional enrichment analysis of the 68 proteins in the *Solanum lycopersicum* proteome containing overlapping N-myristoylation motifs and cTPs. BP: biological process ontology; MF: molecular function ontology; CC: cellular component ontology.

(**E**) Functional enrichment analysis of the 107 proteins in the *Oriza sativa* subsp. *japonica* proteome containing overlapping N-myristoylation motifs and cTPs. BP: biological process ontology; MF: molecular function ontology; CC: cellular component ontology.

(**F**) Functional enrichment analysis of the 19 proteins in the *Chlamydomonas reinhardtii* proteome containing overlapping N-myristoylation motifs and cTPs. BP: biological process ontology; MF: molecular function ontology; CC: cellular component ontology.

(**G**) Functional enrichment analysis of the 30 proteins in the *Marchantia polymorpha* proteome containing overlapping N-myristoylation motifs and cTPs. BP: biological process ontology; MF: molecular function ontology; CC: cellular component ontology.

(**H**) Functional enrichment analysis of the 21 proteins in the *Physcomitrella patens* proteome containing overlapping N-myristoylation motifs and cTPs. BP: biological process ontology; MF: molecular function ontology; CC: cellular component ontology.

Figure S6. The *A. thaliana*-encoded Calcium Protein Kinase 16 (CPK16) employs overlapping targeting signals to re-localize from PM to chloroplasts upon activation of defence and promote chloroplast-mediated defence, Related to Figure 6.

(**A**) Pretreatment with benzothiazole, an inhibitor of NMTs (100 µM, 18 h and 6 h prior to visualization), impaired the PM accumulation of CPK16 from *A. thaliana* upon transient expression in *N. benthamiana* leaves. Dimethyl sulfoxide (DMSO) was used as a mock solvent control. Scale bar = 10 µm. BT: Benzothiazole. AF: Autofluorescence.

(**B**) CPK16-GFP PM/chloroplasts intensity ratio upon flg22 or mock treatment (from Figure 6D), quantified using ImageJ. Bars represent SE of n = 6. Asterisks indicate a statistically significant difference (****P* value = 0.0002) according to a two-tailed comparisons *t*-test.

(**C**) Expression of *CPK16* detected by qRT-PCR in four-week-old plants over-expressing CPK16 or $CPK16_{G2A}$. Data are mean ± SE of n= 6.

(**D**) Pictures of two-, three-, and four-week-old *35S:CPK16* and *35S:CPK16*$_{G2A}$ transgenic Arabidopsis lines.

(**E**) Kinetics of ROS production as relative luminescence units (RLU) during 60 min in response to the elicitor flg22 in four-week-old Arabidopsis transgenic lines over-expressing CPK16 (from Figure 6F). Error bars indicate SE (n = 16) ($P = 0.666$, considered not significant, according to a one-way ANOVA). Experiments were repeated at least three times with similar results; results from one experiment are shown.

(**F**) Total luminescence from calcium burst after elicitation with 1 µM flg22 in *N. benthamiana* leaves transiently overexpressing CPK16 or $CPK16_{G2A}$ in three independent replicates (from Figure 6H). Values represent the average of six plants. Asterisks indicate a statistically significant difference (*$P < 0.001$, ****$P < 0.0001$) according to a two-tailed comparisons *t*-test.

(**G**) *Pto* DC3000 growth in transgenic Arabidopsis plants overexpressing CPK16 or $CPK16_{G2A}$ in four independent replicates (from Figure 6G). Values of each replicate were calculated from three different leaves of four independent plants. Data are mean ± SE. Asterisks indicate a statistically significant difference (*$P < 0.05$, **$P < 0.01$, ***$P < 0.001$) according to a one-way ANOVA with post-hoc Dunnett's multiple comparisons test.

EV: empty vector.

STAR METHODS

RESOURCE AVAILABILITY

Lead Contact

Further information and requests for resources should be directed to and will be fulfilled by the Lead Contact, Rosa Lozano-Duran (lozano-duran@sibs.ac.cn).

Materials Availability

Plasmids and transgenic plant seeds generated in this study will be made available on request; a completed Materials Transfer Agreement may be requested if there is potential for commercial application.

Data and Code Availability

This study did not generate any unique datasets or code.

KEY RESOURCES TABLE

REAGENT or RESOURCE	SOURCE	IDENTIFIER
Antibodies		
Mouse monoclonal anti-GFP (1:5,000)	Abiocode, Agoura Hills, CA, USA	Cat#M0802-3a
Rat monoclonal [5F8] anti-RFP (1:5,000)	ChromoTek, Munich, Germany	Cat#5f8-100; RRID:AB_2336064
Mouse monoclonal anti-Myc (1:5,000)	Cell Signaling Technology, Danvers, Massachusetts	Cat#2276; RRID:AB_331783
Rabbit anti-POR (1:5,000)	Agrisera	Cat#AS05 067; RRID:AB_1031763
Rabbit anti-psbO (1:10,000)	Agrisera	Cat#AS05 092; RRID:AB_1031788
Rabbit anti-LhcB1 (1:10,000)	Agrisera	Cat#AS01 004; RRID:AB_1832079
Rabbit anti-RbcL (1:10,000)	Agrisera	Cat#AS03 037; RRID:AB_2175406
Goat anti-mouse IgG (H+L) HRP conjugate (1:10,000)	Bio-Rad	Cat#170-6516; RRID:AB_11125547
Goat anti-rat IgG-HRP (1:10,000)	Santa Cruz	Cat#sc-2006; RRID:AB_1125219
Goat anti-rabbit IgG-peroxidase (1:10,000)	Jackson ImmunoResearch Labs	Cat#111-035-003; RRID:AB_2313567
Bacterial and Virus Strains		
Escherichia coli DB3.1	Transgen Biotech, China	Cat#CD531
E. coli DH5α	Transgen Biotech, China	Cat#CD501
Agrobacterium tumefaciens GV3101	Shanghai YiXin Biological Technology Co., LTD, China	Cat#AC1001
Pseudomonas syringae pv. tomato DC3000	Cuppels, 1986	N/A
Pseudomonas syringae pv. tomato DC3000 *hopQ1-1* mutant	Rufian et al., 2018	N/A

Tomato yellow leaf curl virus (TYLCV)	Morilla et al., 2005	NCBI:txid220938
Chemicals, Peptides, and Recombinant Proteins		
Salicylic acid	Sigma-Aldrich	Cat#S7401-500G
Coelenterazine, native	Sigma-Aldrich	Cat#C2230
Aniline blue, water soluble	Sangon Biotech	Cat#A500083-0025
Luminol	Sigma-Aldrich	Cat#123072
Horseradish peroxidase (HRP)	Sigma-Aldrich	Cat#77332
Flg22 (TRLSSGLKINSAKDDAAGLQIA)	Abclonal	N/A
Elf18 (SKEKFERTKPHVNVGTIG)	ABclonal	N/A
AtPep1 (ATKVKAKQRGKEKVSSGRPGQHN)	EZBiolabs	N/A
GFP-Trap Agarose	ChromoTek, Munich, Germany	Cat#gta-20; RRID:AB_2631357
RFP-Trap Agarose	ChromoTek, Munich, Germany	Cat#rta-20; RRID:AB_2631362
Protease Inhibitor	Sigma-Aldrich	Cat#P8340
Protease Inhibitor SIGMAFAST^{TM}	Sigma-Aldrich	Cat#S820
Cycloheximide	Xiya Reagent, China	Cat#U5298
K252a	Sigma-Aldrich	Cat#420298-M
Benzothiazole	Sigma-Aldrich	Cat#101338-5G
Acetosyringone	Sigma-Aldrich	Cat#D134406
*Eco*RI-HF®	New England BioLabs	Cat#R3101S
*Sac*I-HF®	New England BioLabs	Cat#R3156S
Q5® High-Fidelity DNA Polymerase	New England BioLabs	Cat#M0491S
T4 DNA Ligase	New England BioLabs	Cat#M0202S
Thermolysin	Calbiochem, Japan	Cat#58656
Critical Commercial Assays		
Plant RNA Kit (200)	Omega	Cat#R6827-02
RNeasy Plant Mini Kit (50)	Qiagen	Cat#74904
2xHLingene PCR Master mix	HLing	Cat#021-52271015
iScript gDNA Clear cDNA Synthesis Kit	BIO-RAD	Cat#172-5035
Hieff qPCR SYBR Green Master Mix	YEASEN	Cat#11201ES
pENTR/D-TOPO Cloning Kit	Invitrogen	Cat#45-0218
Gateway LR Clonase II Enzyme Mix	Invitrogen	Cat#11791-020
AxyPrep Plasmid Miniprep Kit 250-prep	Axygen	Cat#AP-MN-P-250
AxyPrep DNA Gel Extraction Kit 250-prep	Axygen	Cat#AP-GX-250
QuikChange Lightning Site-Directed Mutagenesis Kit	Agilent Technologies	Cat#210518-5
Deposited Data		
RNA-Seq datasets	This paper	GSE148575
EXPERIMENTAL MODELS: ORGANISMS/STRAINS		
Strain name and Genotype	**Source**	**Method**
Arabidopsis thaliana: WT Col-0	NASC (N6673)	NCBI:txid3702
A. thaliana NahG	Lawton et al., 1995	Transgenic Col-0
A. thaliana sid2/NahG	Heck et al., 2003	*sid2* mutant
A. thaliana eds5-1	Nawrath et al., 2002	Ethylmethane sulfonate
A. thaliana cas-1	Nomura et al., 2008	T-DNA insertion line
A. thaliana pGWB2	Rosas-Diaz et al., 2018	Transgenic Col-0
A. thaliana pGWB5	Rosas-Diaz et al., 2018	Transgenic Col-0
A. thaliana GFP	Wang et al., 2019	Transgenic Col-0
A. thaliana RFP	This paper	Transgenic Col-0
A. thaliana C4	Rosas-Diaz et al., 2018	Transgenic Col-0
A. thaliana $C4_{G2A}$	Rosas-Diaz et al., 2018	Transgenic Col-0
A. thaliana C4-GFP	This paper	Transgenic Col-0
A. thaliana $C4_{G2A}$*-GFP*	This paper	Transgenic Col-0
A. thaliana C4-RFP	This paper	Transgenic Col-0
A. thaliana $C4_{G2A}$*-RFP*	This paper	Transgenic Col-0
A. thaliana CPK16	This paper	Transgenic Col-0
A. thaliana $CPK16_{G2A}$	This paper	Transgenic Col-0
A. thaliana CPK16-GFP	This paper	Transgenic Col-0
A. thaliana $CPK16_{G2A}$*-GFP*	This paper	Transgenic Col-0
A. thaliana GALA1-GFP	This paper	Transgenic Col-0
A. thaliana $GALA1_{G2A}$*-GFP*	This paper	Transgenic Col-0
A. thaliana GALA3-GFP	This paper	Transgenic Col-0
A. thaliana $GALA3_{G2A}$*-GFP*	This paper	Transgenic Col-0
Solanum lycopersicum NahG	Brading et al., 2000	Transgenic "Moneymaker"
Oligonucleotides		

See Table S9		
Recombinant DNA		
See Table S8		
SOFTWARE AND ALGORITHMS		
Identifier	**Source**	**Link**
Image J	Schneider et al., 2012	https://imagej.nih.gov/ij/
MegAilgn	DNASTAR Lasergene 7.1.0	https://www.dnastar.com
GraphPad Prism 7	GraphPad Software	https://www.graphpad.com/
LAS-X 2.01	Leica	https://www.leica-microsystems.com/products/confocal-microscopes/
Hitachi HT7700 2.17	Hitachi	https://www.hitachi-hightech.com/global/product_detail/?pn=em-ht7700
Indigo 2.0.5.0	Berthold	https://www.berthold-bio.com/in-vivo-imaging-systems/details/product/nightshade-lb-985/action/show.html
Primer3web version 4.1.0	ELIXIR Estonia	http://primer3.ut.ee/
SGN VIGS Tool	Sol Genomics Network	http://vigs.solgenomics.net/
ChloroP 1.1 Server	DTU Bioinformatics. Department of Bio and Health Informatics	http://www.cbs.dtu.dk/services/ChloroP/
TMHMM Server 2.0	DTU Bioinformatics. Department of Bio and Health Informatics	http://www.cbs.dtu.dk/services/TMHMM/
Myristoylator	ExPASy	https://web.expasy.org/myristoylator/
eulerr	eulerr	https://cran.r-project.org/web/packages/eulerr/index.html
topGO	Bioconductor	https://bioconductor.org/packages/release/bioc/html/topGO.html
DATA SOURCE		
Organism	**Source**	**Link**
Plant viruses	NCBI Virus	https://www.ncbi.nlm.nih.gov/labs/virus/vssi/#/virus?SeqType_s=Protein&VirusLineage_ss=Viruses, taxid:10239&Flags_csv=refseq&HostLineage_ss=green plants, taxid:33090
Ralstonia solanacearum GMI1000	Uniprot	https://www.uniprot.org/proteomes/UP000001436
Arabidopsis thaliana	TAIR	http://www.arabidopsis.org/download_files/Proteins/TAIR10_protein_lists/TAIR10_pep_20101214
Solanum lycopersicum	Sol Genomics Network	ftp://ftp.solgenomics.net/tomato_genome/annotation/ITAG3.2_release/ITAG3.2_proteins.fasta
Oryza sativa subsp. *japonica*	Rice Genome Annotation Project	http://rice.plantbiology.msu.edu/pub/data/Eukaryotic_Projects/o_sativa/annotation_dbs/pseudomolecules/version_7.0/all.dir/all.pep

EXPERIMENTAL MODEL AND SUBJECT DETAILS

Plant material

All Arabidopsis mutants and transgenic plants used in this work are in the ecotype Columbia (Col-0) background. The Arabidopsis *35S:C4* and *35S:C4$_{G2A}$* lines are described in Rosas-Diaz et al. (2018). To generate Arabidopsis transgenic lines, wild-type *Arabidopsis* plants were transformed

with the corresponding construct (see also KEY RESOURCES TABLE and METHODS DETAILS) using the floral dipping method (Zhang et al., 2006; Clough and Bent, 1998). The *NahG* (Lawton et al., 1995), *sid2/NahG* (Heck et al., 2003), *eds5-1* (Nawrath et al., 2002), and *cas-1* (Nomura et al., 2008) lines were previously described. The *Solanum lycopersicum* "Moneymaker" *NahG* transgenic plants are described in Brading et al., 2000.

Plant growth conditions

For all *in vitro* experiments, Arabidopsis seeds were surface-sterilized in 70% EtOH for 10 min, then washed twice in 99% ethanol and dried in sterile conditions. Seeds were stratified at 4°C in the dark on 1% half Murashige and Skoog (MS) agar plates with sucrose for all experiments, or without sucrose for the determination of maximum photochemical efficiency of photosystem II.

Arabidopsis plants were grown in a controlled growth chamber in long-day conditions (16 h light/8 h dark) at 22°C for all experiments except for bacterial infections and callose deposition, for which plants were grown in a controlled growth chamber in short-day conditions (8 h light/16 h dark) at 22°C. *Nicotiana benthamiana* and tomato (cv. Moneymaker) plants were grown in a controlled growth chamber in long-day conditions (16 h light/8 h dark) at 25°C.

Bacterial strains and growth conditions

Agrobacterium tumefaciens strain GV3101 harbouring the corresponding binary vectors were liquid-cultured in LB medium (1% tryptone, 0.5% yeast extract and 1% NaCl) with the appropriate antibiotics at 28°C overnight. Bacterial cultures were centrifuged at 4,000 g for 10 min and resuspended in the infiltration buffer (10 mM $MgCl_2$, 10 mM MES pH 5.6, 150 µM acetosyringone) to an OD_{600} = 0.2-1. Bacterial suspensions were incubated at room temperature in the dark for 2 h before infiltration into the abaxial side of 4-week-old *N. benthamiana* leaves with a 1 mL needle-less syringe. For experiments that required co-infiltration, *Agrobacterium* suspensions carrying different constructs were mixed at 1:1 ratio before infiltration.

Pseudomonas syringae pv. *tomato* DC3000 and *P. syringae* pv. *tomato* DC3000 Δ*hopQ1-1* were cultured on solid LB medium (1% tryptone, 0.5% yeast extract and 0.5% NaCl) with the appropriate antibiotics at 28°C overnight. For spray-inoculation, bacterial suspensions (OD_{600} = 0.2) were prepared in 10 mM $MgCl_2$ with 0.02% Silwet L-77. For infiltration, bacterial suspensions (OD_{600} = 0.0002) were prepared in 10 mM $MgCl_2$ and infiltrated using a needleless syringe. Bacterial growth was determined three days after inoculation by plating 1:10 serial dilutions of leaf extracts on solid LB medium (1% tryptone, 0.5% yeast extract and 0.5% NaCl) with the

appropriate antibiotics; plates were incubated at 28 °C for two days before bacterial cfu were counted.

METHODS DETAILS

Plasmids and cloning

Plasmids and primers used for cloning are summarized in Tables S8 and S9. The TYLCV clone used as template is AJ489258 (NCBI:txid220938); the BCTV clone used as template is M24597 (NCBI:txid268960). The TYLCV_$C4_{1\text{-}8}$ infectious clone is described in Rosas-Diaz et al. (2018). For other viral proteins used in this work, full-length CDS were synthesized (AC4 (EACMV, NCBI:txid374778), GenBank: CAJ78099; CP (CMV, NCBI:txid12305), GenBank: ALT66618; P3 (GFLV, NCBI:txid12274), GenBank AGT42202)). Bacterial effectors (GALA1, UniProtKB/TrEMBL: Q8XRE0; GALA3, UniProtKB/TrEMBL: Q8XTS6) were PCR-amplified from *Ralstonia solanacearum* GMI1000 (NCBI:txid267608). CDS or gene fragments from *A. thaliana*, *N. benthamiana*, and *S. lycopersicum* were obtained by RT-PCR. Vectors from the pGWB and ImpGWB series were kindly provided by Tsuyoshi Nakagawa (Nakagawa et al., 2007a; Nakagawa et al., 2007b). pB7RWG2.0 is described in Karimi et al. (2002). pGTQL1211YN and pGTQL1221YC are described in Lu et al. (2010). The pBIN-CYA(K) plasmid expressing AEQ_{cyt} is described in Mehlmer et al. (2012). In all cases, the pENTR™/D-TOPO® entry vector (Thermo Scientific) or the pDONR™221 entry vector (Thermo Scientific) containing the fragments of interest were recombined into the corresponding destination vectors through a Gateway LR reaction (Thermo Scientific). For virus induced gene silencing (VIGS) assays, homologue genes of *AtTOC75III* and *AtNMT1* were identified in *N. benthamiana* (*NbTOC75III*: Niben101Scf01482g01002, Niben101Scf08757g00006; *NbNMT*: Niben101Scf00747g01011, Niben101Scf00747g01026; Niben101Scf00870g15011). 300-bp conserved gene fragments were selected, PCR-amplified, and cloned into the pTRV2 vector (Liu et al., 2002) by traditional cloning using *Eco*RI and *Sac*I High-Fidelity (HF®) Restriction Endonucleases (NEB) and T4 DNA ligase (NEB). In all cases, PCR products were amplified using Q5® High-Fidelity DNA Polymerase (NEB). See also KEY RESOURCES TABLE and Table S9 for primers details.

Generation of transgenic lines

All plasmids (see also KEY RESOURCES TABLE and Table S8) were transformed by heat shock into *Agrobacterium tumefaciens* GV3101 strain and then transformed into wild-type *Arabidopsis*

plants by the floral dipping method (Clough and Bent, 1998; Zhang et al., 2006) to generate stable transgenic lines.

Transient expression in *Nicotiana benthamiana*

Transient expression assays were performed as described in Wang et al. (2017a) with minor modifications. In brief, the *A. tumefaciens* strain GV3101 harbouring the corresponding binary vectors was liquid-cultured in LB with the appropriate antibiotics at 28°C overnight. Bacterial cultures were centrifuged at 4,000 g for 10 min and resuspended in the infiltration buffer (10 mM $MgCl_2$, 10 mM MES pH 5.6, 150 µM acetosyringone) to an OD_{600} = 0.2-1. Bacterial suspensions were incubated at room temperature in the dark for 2 h before infiltration into the abaxial side of four-week-old *N. benthamiana* leaves with a 1 mL needle-less syringe. For experiments that required co-infiltration, *Agrobacterium* suspensions carrying different constructs were mixed at 1:1 ratio before infiltration.

Elicitor, hormone, and inhibitor treatments

The flg22 peptide from *Pseudomonas syringae pv. tomato* DC3000 (TRLSSGLKINSAKDDAAGLQIA) (Felix et al., 1999; Gómez-Gómez and Boller, 2000), the elf18 peptide from *P. syringae pv. tomato* DC3000 (SKEKFERTKPHVNVGTIG) (Kunze et al., 2004), and the *Arabidopsis thaliana* Plant elicitor peptide 1 (*At*Pep1) (ATKVKAKQRGKEKVSSGRPGQHN) (Yamaguchi et al., 2006) were chemically synthesized by ABclonal (flg22 and elf18) and EZBiolabs (Pep1). The peptides were dissolved in deionized water to a 10 mM stock solution. For hormone treatments, salicylic acid (SA) was purchased from Sigma-Aldrich and dissolved in water to a 20 mM stock solution. For protein synthesis inhibitor treatments, cyclohexamide (CHX) was obtained from Xiya Reagent and dissolved in dimethyl sulfoxide (DMSO) to a 30 mM stock solution. K252a, a reversible cell-permeable, potent inhibitor of phosphorylase kinase, and benzothiazole (BT), a N-myristoyltransferase (NMT) inhibitor, both from Sigma-Aldrich, were dissolved in DMSO to the 100 µM (for K252a (Macho et al., 2014)) and 50 mM (for BT (Mei et al., 2018; Bowyer et al., 2007; Yamazaki et al., 2005)) stock solutions. Water or DMSO were used as a mock solvent controls.

Visualization of protein subcellular localization

For subcellular localization, plant tissues expressing GFP- or RFP-fused proteins were imaged with a Leica TCS SP8 confocal microscope (Leica Microsystems) LAS-X 2.01 software using the preset settings for GFP (Ex: 488 nm, Em: 500-550 nm) and RFP (Ex: 554 nm, Em: 580-630 nm).

Localization of C4-GFP in the presence of each TYLCV protein independently was determined with a Leica SMD confocal microscope (Leica Microsystems) using the following settings: gating 1%, laser 10, gain 90%. With V2: gating 1%, laser 10, gain 30%. For transient expression in *N. benthamiana* leaves, subcellular localization was determined at two days post-infiltration. For localization of the wild-type and the non-myristoylable ($C4_{G2A}$) C4 versions fused to GFP in transgenic Arabidopsis lines, cotyledons of seven-day-old seedlings were used. For localization of the wild-type and the non-myristoylable ($CPK16_{G2A}$) CPK16 versions fused to GFP in transgenic Arabidopsis lines, cotyledons of five-day-old seedlings were used. For VIGS of *NbTOC75III* and *NbNMT*, 21 and 14 dpi plants, respectively, were infiltrated with a suspension of *Agrobacterium* harbouring the corresponding binary vectors expressing GFP-fused proteins for further subcellular localization.

Bimolecular fluorescence complementation (BiFC) assay

BiFC assays were performed in *N. benthamiana* leaves as described previously (Lu et al., 2010). *A. tumefaciens* mixtures carrying the appropriate BiFC constructs were infiltrated into the abaxial side of four-week-old *N. benthamiana* leaves with a 1 mL needle-less syringe. Two days later, samples were imaged with a Leica TCS SP8 confocal microscope (Leica Microsystems) using the preset settings for YFP (Ex: 514 nm, Em: 525-575 nm).

Chloroplast isolation

Chloroplasts were isolated from three-week-old Arabidopsis and four-week-old *N. benthamiana* plants as described previously (Dogra et al., 2019a; Kauss et al., 2012). Briefly, plant leaves were homogenized in chloroplast isolation buffer (50 mM Hepes-KOH pH 8, 5 mM $MgCl_2$, 5 mM EDTA pH 8, 5 mM EGTA pH 8, 10 mM $NaHCO_3$, and 0.33 M D-sorbitol, supplemented with SIGMAFAST™ Protease Inhibitor (1 tablet per 100 ml)). The homogenate was then filtered through four layers of Miracloth and centrifuged at 400 × *g* for 8 min at 4 °C. The pellets were suspended in isolation buffer and loaded onto a two-step Percoll gradient (40:80%) to separate intact and broken chloroplasts. Intact chloroplasts enriched between the two Percoll steps were carefully collected and washed twice with HS buffer (50 mM Hepes-KOH pH 8, and 0.33 M D-sorbitol). Isolated chloroplasts were separated into thylakoid membrane and stroma fractions according to (Wang et al., 2016). The equal amounts of intact chloroplasts (equal amounts of chlorophyll) were lysed in HM buffer (10 mM HEPES-KOH pH 8.0, and 5 mM $MgCl_2$) followed by 10 min incubation on ice. The lysate was then subjected to centrifugation at 2,600 × *g* for 5 min at 4 °C to pellet the membranes. During the course of the fractionation, SIGMAFAST™ Protease

Inhibitor was added to all required buffers (1 tablet per 300 ml buffer). Chlorophyll from separated thylakoid membrane fractions was removed using acetone (Wang et al., 2016). The resulting proteins from thylakoid membrane and stroma fractions were resuspended in 1x Laemmli SDS sample buffer and denatured for 10 min at 95 °C. Equal amounts of the solubilized protein fractions were separated on 10% SDS-PAGE gels and blotted onto PVDF membranes (Bio-Rad). RFP-fused proteins were detected using a rat monoclonal anti-RFP antibody (1:5,000; ChromoTek). Light harvesting complex protein (LhcB1) and Rubisco large subunit (RbcL) proteins were immunochemically detected using rabbit anti-LhcB1 (1:10,000; Agrisera) and rabbit anti-RbcL (1:10,000; Agrisera) antibodies, respectively.

For protein re-localization experiments, total intact isolated chloroplasts were used. Equal amounts of the solubilized protein fractions were separated on 10% SDS-PAGE gels and blotted onto PVDF membranes (Bio-Rad). GFP-fused proteins were detected using a mouse monoclonal anti-GFP antibody (1:5,000; Abiocode); myc-fused proteins were detected using a mouse monoclonal anti-Myc antibody (1:5,000; Cell Signaling Technology).

Immunoprecipitation (IP) using total chloroplast proteins

To detect GALA1$_{G2A}$ and GALA3$_{G2A}$, chloroplasts were isolated from four-week-old *N. benthamiana* plants expressing GALA1/3$_{G2A}$-GFP proteins (2 dpi) as described previously (Dogra et al., 2019a; Kauss et al., 2012). Total chloroplast proteins were isolated by suspending the intact chloroplast in IP buffer (containing 20 mM HEPES-KOH (pH 7.4), 2 mM EDTA, 2 mM EGTA, 25 mM NaF, 1 mM Na_3VO_4, 10% (v/v) glycerol, 100 mM NaCl, 0.5% (v/v) Triton X-100, and SIGMAFAST™ Protease Inhibitor (1 tablet/100 mL)) (Wang et al., 2016). The suspension was kept on a tube rotator for 30 min at 4 °C, followed by centrifugation at maximum speed (21,000 × *g*) in an Eppendorf tabletop centrifuge for 30 min at 4 °C. The supernatant was filtered through a 0.22 µm Millipore Express PES membrane, and proteins were quantified using PierceTM BCA protein assay kit (Thermo Fisher Scientific). GFP-Trap beads (GFP-Trap Agarose; ChromoTek) were added to the equal amounts of isolated chloroplast proteins. The samples were first agitated at room temperature for 1.5-2 h, then the beads were washed four times for 5 min with wash buffer. Finally, the washed beads were resuspended in 100 µl 1x Laemmli SDS sample buffer and incubated for 20 min at 70 °C. Equal amounts of the eluted proteins were separated on 10% SDS-PAGE gels and blotted onto PVDF membranes (Bio-Rad). GFP-fused proteins were detected using mouse monoclonal anti-GFP antibody (1:5,000; Abiocode).

Thylakoid membrane isolation and topology analysis

Thylakoid membranes were isolated from four-week-old plants as described by Kato et al. (2018). Leaves were homogenized in a blender with ice-cold homogenization buffer (0.35 M Sucrose, 50 mM HEPES pH 7.5, 0.5 mM $MgCl_2$, 10 mM NaCl, and 2 mM EDTA). Homogenates were then filtered through Miracloth (Merck Millipore). After centrifugation at 2,380 × *g* for 10 min, the pellet was resuspended in the same buffer. After centrifugation at 300 × *g* for 1 min, the supernatant was centrifuged at 2,380 × *g* for 10 min. The pellets were resuspended in the homogenization buffer and used for further analyses.

For topology analysis, freshly isolated thylakoid membranes were resuspended (0.5 mg chlorophyll/ml) in HS buffer (0.35 M Sucrose, 50 mM HEPES, pH 7.5 mM) and treated with thermolysin (100 µg/ml) for 30 min on ice. The soluble- and pellet-fractions were then separated by centrifugation at 2,380 × *g* for 5 min. Chlorophyll from pellet fractions was removed using acetone. The resulting proteins from pellet and soluble fractions were resuspended in 1x Laemmli SDS sample buffer and denatured for 10 min at 95 °C. Equal amounts of the solubilized protein fractions were separated on 10% SDS-PAGE gels and blotted onto PVDF membranes (Bio-Rad). Protochlorophyllide oxidoreductase (POR) and photosystem II subunit O (PsbO) proteins were immunochemically detected using rabbit anti-POR (1:5,000; Agrisera) and rabbit anti-PsbO (1:10,000; Agrisera) antibodies, respectively.

Affinity-purification and mass spectrometry

Affinity-purification and mass spectrometry (AP-MS) was performed according to Wang et al. (2017b). Data were analysed by Scaffold 4.9 with 99% peptide threshold.

Co-immunoprecipitation (co-IP)

To detect the interaction between C4 and CAS, thylakoid membranes were first isolated. Co-immunoprecipitation (co-IP) was carried out as described previously (Dogra et al., 2019b; Wang et al., 2016). Briefly, freshly isolated thylakoid membranes were resuspended in co-IP buffer and kept on ice for 20 min followed by centrifugation at 21,000 × *g* for 30 min at 4 °C. The supernatant was filtered through a 0.22 µm Millipore Express PES membrane and proteins were quantified using Pierce™ BCA protein assay kit (Thermo Fisher Scientific). Small aliquots were taken as input samples whereas the remaining parts were used for co-IP. RFP-Trap beads (RFP-Trap Agarose; ChromoTek) were added to equal amounts of the co-IP samples. The samples were first agitated at room temperature for 1.5-2 h, then the beads were washed four times for 5 min with wash buffer. Finally, the washed beads were resuspended in 100 µl 1x Laemmli SDS sample buffer and incubated for 20 min at 70 °C. Equal amounts of the eluted proteins were separated

on 10% SDS-PAGE gels and blotted onto PVDF membranes (Bio-Rad). GFP- and RFP-fused proteins were detected using mouse monoclonal anti-GFP antibody (1:5,000; Abiocode) and rat monoclonal anti-RFP antibody (1:5,000; Chromotek), respectively.

Calcium burst measurements

N. benthamiana leaf discs transiently co-expressing aequorin and the construct of interest were floated on Milli-Q water containing 5 µM coelenterazine (Sigma), then kept overnight at 22°C in the dark. A 1 µM solution of the peptide elicitor flg22 was applied to the leaf discs and the transient increase in calcium was immediately recorded. Aequorin luminescence was measured with a NightShade LB 985 In vivo Plant Imaging System (Berthold) equipped with an absolutely light-tight cabinet and a cooled CCD camera; data were analysed with Indigo v2 software.

Bacterial infections

Three-week-old Arabidopsis plants grown under short-day conditions were spray-inoculated with a *Pseudomonas syringae* pv. *tomato* DC3000 inoculum (OD_{600} = 0.2 in 10 mM $MgCl_2$ with 0.02% Silwet L-77) and kept covered for 24 h. Four-week-old Arabidopsis plants grown under short-day conditions were infiltrated with a *Pto* DC3000 inoculum (OD_{600} = 0.0002 in 10 mM $MgCl_2$) using a needleless syringe and kept covered for 24 h.

Four-week-old *N. benthamiana* leaves were infiltrated with a *P. syringae* pv. *tomato* DC3000 Δ*hopQ1-1* suspension (OD_{600} = 0.0002 in 10 mM $MgCl_2$) using a needleless syringe upon transient expression of the construct of interest.

Bacterial growth was determined three days after inoculation by plating 1:10 serial dilutions of leaf extracts; plates were incubated at 28 °C for two days before the bacterial cfu were counted.

Viral infections

Viral infections were performed as described in Lozano-Duran et al. (2011a, b). In brief, for *N. benthamiana* and tomato (cv. Moneymaker), a suspension of *Agrobacterium* carrying the TYLCV infectious clone or a mutant version lacking C4 (TYLCV_$C4_{1-8}$) were syringe-inoculated in the shoot apical meristem of two-week-old plants. For VIGS of *NbCAS* and *SlCAS*, plants were co-inoculated with a suspension of *Agrobacterium* carrying the TYLCV infectious clone or a mutant version lacking C4 (TYLCV_$C4_{1-8}$) and samples were collected at three weeks post-inoculation. For Arabidopsis, the corresponding *Agrobacterium* cells were collected from densely grown plates by scraping and inoculated in the centre of the rosette using a needle. Samples were collected at 21 dpi. DNA was extracted with CTAB (Murray and Thompson, 1980) from the three youngest

apical leaves for *N. benthamiana* and tomato, and from the six youngest leaves of the rosette for *A. thaliana*. Viral DNA accumulation was quantified by qPCR.

Virus induced gene silencing (VIGS) assay

VIGS assays were performed as described by Yu et al. (2019). Briefly, independent cultures of *A. tumefaciens* GV3101 carrying pTRV1 or pTRV2-based constructs were liquid-cultured overnight in LB medium plus appropriate antibiotics. Cultures were resuspended in 10 mM $MgCl_2$, 10 mM MES pH 5.6 and 150 µM acetosyringone to OD_{600}=1, and incubated for 2 h at room temperature in the dark. Cultures were mixed at a 1:1 ratio. Approximately 1 mL of this suspension was used to inoculate the stem and underside of cotyledons of two-week-old *N. benthamiana* and tomato (cv. Moneymaker) plants.

qPCR and qRT-PCR

RNA was extracted using the Plant RNA kit (OMEGA Bio-Tek); cDNA was prepared using the iScript™ gDNA Clear cDNA Synthesis Kit (Bio-Rad) according to the manufacturer's instructions. DNA was extracted with CTAB (Murray and Thompson, 1980). DNA (qPCR) and cDNA (qRT-PCR) were analyzed with Hieff™ qPCR SYBR® Green Master Mix (Yeasen). The reactions were done as follows: 3 min at 95 °C, 40 cycles consisting of 15 s at 95 °C, 30 s at 60 °C. The primers used are described in Table S9. *ACTIN* (*ACT2*) was used as internal reference for DNA extracted from Arabidopsis samples; the *25S ribosomal DNA interspacer* (*ITS*) was used for *N. benthamiana* and tomato DNA samples (Mason et al., 2008). For cDNA samples, *ACT2*, *elongation factor-1 alpha* (*NbEF1α;* Nicot et al., 2005), and *SlACTIN* were used as normalizers for Arabidopsis, *N. benthamiana*, and tomato, respectively.

RNA-sequencing

Transcriptome analyses were performed at the Genomics Core Facility, Shanghai Center for Plant Stress Biology, CAS. Sterilized seeds were sown on ½ MS medium containing 1% sucrose and 0.7% agar. Seeds were stratified for three days in the dark at 4°C and grown in long-day conditions. Five-day-old seedlings were transferred into 24-well plates (Corning™ Costar™, Fisher Scientific) with liquid ½ MS containing 0.8% sucrose and grown for another five days prior to elicitation with 1 µM flg22 during 12 h. Water was used as mock. Four biological replicates were used per genotype. Total RNA (1 µg) from each sample was used for library preparation with NEBNext® Poly(A) mRNA Magnetic Isolation Module (New England BioLabs) and NEBNext Ultra II Directional RNA Library Prep Kit for Illumina (New England BioLabs) following the

manufacturer's instructions. Prepared libraries were assessed for quality using NGS High-Sensitivity kit on a Fragment Analyzer (AATI) and for quantity using Qubit 2.0 fluorometer (Thermo Fisher Scientific). All libraries were sequenced using a paired-end 150 bases protocol (PE150) on an Illumina HiSeq sequencer.

Total SA quantification

Sterilized seeds were sown on ½ MS medium containing 1% sucrose and 0.7% agar. Seeds were stratified for three days in the dark at 4°C and grown in long-day conditions. Five-day-old seedlings were transferred into 24-well plates (Corning™ Costar™, Fisher Scientific) with liquid ½ MS containing 0.8% sucrose and grown for another five days prior to elicitation with 1 µM flg22 during 12 h. Water was used as mock. 25 mg of ten-day-old Arabidopsis seedlings were used for SA quantification. Total SA was extracted with 70% MeOH; 2 ng SA-d4 was used as internal standard. 50 µL of the solution were injected into the LC-MS that was performed in a Waters Liquid chromatography ACQUITY UPLC I-class coupled with AB SCIEX TripleTOF® 5600+ equipped with an ACQUITY UPLC BECH C18 1.7 µm VanGuardTM Pre-Column 2.1x5 mm column. The analytical column used was ACQUITY UPLC BECH C18 1.7 µm 2.1x150 mm column. The results were analyzed by Peakview 1.2.

Seedling growth inhibition

Sterilized seeds were sown on ½ MS medium containing 1% sucrose and 0.7% agar. Seeds were stratified for three days in the dark at 4°C and grown in long-day conditions. Five-day-old seedlings were transferred into 48-well plates (Corning™ Costar™, Fisher Scientific) with liquid ½ MS containing 0.8% sucrose with or without the desired peptides (elf18 or flg22 at 10 nM and 100 nM concentration) and grown for another ten days. Fresh weight of 12-16 seedlings was measured using a precision balance.

Reactive oxygen species measurement

Measurement of PAMP-triggered reactive oxygen species (ROS) was performed as previously described (Sang and Macho, 2017). Leaf discs from four- to five-week-old Arabidopsis plants grown in short-day conditions or *N. benthamiana* leaf discs transiently expressing the construct of interest were placed in white 96-well plates (OptiPlate™-96, PerkinElmer) with water overnight. The following day, water was replaced by a solution containing 100 nM flg22, 100 µM luminol, and 20 µg/mL HRP, and luminescence was measured in a microplate reader (Varioskan flash,

Thermo Scientifc) for 60 min. For data analysis, both relative luminescence units (RLU) produced every minute upon flg22 treatment and total RLU over the duration of 60 min were plotted.

Callose deposition

Three- to four-week-old Arabidopsis plants grown in short-day conditions were infiltrated with 1 µM flg22 solution or water using a needle-less syringe. Infiltrated leaves were collected 24 h later and placed in 6-well plates. Chlorophyll was removed by incubating the tissue in ethanol (90% v/v) at 37 °C, followed by two washes with ethanol (75% v/v) for 1 h, and one in dH_2O for 1h. The distained leaves were vacuum-infiltrated with 0.05% aniline blue and incubated for 1h. Then, aniline blue was removed and leaves were embedded in 50% glycerol and conserved at 4 °C in the dark before visualization. Callose deposits were visualized under UV illumination (Ex: 405 nm, Em: 448–525 nm) and quantified using Image J.

Transmission electron microscopy

Ten-day-old Arabidopsis seedlings were used for TEM observation. Samples were cut into sections of about 1mm×2mm and pre-fixed in 2.5% glutaraldehyde in 0.1M phosphate buffer (PBS, pH7.4) at 4°C for three days, followed by three washes with PBS buffer. Samples were post-fixed in 1% osmic acid overnight at 4°C, followed by three washes with 0.1M PBS, then dehydrated with a gradient ethanol-acetone series and gradient-infiltrated and embedded in Spurr resin. Ultra-thin resin sections (70 nm) were cut by a diamond knife on a Leica UC7 ultramicrotome, mounted on copper grids, and stained by 2% uranyl acetate and 0.5% lead citrate. The sections were observed and photographed using a transmission electron microscope H7700 (Hitachi, Japan).

Determination of maximum photochemical efficiency of photosystem II (Fv/Fm)

The Fv/Fm was determined with a FluorCam system (FC800-C/1010GFP; Photon Systems Instruments) containing a CCD camera and an irradiation system following the manufacturer's instructions. Seedlings were grown in ½ MS without sucrose agar medium under constant light (low light intensity: 40 µmol m^{-2} s^{-1}; high light intensity: 80 µmol m^{-2} s^{-1}) for five days under normal temperature (22°C), followed by five days in constant light (very high intensity: 300 µmol m^{-2} s^{-1}) under cold stress conditions (10°C), when Fv/Fm was recorded every day (D: day; D0 to D5: from day 0 to day 5); seedlings were then transferred to the initial conditions, and Fv/Fm was recorded at the indicated time points (R: recovery; R_2h: 2 h after recovery; R_D1 to R_D5: from day 1 to day 5 after recovery).

Prediction of N-myrisotylation motif and chloroplast transit peptide

In all cases, the N-terminal myristoylation motif and the cTP were predicted by Expasy Myristoylator (https://web.expasy.org/myristoylator/) and ChloroP (http://www.cbs.dtu.dk/services/ChloroP/), respectively.

For plant viruses, we extracted the "Genbank organism" corresponding to plant virus from the tab-delimited text file downloaded from DPV (www.dpvweb.net/seqs/seqlist.zip) and used NCBI Entrez Direct (https://www.ncbi.nlm.nih.gov/books/NBK179288/) to download all the plant virus protein sequences in FASTA format. Proteins starting with methionine (M) followed by glycine (G) were selected for further analyses. Then, redundancy was removed using CD-HIT (http://weizhongli-lab.org/cd-hit/). A total of 3,229 non-redundant plant virus proteins were used to predict the N-terminal myristoylation and cTP. For *Ralstonia solanacearum* GMI1000, a total of 5,002 protein sequences were downloaded from UniProt (https://www.uniprot.org/proteomes/UP000001436). For Arabidopsis, the annotated proteins (35,386) were downloaded from http://www.arabidopsis.org/download_files/Proteins/TAIR10_protein_lists/TAIR10_pep_20101214. Proteins starting with MG (3,278) were selected for further analyses. For tomato (*Solanum lycopersicum*), the annotated tomato proteins (35,768) were downloaded from ftp://ftp.solgenomics.net/tomato_genome/annotation/ITAG3.2_release/ITAG3.2_proteins.fasta. Proteins starting with MG (3,456) were selected for further analyses. For rice (*Oryza sativa* subsp. *japonica*), the annotated proteins (66,338) were downloaded from http://rice.plantbiology.msu.edu/pub/data/Eukaryotic_Projects/o_sativa/annotation_dbs/pseudomolecules/version_7.0/all.dir/all.pep. Proteins starting with MG (5,954) were selected for further analyses. For *Chlamydomonas reinhardtii*, a total of 18,829 protein sequences were downloaded from UniProt (https://www.uniprot.org/proteomes/UP000006906). For *Marchantia polymorpha*, a total of 40,580 protein sequences were downloaded from UniProt (https://www.uniprot.org/uniprot/?query=Marchantia%20polymorpha). For *Physcomitrella patens*, a total of 30,858 protein sequences were downloaded from UniProt (https://www.uniprot.org/proteomes/UP000006727).

Bioinformatic analyses

GO term analyses were conducted with topGO (https://bioconductor.org/packages/release/bioc/html/topGO.html); Venn diagrams were drawn by eulerr (https://cran.r-project.org/web/packages/eulerr/index.html).

Accession Numbers

Sequence information of the proteins studied in this article can be found in Table S10. Accession numbers were obtained from the Arabidopsis TAIR database (https://www.arabidopsis.org), National Center for Biotechnology Information (https://www.ncbi.nlm.nih.gov), UniProt (https://www.uniprot.org/uniprot/), and the Sol Genomics Network website (https://solgenomics.net/).

QUANTIFICATION AND STATISTICAL ANALYSIS

To quantify the PM/chloroplasts-localized fluorescence intensity when expressing proteins fused to GFP, confocal images were analysed with the ImageJ software (https://imagej.nih.gov/ij/). In short, first we set a defined “Region of Interest” (ROI) size. Second, “Grey Mean Value” from the “Set Measurements” of the “Analyze” menu in the tool bar was checked and values of the selected areas exported into a spreadsheet. The final relative quantification values are the ratio of PM to chloroplast fluorescence intensity.

For callose deposition, images were analysed with the ImageJ software (https://imagej.nih.gov/ij/). Briefly, images were transformed to 8 bits type, and a “Gaussian Blur” filter was applied keeping the default value for “Sigma (Radius)” for all images. The threshold was set for each image where the background noise of the vasculature disappeared. Note that this threshold value is not fixed between different images and can be adjusted according to their staining intensity. Next, “Analyze Particles” from the tool bar was used to record the number of callose deposits, and the average number (with SD) of callose deposits per 2.5 mm^2 was indicated.

For western blots, images were analysed with the ImageJ software (https://imagej.nih.gov/ij/); quantifications reflect the relative amount as a ratio of the intensity of each band relative to the lane’s loading control. First, “Grey Mean Value” from the “Set Measurements” of the “Analyze” menu in the tool bar was checked. Second, a “Region of Interest (ROI)” to contain the largest band of the row was defined for each blot. To make measurements, “Measure” under the “Analyze” menu was used. All the obtained values were exported into a spreadsheet. The final relative quantification values are the ratio of net band to net loading control.

All statistical analyses were done with the GraphPad Prism 7.0 software (https://www.graphpad.com/). A two-tailed comparisons *t*-test or a one-way ANOVA with post-hoc Student’s test, Dunnett's or Tukey's multiple comparisons test were performed as appropriate.

Details about the statistical approaches used can be found in the figure legends. Data are represented as mean ± SD or SE, as indicated; “n” represents number of samples.

ADDITIONAL RESOURCES

The RNA-Seq datasets are deposited in the Genome Expression Omnibus under the accession number GEO: GSE148575.

SUPPLEMENTAL TABLES

Table S1. Identity of the 78 proteins containing both an N-myristoylation motif and a cTP from the Arabidopsis predicted proteome, Related to Figure 5.

Table S2. Identity of the 26 proteins corresponding to 19 unique genes common to the Arabidopsis, tomato, and rice proteomes containing both an N-myristoylation motif and a cTP, Related to Figure 5.

Table S3. Identity of the 68 proteins containing both an N-myristoylation motif and a cTP from the predicted *Solanum lycopersicum* proteome, Related to Figure 5.

Table S4. Identity of the 107 proteins containing both an N-myristoylation motif and a cTP from the predicted *Oryza sativa* subsp. *japonica* proteome, Related to figure 5.

Table S5. Identity of the 19 proteins containing both an N-myristoylation motif and a cTP from the predicted *Chlamydomonas reinhardtii* proteome, Related to Figure 5.

Table S6. Identity of the 30 proteins containing both an N-myristoylation motif and a cTP from the predicted *Marchantia polymorpha* proteome, Related to Figure 5.

Table S7. Identity of the 21 proteins containing both an N-myristoylation motif and a cTP from the predicted *Physcomitrella patens* proteome, Related to Figure 5.

Table S8: Plasmids generated in this work.

Table S9: Primers used in this work.

Table S10: Sequence information of the proteins studied in this work. Accession numbers were obtained from the Arabidopsis TAIR database (https://www.arabidopsis.org), National Center for Biotechnology Information (https://www.ncbi.nlm.nih.gov), UniProt (https://www.uniprot.org/uniprot/), and the Sol Genomics Network website (https://solgenomics.net/).

REFERENCES

Bhattacharyya, D., Gnanasekaran, P., Kumar, R.K., Kushwaha, N.K., Sharma, V.K., Yusuf, M.A., and Chakraborty, S. (2015). A geminivirus betasatellite damages the structural and functional integrity of chloroplasts leading to symptom formation and inhibition of photosynthesis. Journal of experimental botany *66*, 5881-5895.

Boisson, B., Giglione, C., and Meinnel, T. (2003). Unexpected protein families including cell defense components feature in the N-myristoylome of a higher eukaryote. The Journal of biological chemistry *278*, 43418-43429.

Bowyer, P.W., Gunaratne, R.S., Grainger, M., Withers-Martinez, C., Wickramsinghe, S.R., Tate, E.W., Leatherbarrow, R.J., Brown, K.A., Holder, A.A., and Smith, D.F. (2007). Molecules incorporating a benzothiazole core scaffold inhibit the N-myristoyltransferase of Plasmodium falciparum. The Biochemical journal *408*, 173-180.

Brading, P.A., Hammond-Kosack, K.E., Parr, A., and Jones, J.D. (2000). Salicylic acid is not required for Cf-2- and Cf-9-dependent resistance of tomato to Cladosporium fulvum. The Plant journal : for cell and molecular biology *23*, 305-318.

Chan, K.X., Phua, S.Y., Crisp, P., McQuinn, R., and Pogson, B.J. (2016). Learning the Languages of the Chloroplast: Retrograde Signaling and Beyond. Annual review of plant biology *67*, 25-53.

Chen, H., Zhang, Z., Teng, K., Lai, J., Zhang, Y., Huang, Y., Li, Y., Liang, L., Wang, Y., Chu, C., *et al.* (2010). Up-regulation of LSB1/GDU3 affects geminivirus infection by activating the salicylic acid pathway. The Plant journal : for cell and molecular biology *62*, 12-23.

Clough, S.J., and Bent, A.F. (1998). Floral dip: a simplified method for Agrobacterium-mediated transformation of Arabidopsis thaliana. The Plant journal : for cell and molecular biology *16*, 735-743.

Cuppels, D.A. (1986). Generation and Characterization of Tn5 Insertion Mutations in Pseudomonas syringae pv. tomato. Applied and environmental microbiology *51*, 323-327.

Cutolo, E., Parvin, N., Ruge, H., Pirayesh, N., Roustan, V., Weckwerth, W., Teige, M., Grieco, M., Larosa, V., and Vothknecht, U.C. (2019). The High Light Response in Arabidopsis Requires the Calcium Sensor Protein CAS, a Target of STN7- and STN8-Mediated Phosphorylation. Frontiers in plant science *10*, 974.

de Souza, A., Wang, J.Z., and Dehesh, K. (2017). Retrograde Signals: Integrators of Interorganellar Communication and Orchestrators of Plant Development. Annual review of plant biology *68*, 85-108.

de Torres Zabala, M., Littlejohn, G., Jayaraman, S., Studholme, D., Bailey, T., Lawson, T., Tillich, M., Licht, D., Bolter, B., Delfino, L.*, et al.* (2015). Chloroplasts play a central role in plant defence and are targeted by pathogen effectors. Nature plants *1*, 15074.

Ding, X., Jimenez-Gongora, T., Krenz, B., and Lozano-Duran, R. (2019). Chloroplast clustering around the nucleus is a general response to pathogen perception in Nicotiana benthamiana. Molecular plant pathology *20*, 1298-1306.

Dogra, V., Li, M., Singh, S., Li, M., and Kim, C. (2019). Oxidative post-translational modification of EXECUTER1 is required for singlet oxygen sensing in plastids. Nature communications *10*, 2834.

Exposito-Rodriguez, M., Borges, A.A., Borges-Perez, A., and Perez, J.A. (2008). Selection of internal control genes for quantitative real-time RT-PCR studies during tomato development process. BMC plant biology *8*, 131.

Fan, P., Wang, H., Xue, H., Rosas-Diaz, T., Tang, W., Zhang, H., Xu, L., and Lozano-Duran, R. (2019). The receptor-like kinases BAM1 and BAM2 promote the cell-to-cell movement of miRNA in the root stele to regulate xylem patterning. bioRxiv, 603415.

Felix, G., Duran, J.D., Volko, S., and Boller, T. (1999). Plants have a sensitive perception system for the most conserved domain of bacterial flagellin. The Plant journal : for cell and molecular biology *18*, 265-276.

Fondong, V.N., Reddy, R.V., Lu, C., Hankoua, B., Felton, C., Czymmek, K., and Achenjang, F. (2007). The consensus N-myristoylation motif of a geminivirus AC4 protein is required for membrane binding and pathogenicity. Molecular plant-microbe interactions : MPMI *20*, 380-391.

Gao, C., Xu, H., Huang, J., Sun, B., Zhang, F., Savage, Z., Duggan, C., Yan, T., Wu, C.H., Wang, Y.*, et al.* (2020). Pathogen manipulation of chloroplast function triggers a light-dependent immune recognition. Proceedings of the National Academy of Sciences of the United States of America.

Gnanasekaran, P., Ponnusamy, K., and Chakraborty, S. (2019). A geminivirus betasatellite encoded betaC1 protein interacts with PsbP and subverts PsbP-mediated antiviral defence in plants. Molecular plant pathology *20*, 943-960.

Gomez-Gomez, L., and Boller, T. (2000). FLS2: an LRR receptor-like kinase involved in the perception of the bacterial elicitor flagellin in Arabidopsis. Molecular cell *5*, 1003-1011.

Heck, S., Grau, T., Buchala, A., Metraux, J.P., and Nawrath, C. (2003). Genetic evidence that expression of NahG modifies defence pathways independent of salicylic acid biosynthesis in the Arabidopsis-Pseudomonas syringae pv. tomato interaction. The Plant journal : for cell and molecular biology *36*, 342-352.

Jelenska, J., van Hal, J.A., and Greenberg, J.T. (2010). Pseudomonas syringae hijacks plant stress chaperone machinery for virulence. Proceedings of the National Academy of Sciences of the United States of America *107*, 13177-13182.

Jelenska, J., Yao, N., Vinatzer, B.A., Wright, C.M., Brodsky, J.L., and Greenberg, J.T. (2007). A J domain virulence effector of Pseudomonas syringae remodels host chloroplasts and suppresses defenses. Current biology : CB *17*, 499-508.

Ji, L.H., and Ding, S.W. (2001). The suppressor of transgene RNA silencing encoded by Cucumber mosaic virus interferes with salicylic acid-mediated virus resistance. Molecular plant-microbe interactions : MPMI *14*, 715-724.

Kachroo, P., Yoshioka, K., Shah, J., Dooner, H.K., and Klessig, D.F. (2000). Resistance to turnip crinkle virus in Arabidopsis is regulated by two host genes and is salicylic acid dependent but NPR1, ethylene, and jasmonate independent. The Plant cell *12*, 677-690.

Karimi, M., Inze, D., and Depicker, A. (2002). GATEWAY vectors for Agrobacterium-mediated plant transformation. Trends in plant science *7*, 193-195.

Kato, Y., Hyodo, K., and Sakamoto, W. (2018). The Photosystem II Repair Cycle Requires FtsH Turnover through the EngA GTPase. Plant physiology *178*, 596-611.

Kauss, D., Bischof, S., Steiner, S., Apel, K., and Meskauskiene, R. (2012). FLU, a negative feedback regulator of tetrapyrrole biosynthesis, is physically linked to the final steps of the Mg(++)-branch of this pathway. FEBS letters *586*, 211-216.

1409 Krenz, B., Windeisen, V., Wege, C., Jeske, H., and Kleinow, T. (2010). A plastid-targeted heat
1410 shock cognate 70kDa protein interacts with the Abutilon mosaic virus movement protein.
1411 Virology *401*, 6-17.

1412 Kunze, G., Zipfel, C., Robatzek, S., Niehaus, K., Boller, T., and Felix, G. (2004). The N terminus
1413 of bacterial elongation factor Tu elicits innate immunity in Arabidopsis plants. The Plant
1414 cell *16*, 3496-3507.

1415 Lawton, K., Weymann, K., Friedrich, L., Vernooij, B., Uknes, S., and Ryals, J. (1995). Systemic
1416 acquired resistance in Arabidopsis requires salicylic acid but not ethylene. Molecular plant-
1417 microbe interactions : MPMI *8*, 863-870.

1418 Li, G., Froehlich, J.E., Elowsky, C., Msanne, J., Ostosh, A.C., Zhang, C., Awada, T., and Alfano,
1419 J.R. (2014). Distinct Pseudomonas type-III effectors use a cleavable transit peptide to
1420 target chloroplasts. The Plant journal : for cell and molecular biology *77*, 310-321.

1421 Li, T., Huang, Y., Xu, Z.S., Wang, F., and Xiong, A.S. (2019). Salicylic acid-induced differential
1422 resistance to the Tomato yellow leaf curl virus among resistant and susceptible tomato
1423 cultivars. BMC plant biology *19*, 173.

1424 Liu, Y., Lan, X., Song, S., Yin, L., Dry, I.B., Qu, J., Xiang, J., and Lu, J. (2018). In Planta Functional
1425 Analysis and Subcellular Localization of the Oomycete Pathogen Plasmopara viticola
1426 Candidate RXLR Effector Repertoire. Frontiers in plant science *9*, 286.

1427 Liu, Y., Schiff, M., Marathe, R., and Dinesh-Kumar, S.P. (2002). Tobacco Rar1, EDS1 and
1428 NPR1/NIM1 like genes are required for N-mediated resistance to tobacco mosaic virus.
1429 The Plant journal : for cell and molecular biology *30*, 415-429.

1430 Lozano-Duran, R., Rosas-Diaz, T., Gusmaroli, G., Luna, A.P., Taconnat, L., Deng, X.W., and
1431 Bejarano, E.R. (2011a). Geminiviruses subvert ubiquitination by altering CSN-mediated
1432 derubylation of SCF E3 ligase complexes and inhibit jasmonate signaling in Arabidopsis
1433 thaliana. The Plant cell *23*, 1014-1032.

1434 Lozano-Duran, R., Rosas-Diaz, T., Luna, A.P., and Bejarano, E.R. (2011b). Identification of host
1435 genes involved in geminivirus infection using a reverse genetics approach. PloS one *6*,
1436 e22383.

1437 Lu, Q., Tang, X., Tian, G., Wang, F., Liu, K., Nguyen, V., Kohalmi, S.E., Keller, W.A., Tsang, E.W.,
1438 Harada, J.J.*, et al.* (2010). Arabidopsis homolog of the yeast TREX-2 mRNA export

complex: components and anchoring nucleoporin. The Plant journal : for cell and molecular biology *61*, 259-270.

Macho, A.P., Schwessinger, B., Ntoukakis, V., Brutus, A., Segonzac, C., Roy, S., Kadota, Y., Oh, M.H., Sklenar, J., Derbyshire, P.*, et al.* (2014). A bacterial tyrosine phosphatase inhibits plant pattern recognition receptor activation. Science *343*, 1509-1512.

Maimbo, M., Ohnishi, K., Hikichi, Y., Yoshioka, H., and Kiba, A. (2007). Induction of a small heat shock protein and its functional roles in Nicotiana plants in the defense response against Ralstonia solanacearum. Plant physiology *145*, 1588-1599.

Malamy, J., Carr, J.P., Klessig, D.F., and Raskin, I. (1990). Salicylic Acid: a likely endogenous signal in the resistance response of tobacco to viral infection. Science *250*, 1002-1004.

Mason, G., Caciagli, P., Accotto, G.P., and Noris, E. (2008). Real-time PCR for the quantitation of Tomato yellow leaf curl Sardinia virus in tomato plants and in Bemisia tabaci. Journal of virological methods *147*, 282-289.

Mehlmer, N., Parvin, N., Hurst, C.H., Knight, M.R., Teige, M., and Vothknecht, U.C. (2012). A toolset of aequorin expression vectors for in planta studies of subcellular calcium concentrations in Arabidopsis thaliana. Journal of experimental botany *63*, 1751-1761.

Mei, Y., Wang, Y., Hu, T., Yang, X., Lozano-Duran, R., Sunter, G., and Zhou, X. (2018). Nucleocytoplasmic Shuttling of Geminivirus C4 Protein Mediated by Phosphorylation and Myristoylation Is Critical for Viral Pathogenicity. Molecular plant *11*, 1466-1481.

Morilla, G., Janssen, D., Garcia-Andres, S., Moriones, E., Cuadrado, I.M., and Bejarano, E.R. (2005). Pepper (Capsicum annuum) Is a Dead-End Host for Tomato yellow leaf curl virus. Phytopathology *95*, 1089-1097.

Moury, B. (2004). Differential selection of genes of cucumber mosaic virus subgroups. Molecular biology and evolution *21*, 1602-1611.

Mukaihara, T., Tamura, N., and Iwabuchi, M. (2010). Genome-wide identification of a large repertoire of Ralstonia solanacearum type III effector proteins by a new functional screen. Molecular plant-microbe interactions : MPMI *23*, 251-262.

Murray, M.G., and Thompson, W.F. (1980). Rapid isolation of high molecular weight plant DNA. Nucleic acids research *8*, 4321-4325.

Nakagawa, T., Kurose, T., Hino, T., Tanaka, K., Kawamukai, M., Niwa, Y., Toyooka, K., Matsuoka, K., Jinbo, T., and Kimura, T. (2007a). Development of series of gateway binary vectors, pGWBs, for realizing efficient construction of fusion genes for plant transformation. Journal of bioscience and bioengineering *104*, 34-41.

Nakagawa, T., Suzuki, T., Murata, S., Nakamura, S., Hino, T., Maeo, K., Tabata, R., Kawai, T., Tanaka, K., Niwa, Y.*, et al.* (2007b). Improved Gateway binary vectors: high-performance vectors for creation of fusion constructs in transgenic analysis of plants. Bioscience, biotechnology, and biochemistry *71*, 2095-2100.

Nawrath, C., Heck, S., Parinthawong, N., and Metraux, J.P. (2002). EDS5, an essential component of salicylic acid-dependent signaling for disease resistance in Arabidopsis, is a member of the MATE transporter family. The Plant cell *14*, 275-286.

Nicot, N., Hausman, J.F., Hoffmann, L., and Evers, D. (2005). Housekeeping gene selection for real-time RT-PCR normalization in potato during biotic and abiotic stress. Journal of experimental botany *56*, 2907-2914.

Nomura, H., Komori, T., Kobori, M., Nakahira, Y., and Shiina, T. (2008). Evidence for chloroplast control of external Ca2+-induced cytosolic Ca2+ transients and stomatal closure. The Plant journal : for cell and molecular biology *53*, 988-998.

Nomura, H., Komori, T., Uemura, S., Kanda, Y., Shimotani, K., Nakai, K., Furuichi, T., Takebayashi, K., Sugimoto, T., Sano, S.*, et al.* (2012). Chloroplast-mediated activation of plant immune signalling in Arabidopsis. Nature communications *3*, 926.

Petre, B., Lorrain, C., Saunders, D.G., Win, J., Sklenar, J., Duplessis, S., and Kamoun, S. (2016). Rust fungal effectors mimic host transit peptides to translocate into chloroplasts. Cellular microbiology *18*, 453-465.

Qi, G., Chen, J., Chang, M., Chen, H., Hall, K., Korin, J., Liu, F., Wang, D., and Fu, Z.Q. (2018). Pandemonium Breaks Out: Disruption of Salicylic Acid-Mediated Defense by Plant Pathogens. Molecular plant *11*, 1427-1439.

Rekhter, D., Ludke, D., Ding, Y., Feussner, K., Zienkiewicz, K., Lipka, V., Wiermer, M., Zhang, Y., and Feussner, I. (2019). Isochorismate-derived biosynthesis of the plant stress hormone salicylic acid. Science *365*, 498-502.

Rodriguez-Herva, J.J., Gonzalez-Melendi, P., Cuartas-Lanza, R., Antunez-Lamas, M., Rio-Alvarez, I., Li, Z., Lopez-Torrejon, G., Diaz, I., Del Pozo, J.C., Chakravarthy, S., *et al.* (2012). A bacterial cysteine protease effector protein interferes with photosynthesis to suppress plant innate immune responses. Cellular microbiology *14*, 669-681.

Roossinck, M.J. (2002). Evolutionary history of Cucumber mosaic virus deduced by phylogenetic analyses. Journal of virology *76*, 3382-3387.

Rosas-Diaz, T., Zhang, D., Fan, P., Wang, L., Ding, X., Jiang, Y., Jimenez-Gongora, T., Medina-Puche, L., Zhao, X., Feng, Z., *et al.* (2018). A virus-targeted plant receptor-like kinase promotes cell-to-cell spread of RNAi. Proceedings of the National Academy of Sciences of the United States of America *115*, 1388-1393.

Rufian, J.S., Lucia, A., Rueda-Blanco, J., Zumaquero, A., Guevara, C.M., Ortiz-Martin, I., Ruiz-Aldea, G., Macho, A.P., Beuzon, C.R., and Ruiz-Albert, J. (2018). Suppression of HopZ Effector-Triggered Plant Immunity in a Natural Pathosystem. Frontiers in plant science *9*, 977.

Sang, Y., and Macho, A.P. (2017). Analysis of PAMP-Triggered ROS Burst in Plant Immunity. Methods in molecular biology *1578*, 143-153.

Sang, Y., Yu, W., Zhuang, H., Wei, Y., Derevnina, L., Yu, G., Luo, J., and Macho, A.P. (2020). Intra-strain Elicitation and Suppression of Plant Immunity by Ralstonia solanacearum Type-III Effectors in Nicotiana benthamiana. Plant Communications *100025*.

Schneider, C.A., Rasband, W.S., and Eliceiri, K.W. NIH Image to ImageJ: 25 years of image analysis.

Segonzac, C., Feike, D., Gimenez-Ibanez, S., Hann, D.R., Zipfel, C., and Rathjen, J.P. (2011). Hierarchy and roles of pathogen-associated molecular pattern-induced responses in Nicotiana benthamiana. Plant physiology *156*, 687-699.

Serrano, I., Audran, C., and Rivas, S. (2016). Chloroplasts at work during plant innate immunity. Journal of experimental botany *67*, 3845-3854.

Stael, S., Bayer, R.G., Mehlmer, N., and Teige, M. (2011). Protein N-acylation overrides differing targeting signals. FEBS letters *585*, 517-522.

Tang, L., Yang, G., Ma, M., Liu, X., Li, B., Xie, J., Fu, Y., Chen, T., Yu, Y., Chen, W.*, et al.* (2020). An effector of a necrotrophic fungal pathogen targets the calcium-sensing receptor in chloroplasts to inhibit host resistance. Molecular plant pathology.

Thelen, M., Rosen, A., Nairn, A.C., and Aderem, A. (1991). Regulation by phosphorylation of reversible association of a myristoylated protein kinase C substrate with the plasma membrane. Nature *351*, 320-322.

Wang, L., Ding, X., Xiao, J., Jimenez-Gomicronngora, T., Liu, R., and Lozano-Duran, R. (2017a). Inference of a Geminivirus-Host Protein-Protein Interaction Network through Affinity Purification and Mass Spectrometry Analysis. Viruses *9*.

Wang, L., Kim, C., Xu, X., Piskurewicz, U., Dogra, V., Singh, S., Mahler, H., and Apel, K. (2016). Singlet oxygen- and EXECUTER1-mediated signaling is initiated in grana margins and depends on the protease FtsH2. Proceedings of the National Academy of Sciences of the United States of America *113*, E3792-3800.

Wang, L., Tan, H., Wu, M., Jimenez-Gongora, T., Tan, L., and Lozano-Duran, R. (2017b). Dynamic Virus-Dependent Subnuclear Localization of the Capsid Protein from a Geminivirus. Frontiers in plant science *8*, 2165.

Wang, Y., Li, Y., Rosas-Diaz, T., Caceres-Moreno, C., Lozano-Duran, R., and Macho, A.P. (2019). The IMMUNE-ASSOCIATED NUCLEOTIDE-BINDING 9 Protein Is a Regulator of Basal Immunity in Arabidopsis thaliana. Molecular plant-microbe interactions : MPMI *32*, 65-75.

Xiao, Y., Wang, J., and Dehesh, K. (2013). Review of stress specific organelles-to-nucleus metabolic signal molecules in plants. Plant science : an international journal of experimental plant biology *212*, 102-107.

Xu, Q., Tang, C., Wang, X., Sun, S., Zhao, J., Kang, Z., and Wang, X. (2019). An effector protein of the wheat stripe rust fungus targets chloroplasts and suppresses chloroplast function. Nature communications *10*, 5571.

Yamaguchi, Y., Pearce, G., and Ryan, C.A. (2006). The cell surface leucine-rich repeat receptor for AtPep1, an endogenous peptide elicitor in Arabidopsis, is functional in transgenic tobacco cells. Proceedings of the National Academy of Sciences of the United States of America *103*, 10104-10109.

Yamazaki, K., Kaneko, Y., Suwa, K., Ebara, S., Nakazawa, K., and Yasuno, K. (2005). Synthesis of potent and selective inhibitors of Candida albicans N-myristoyltransferase based on the benzothiazole structure. Bioorganic & medicinal chemistry *13*, 2509-2522.

Yu, G., Xian, L., Sang, Y., and Macho, A.P. (2019). Cautionary notes on the use of Agrobacterium-mediated transient gene expression upon SGT1 silencing in Nicotiana benthamiana. The New phytologist *222*, 14-17.

Zhang, X., Henriques, R., Lin, S.S., Niu, Q.W., and Chua, N.H. (2006). Agrobacterium-mediated transformation of Arabidopsis thaliana using the floral dip method. Nature protocols *1*, 641-646.

Zhang, Y., and Li, X. (2019). Salicylic acid: biosynthesis, perception, and contributions to plant immunity. Current opinion in plant biology *50*, 29-36.

Zhao, J., Zhang, X., Hong, Y., and Liu, Y. (2016). Chloroplast in Plant-Virus Interaction. Frontiers in microbiology *7*, 1565.

Zhu, J.K. (2016). Abiotic Stress Signaling and Responses in Plants. Cell *167*, 313-324.

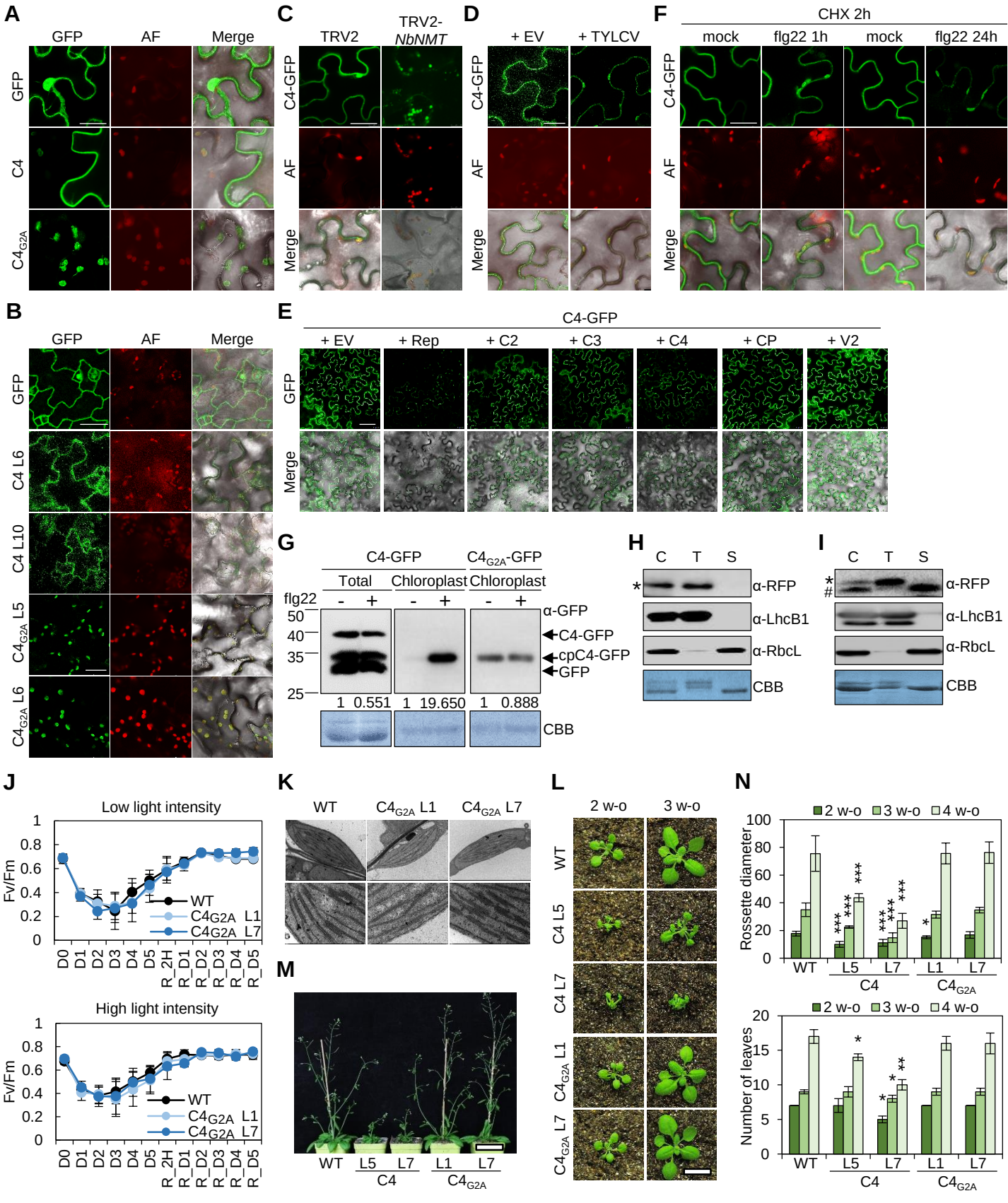
A
GFP
AF
Merge
C4
C4G2A
B
C4 L6
C4 L10
C4G2A L5
C4G2A L6
C
TRV2
TRV2-NbNMT
C4-GFP
D
+ EV
+ TYLCV
F
CHX 2h
mock
flg22 1h
flg22 24h
flg22 24h
E
+ Rep
+ C2
+ C3
+ C4
+ CP
+ V2
G
C4G2A-GFP
Total
Chloroplast
flg22
α-GFP
C4-GFP
cpC4-GFP
GFP
50
40
35
25
1 0.551 1 19.650 1 0.888
CBB
H
I
C T S
α-RFP
α-LhcB1
α-RbcL
CBB
J
Low light intensity
High light intensity
Fv/Fm
WT
C4G2A L1
C4G2A L7
D0 D1 D2 D3 D4 D5 R_2H R_D1 R_D2 R_D3 R_D4 R_D5
K
WT
C4G2A L1
C4G2A L7
L
2 w-o
3 w-o
WT
C4 L5
C4 L7
C4G2A L1
C4G2A L7
M
WT L5 L7 L1 L7
C4 C4G2A
N
2 w-o 3 w-o 4 w-o
Rossette diameter
Number of leaves
WT L5 L7 L1 L7
C4 C4G2A

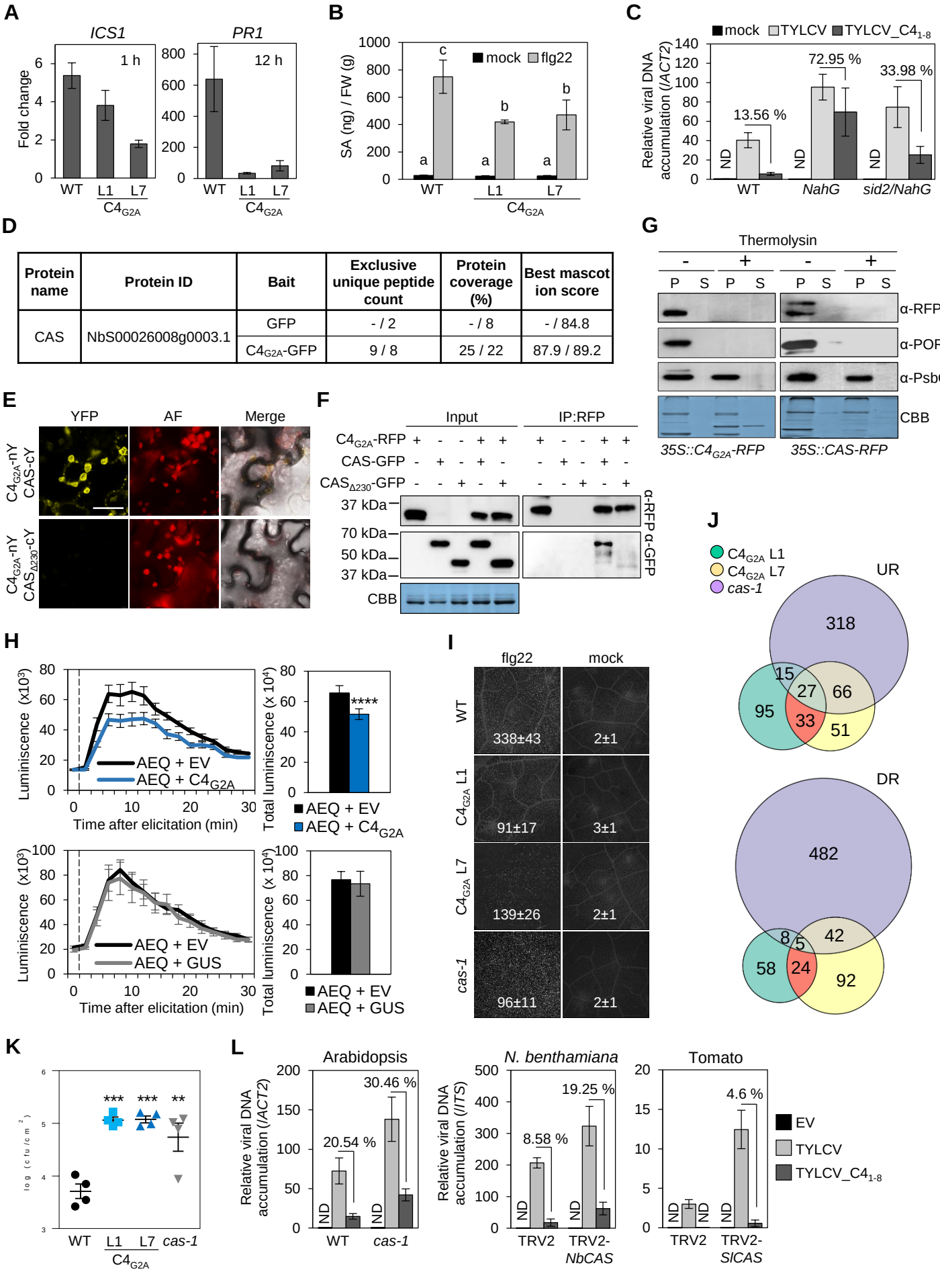
A
ICS1
PR1
1 h
12 h
Fold change
WT
L1
L7
C4G2A
B
mock
flg22
SA (ng) / FW (g)
C
mock
TYLCV
TYLCV_C41-8
Relative viral DNA accumulation (/ACT2)
13.56 %
72.95 %
33.98 %
ND
WT
NahG
sid2/NahG
D
Protein name
Protein ID
Bait
Exclusive unique peptide count
Protein coverage (%)
Best mascot ion score
CAS
NbS00026008g0003.1
GFP
- / 2
- / 8
- / 84.8
C4G2A-GFP
9 / 8
25 / 22
87.9 / 89.2
E
YFP
AF
Merge
C4G2A-nY CAS-cY
C4G2A-nY CASΔ230-cY
F
Input
IP:RFP
C4G2A-RFP
CAS-GFP
CASΔ230-GFP
37 kDa
70 kDa
50 kDa
CBB
α-RFP
α-GFP
G
Thermolysin
P
S
α-RFP
α-POR
α-PsbO
CBB
35S::C4G2A-RFP
35S::CAS-RFP
H
Luminiscence (x10³)
Time after elicitation (min)
AEQ + EV
AEQ + C4G2A
AEQ + GUS
Total luminiscence (x 10⁴)
****
I
flg22
mock
WT
C4G2A L1
C4G2A L7
cas-1
338±43
2±1
91±17
3±1
139±26
2±1
96±11
2±1
J
C4G2A L1
C4G2A L7
cas-1
UR
318
15
27
66
95
33
51
DR
482
8
5
42
58
24
92
K
log (cfu/cm²)
***
***
**
WT
L1
L7
cas-1
C4G2A
L
Arabidopsis
N. benthamiana
Tomato
Relative viral DNA accumulation (/ACT2)
Relative viral DNA accumulation (/ITS)
20.54 %
30.46 %
8.58 %
19.25 %
4.6 %
ND
WT
cas-1
TRV2
TRV2-NbCAS
TRV2-SlCAS
EV
TYLCV
TYLCV_C41-8

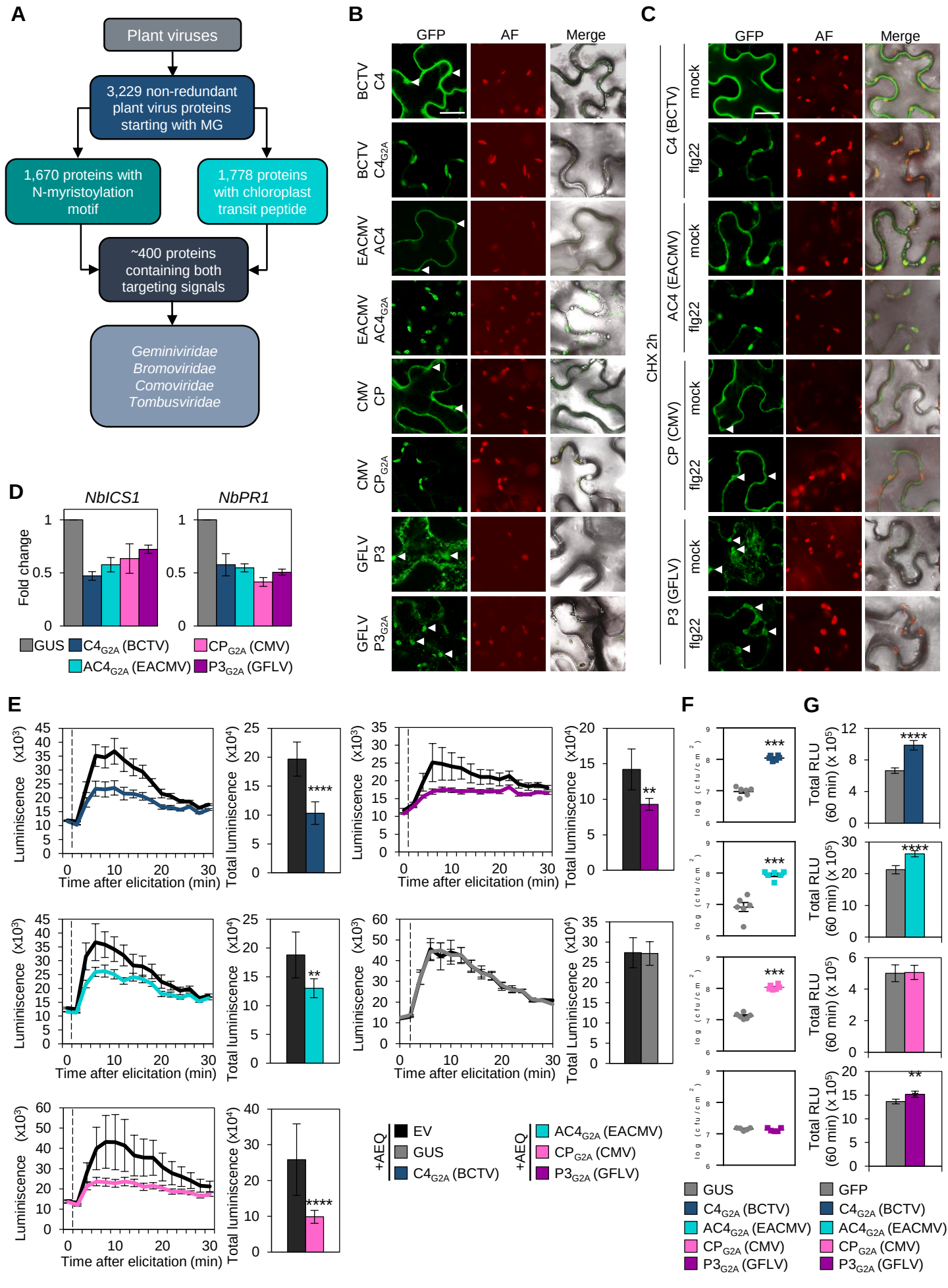
A
Plant viruses
3,229 non-redundant plant virus proteins starting with MG
1,670 proteins with N-myristoylation motif
1,778 proteins with chloroplast transit peptide
~400 proteins containing both targeting signals
Geminiviridae
Bromoviridae
Comoviridae
Tombusviridae
B
GFP
AF
Merge
BCTV C4
BCTV C4G2A
EACMV AC4
EACMV AC4G2A
CMV CP
CMV CPG2A
GFLV P3
GFLV P3G2A
C
CHX 2h
C4 (BCTV)
AC4 (EACMV)
CP (CMV)
P3 (GFLV)
mock
flg22
D
NbICS1
NbPR1
Fold change
GUS
C4G2A (BCTV)
CPG2A (CMV)
AC4G2A (EACMV)
P3G2A (GFLV)
E
Luminiscence (x10³)
Time after elicitation (min)
Total luminiscence (x10⁴)
+AEQ
EV
GUS
C4G2A (BCTV)
AC4G2A (EACMV)
CPG2A (CMV)
P3G2A (GFLV)
F
log (cfu/cm²)
G
Total RLU (60 min) (x 10⁵)
GFP

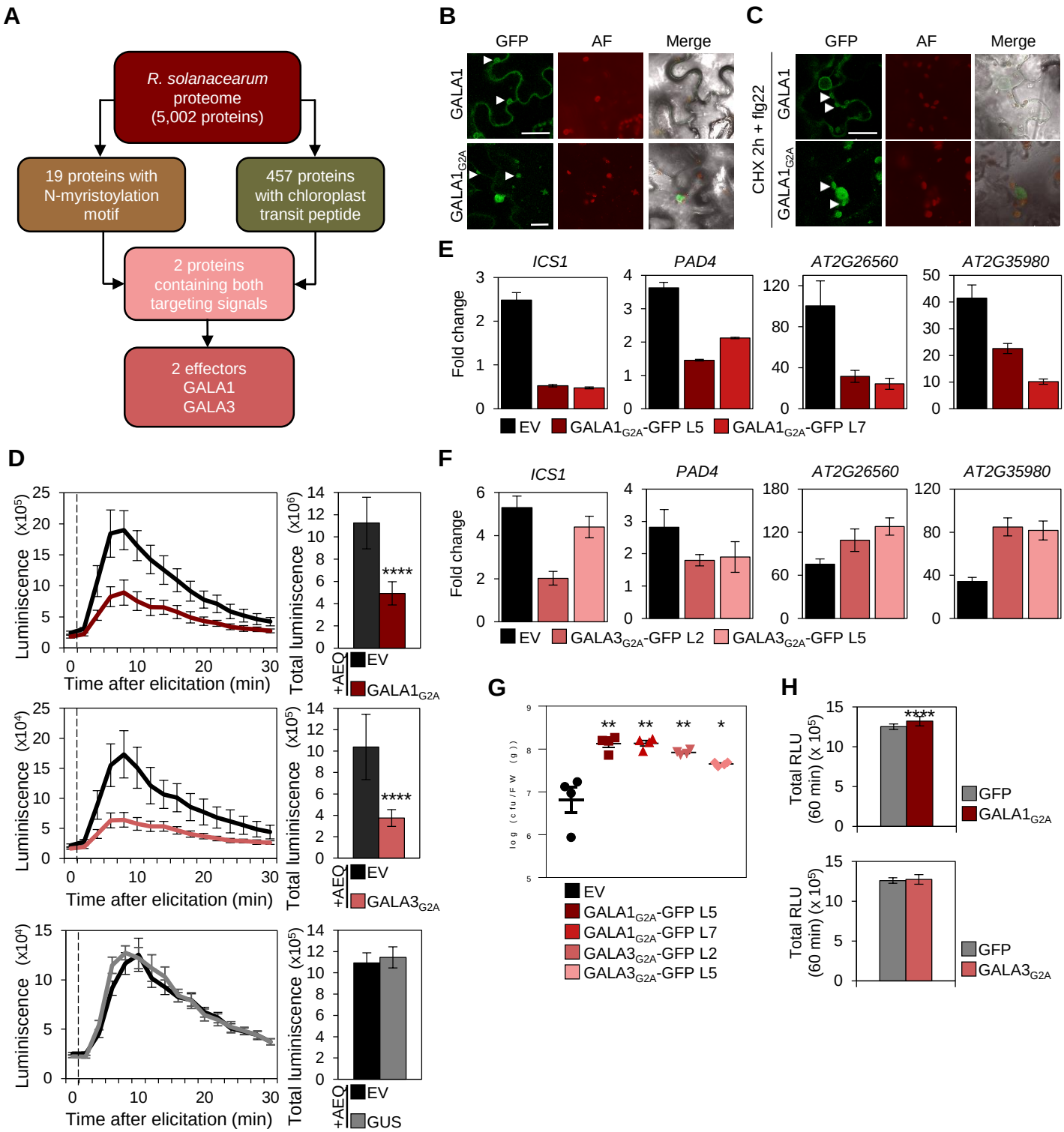
A
R. solanacearum proteome (5,002 proteins)
19 proteins with N-myristoylation motif
457 proteins with chloroplast transit peptide
2 proteins containing both targeting signals
2 effectors GALA1 GALA3
B
GFP
AF
Merge
GALA1
GALA1G2A
C
CHX 2h + flg22
E
ICS1
PAD4
AT2G26560
AT2G35980
Fold change
EV
GALA1G2A-GFP L5
GALA1G2A-GFP L7
D
Luminiscence (x10^5)
Time after elicitation (min)
Total luminiscence (x10^6)
+AEO
EV
GALA1G2A
Luminiscence (x10^4)
Total luminiscence (x10^5)
GALA3G2A
Luminiscence (x10^4)
Total luminiscence (x10^5)
GUS
F
GALA3G2A-GFP L2
GALA3G2A-GFP L5
G
log (cfu/FW (g))
EV
GALA1G2A-GFP L5
GALA1G2A-GFP L7
GALA3G2A-GFP L2
GALA3G2A-GFP L5
H
Total RLU (60 min) (x 10^5)
GFP
GALA1G2A
GALA3G2A

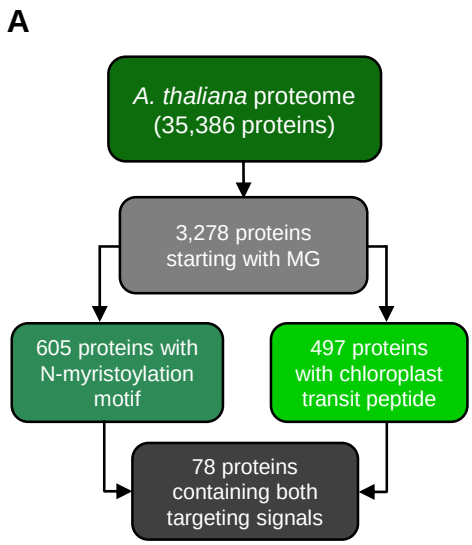

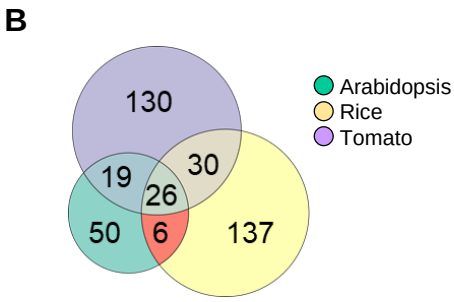

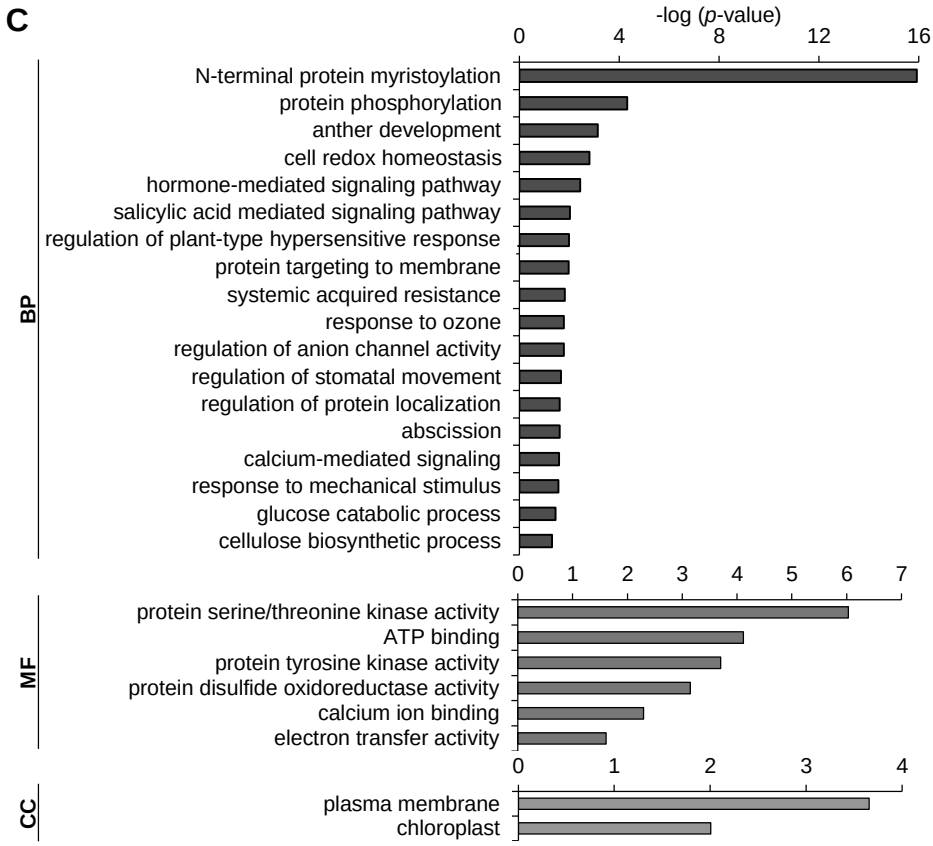

D

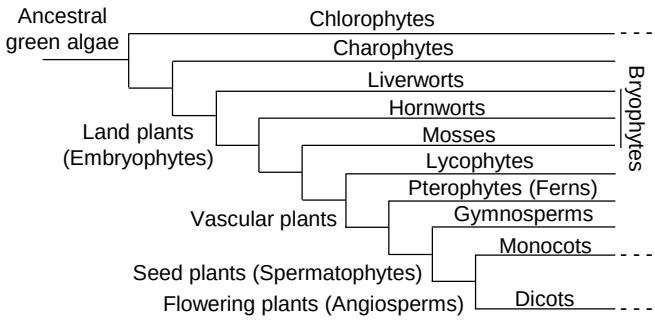

	Proteins containing N-myr and cTP / Total proteome	Proteins containing N-myr and cTP / Total proteome (%)
Chlamydomonas reinhardtii	19 / 18829	0.101
Marchantia polymorpha	30 / 40580	0.074
Physcomitrella patens	21 / 30858	0.068
Oryza sativa	107 / 66338	0.161
Solanum lycopersicum	68 / 35768	0.190
Arabidopsis thaliana	78 / 35386	0.220

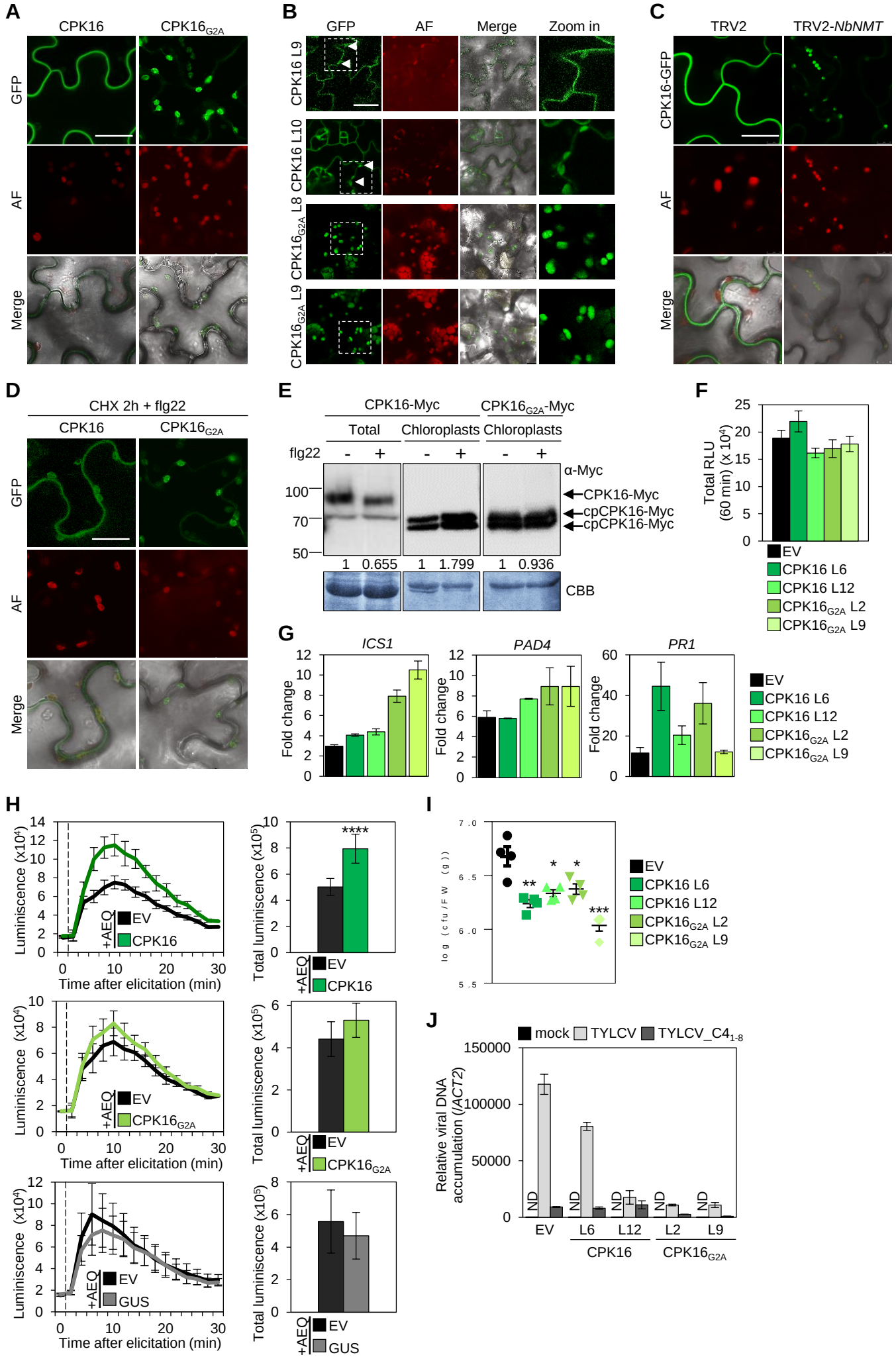
A
CPK16
CPK16G2A
GFP
AF
Merge
B
GFP
AF
Merge
Zoom in
CPK16 L9
CPK16 L10
CPK16G2A L8
CPK16G2A L9
C
TRV2
TRV2-NbNMT
CPK16-GFP
AF
Merge
D
CHX 2h + flg22
CPK16
CPK16G2A
GFP
AF
Merge
E
CPK16-Myc
CPK16G2A-Myc
Total
Chloroplasts
Chloroplasts
flg22
- + - + - +
α-Myc
100
70
50
CPK16-Myc
cpCPK16-Myc
cpCPK16-Myc
1 0.655 1 1.799 1 0.936
CBB
F
Total RLU (60 min) (x 10^4)
25
20
15
10
5
0
EV
CPK16 L6
CPK16 L12
CPK16G2A L2
CPK16G2A L9
G
ICS1
PAD4
PR1
Fold change
12
10
8
6
4
2
0
60
40
20
EV
CPK16 L6
CPK16 L12
CPK16G2A L2
CPK16G2A L9
H
Luminiscence (x10^4)
Time after elicitation (min)
+AEQ
EV
CPK16
CPK16G2A
GUS
Total luminiscence (x10^5)
****
I
log (cfu/FW (g))
7.0
6.5
6.0
5.5
**
*
*
***
EV
CPK16 L6
CPK16 L12
CPK16G2A L2
CPK16G2A L9
J
mock
TYLCV
TYLCV_C4 1-8
Relative viral DNA accumulation (/ACT2)
150000
100000
50000
0
ND
EV
L6
L12
L2
L9
CPK16
CPK16G2A

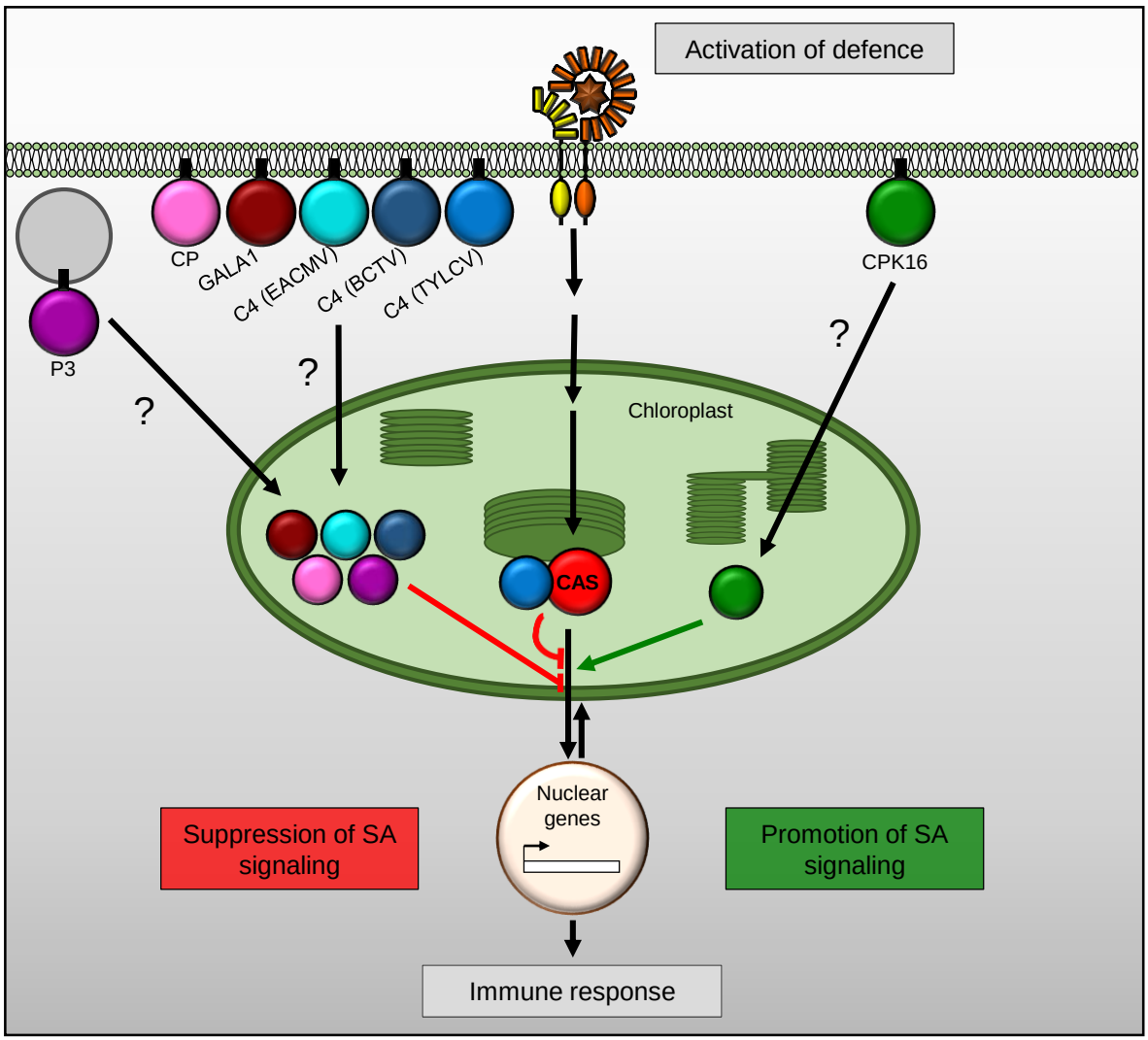
Activation of defence
CP
GALA1
C4 (EACMV)
C4 (BCTV)
C4 (TYLCV)
CPK16
P3
?
?
?
Chloroplast
CAS
Nuclear genes
Suppression of SA signaling
Promotion of SA signaling
Immune response

A

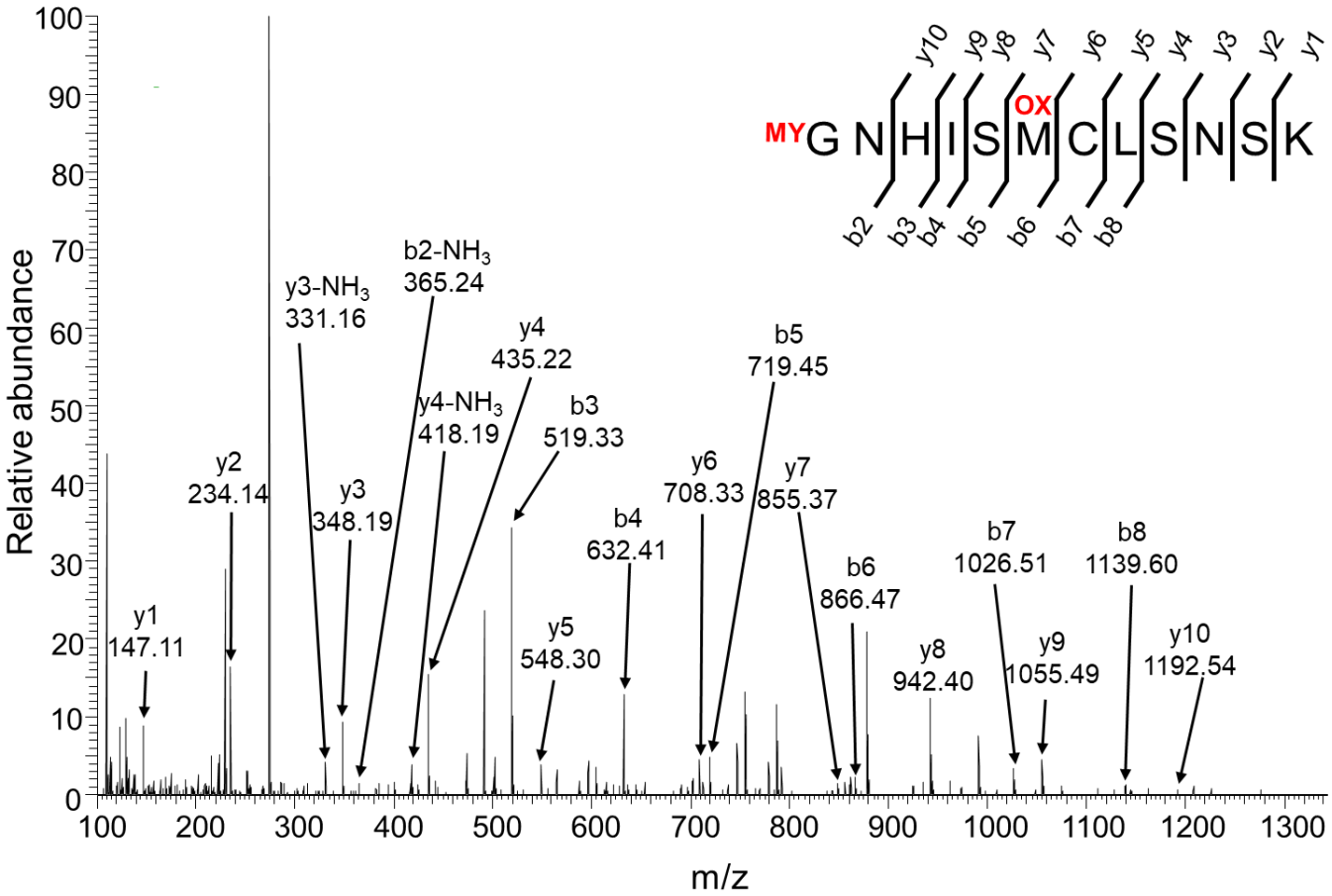

B

Replicate	Sequence	Mass (Da)		Charge state	Probability (%)	Modification
		Observed	Actual			
1	(M)GNHISMCLSNSK(A)	787.41	1572.80	+2	61	(G2) Myristoyl (+210) (M7) Oxidation (+16)
2	(M)GNHISMCLSNSK(A)	787.41	1572.81	+2	100	(G2) Myristoyl (+210) (M7) Oxidation (+16)
	(M)GNHISMCLSNSK(A)	703.31	1404.61	+2	100	(G2) Acetyl (+42) (M7) Oxidation (+16)
	(M)GNHISMCLSNSK(A)	682.31	1362.60	+2	100	(M7) Oxidation (+16)
	(M)GNHISMCLSNSK(A)	682.31	1362.60	+2	87	(M7) Oxidation (+16)

C

D

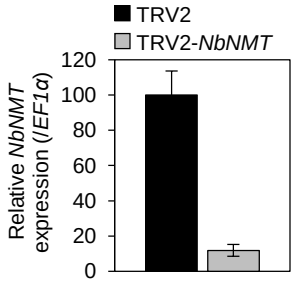

E

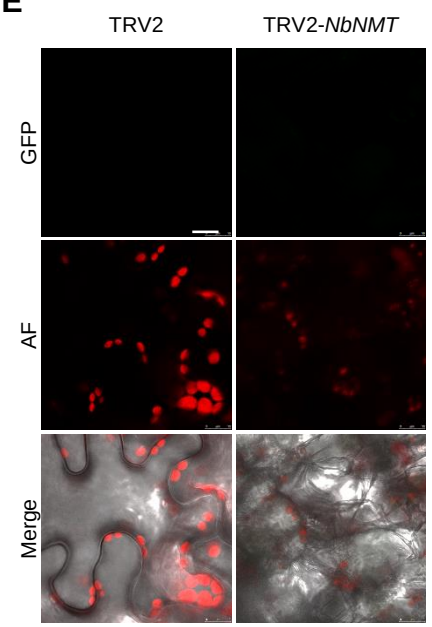

F

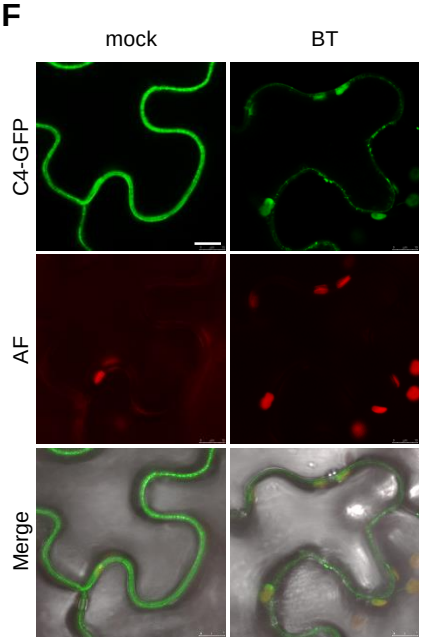

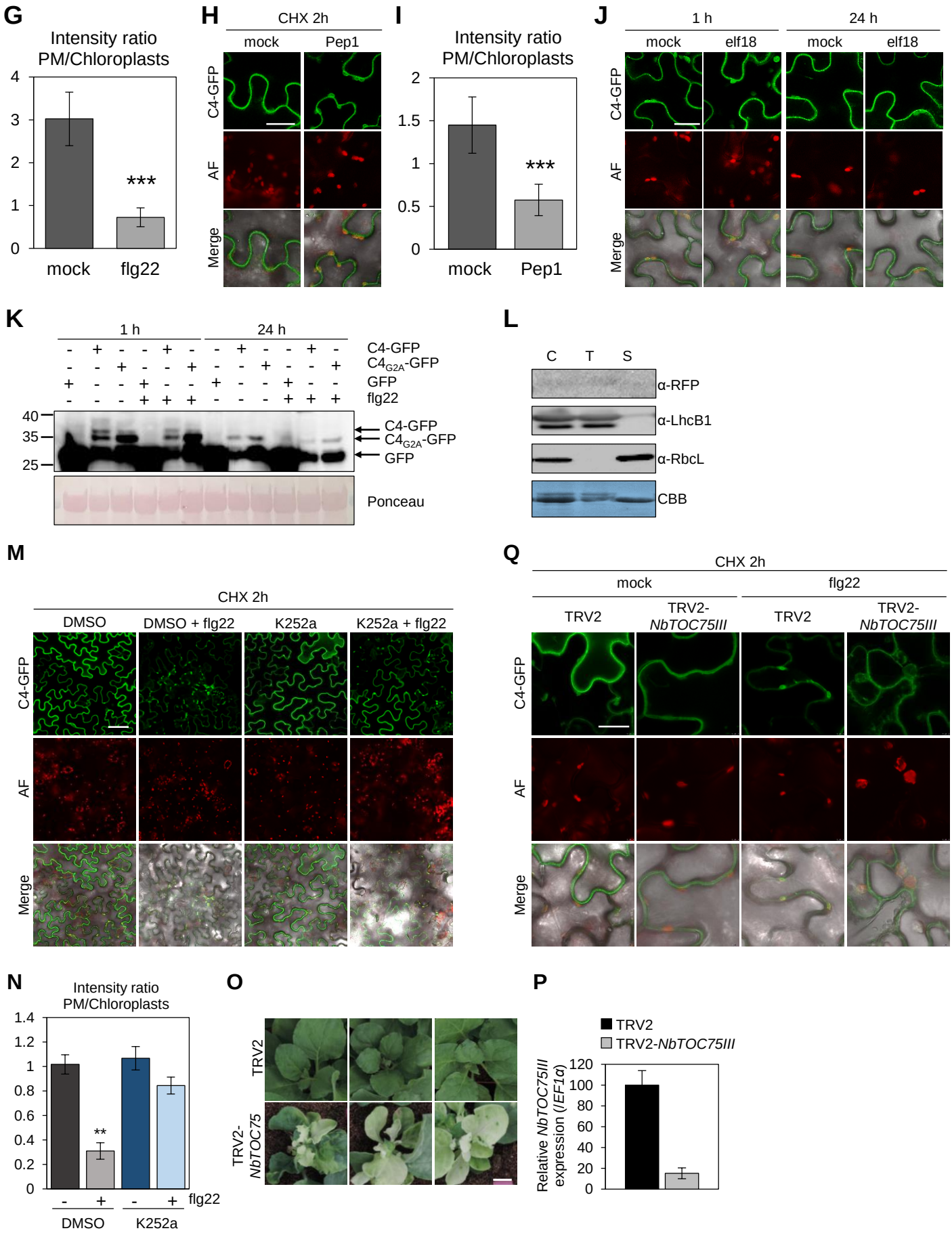
G
Intensity ratio
PM/Chloroplasts
4
3
2
1
0
***
mock
flg22
H
CHX 2h
mock
Pep1
C4-GFP
AF
Merge
I
Intensity ratio
PM/Chloroplasts
2
1.5
1
0.5
0
***
mock
Pep1
J
1 h
24 h
mock
elf18
mock
elf18
C4-GFP
AF
Merge
K
1 h
24 h
C4-GFP
C4G2A-GFP
GFP
flg22
40
35
25
C4-GFP
C4G2A-GFP
GFP
Ponceau
L
C
T
S
α-RFP
α-LhcB1
α-RbcL
CBB
M
CHX 2h
DMSO
DMSO + flg22
K252a
K252a + flg22
C4-GFP
AF
Merge
Q
CHX 2h
mock
flg22
TRV2
TRV2-NbTOC75III
TRV2
TRV2-NbTOC75III
C4-GFP
AF
Merge
N
Intensity ratio
PM/Chloroplasts
1.4
1.2
1
0.8
0.6
0.4
0.2
0
**
flg22
DMSO
K252a
O
TRV2
TRV2-NbTOC75
P
TRV2
TRV2-NbTOC75III
Relative NbTOC75III expression (IEF1α)
120
100
80
60
40
20
0

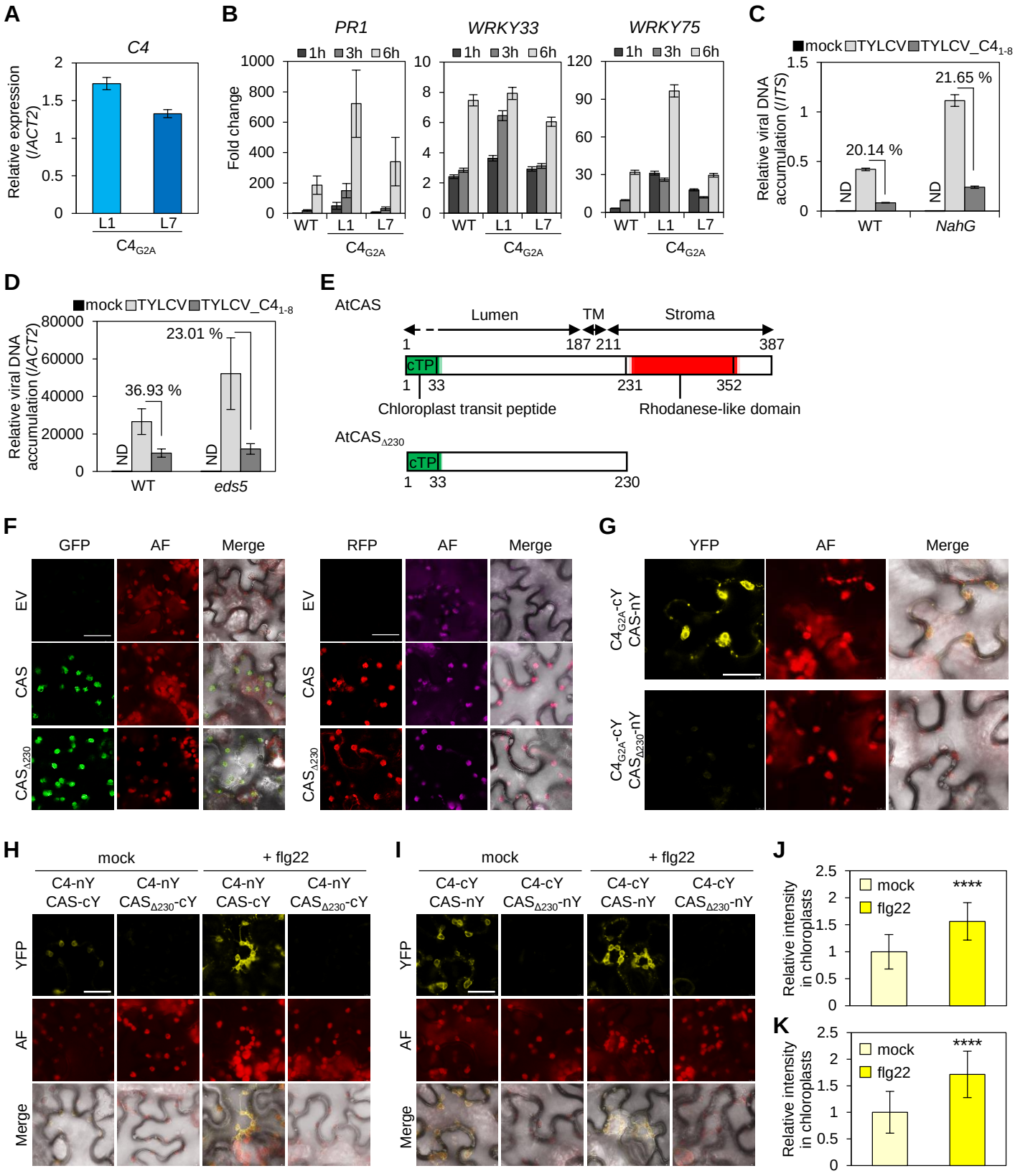

L

	Total luminescence ± SE (x10^4)			
	EV	$C4_{G2A}$	EV	GUS
R1	65.652 ± 4.798	51.686 ± 3.511****	76.832 ± 4.403	74.016 ± 5.890
R2	47.270 ± 3.331	40.830 ± 2.591***	38.524 ± 5.297	46.622 ± 5.872
R3	71.056 ± 8.003	53.420 ± 3.342***	47.605 ± 3.847	47.744 ± 2.942

M

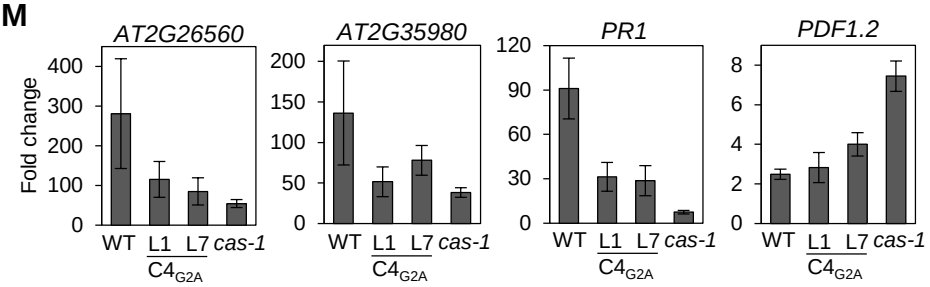

N

	log (cfu/cm^2) ± SE			
	WT	**C4$_{G2A}$ L1**	**C4$_{G2A}$ L7**	***cas-1***
R1	5.381 ± 0.055	6.251 ± 0.079***	6.302 ± 0.165***	5.861 ± 0.192*
R2	2.927 ± 0.129	4.268 ± 0.188***	4.666 ± 0.167***	4.807 ± 0.089***
R3	3.708 ± 0.137	5.062 ± 0.083***	5.041 ± 0.079***	5.002 ± 0.048***

O

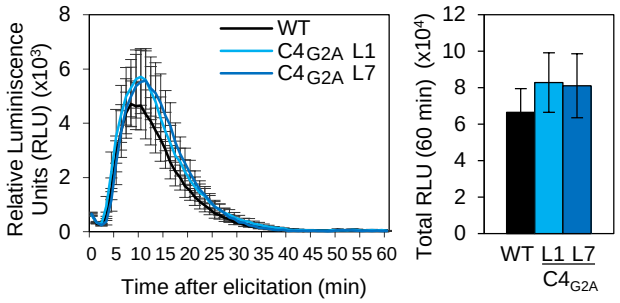

P

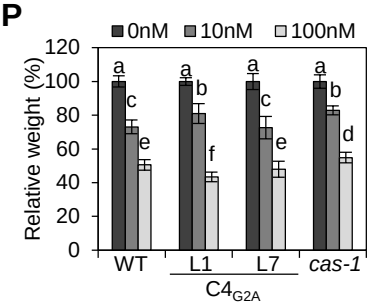

Q

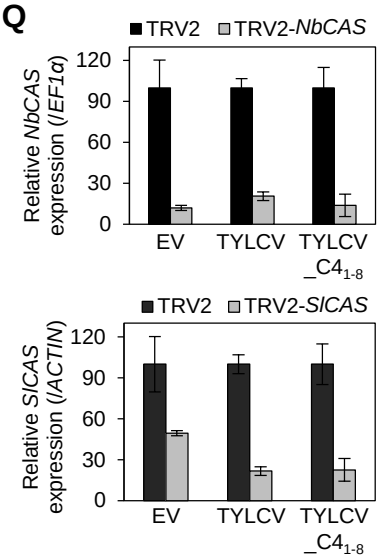

A

Family	Subfamily	Genus	Type of genome	Number of proteins containing both targeting signals
Geminiviridae		Begomovirus	dsDNA	390
		Capulavirus	dsDNA	1
		Curtovirus	dsDNA	5
		Topocuvirus	dsDNA	1
		Turncurtovirus	dsDNA	1
Bromoviridae		Cucumovirus	(+)ssRNA	1
Secoviridae	Comovirinae	Nepovirus	(+)ssRNA	1
Tombusviridae	Calvusvirinae	Umbravirus	(+)ssRNA	1

B

Genus	Species	Isolate	Accession number	Protein	Protein ID	AA	myr	cTP (AA)
Curtovirus	*Beet curly top virus* (*BCTV*)	California [Logan]	M24597	C4	ADD82466	85	yes	69
Begomovirus	*East African cassava mosaic virus* (*EACMV*)	EACMV-KE2[K48]	AJ717542	AC4	CAJ78099	77	yes	49
Cucumovirus	*Cucumber mosaic virus* (*CMV*)	DN2-1	KT302169	CP	ALT66618	218	yes	25
Nepovirus	*Grapevine fanleaf virus* (*GFLV*)	SACH44	KC900164	P3	AGT42202	338	yes	42

C

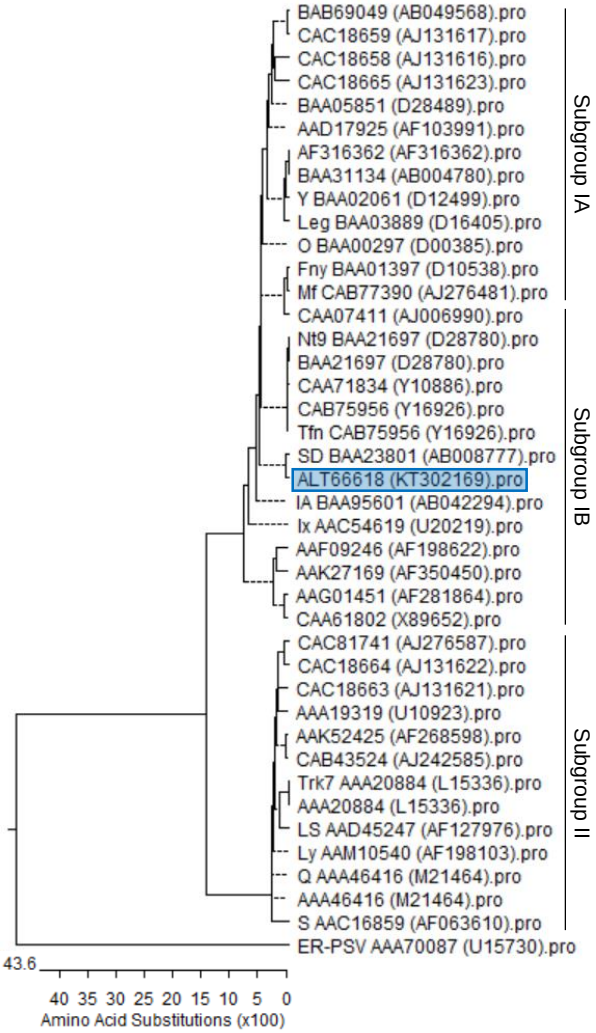

D

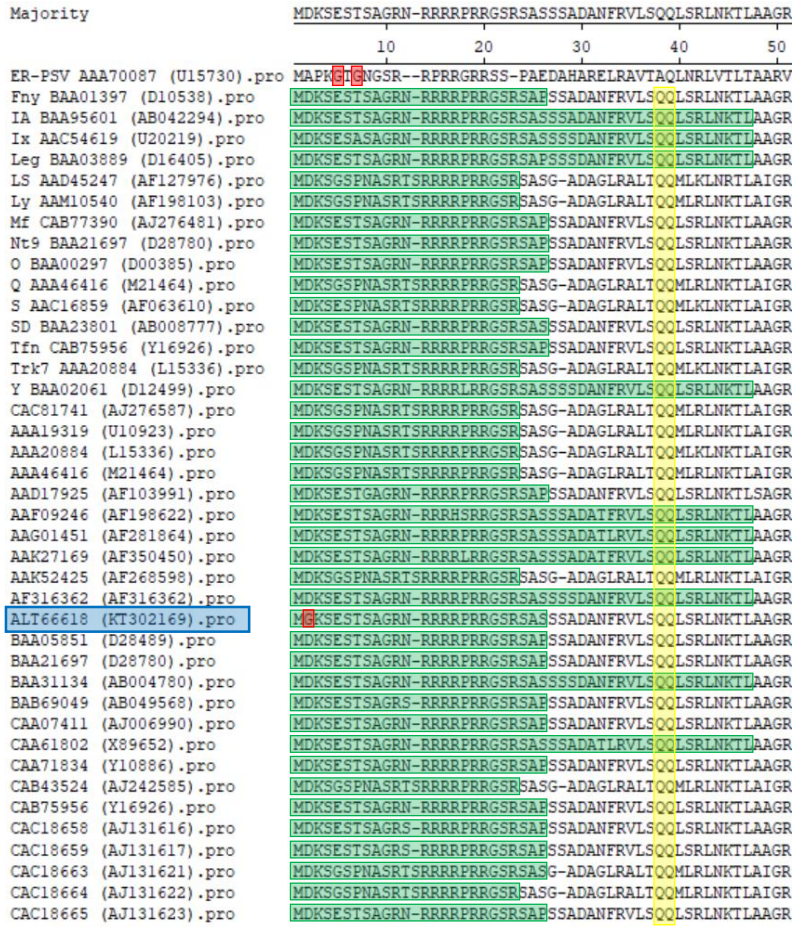

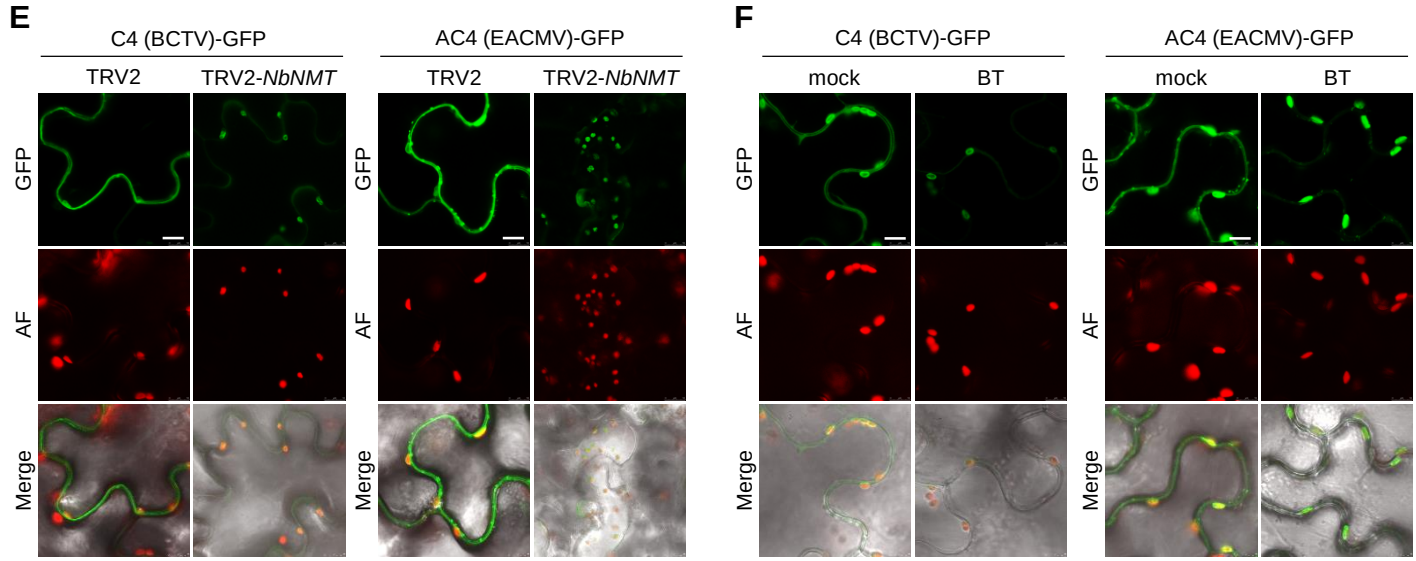

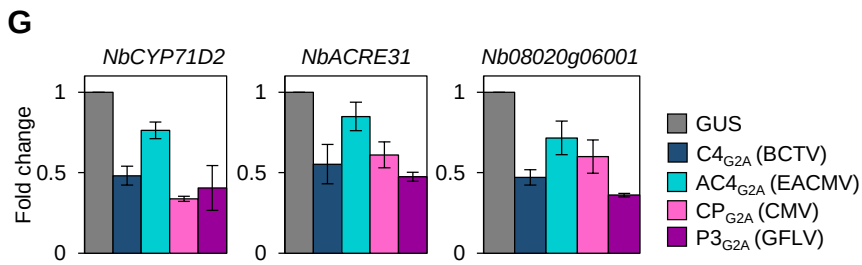

H

	Total luminescence ± SE (x10^4)							
	EV	**C4$_{G2A}$ (BCTV)**	**EV**	**AC4$_{G2A}$ (EACMV)**	**EV**	**CP$_{G2A}$ (CMV)**	**EV**	**P3$_{G2A}$ (GFLV)**
R1	19.672 ± 2.938	10.336 ± 1.946****	32.244 ± 3.464	22.606 ± 2.543****	17.464 ± 2.753	11.490 ± 7.297**	14.208 ± 2.869	9.300 ± 0.832**
R2	17.314 ± 4.921	10.458 ± 1.469**	18.804 ± 3.982	13.020 ± 1.632***	25.840 ± 9.995	9.856 ± 1.777****	40.301 ± 3.777	35.415 ± 4.368**
R3	42.844 ± 6.210	42.692 ± 5.539	11.242 ± 1.639	5.422 ± 0.972****	18.528 ± 2.561	15.648 ± 1.944*	20.840 ± 3.569	17.982 ± 2.967

	Total luminescence ± SE (x10^4)	
	EV	**GUS**
R1	27.370 ± 3.730	27.190 ± 2.906
R2	55.724 ± 19.385	46.944 ± 14.336
R3	19.132 ± 4.089	25.374 ± 4.499

I

	log (cfu/cm^2) ± SE							
	GUS	**C4$_{G2A}$ (BCTV)**	**GUS**	**AC4$_{G2A}$ (EACMV)**	**GUS**	**CP$_{G2A}$ (CMV)**	**GUS**	**P3$_{G2A}$ (GFLV)**
R1	6.918 ± 0.129	7.943 ± 0.048***	6.979 ± 0.052	8.043 ± 0.028***	7.124 ± 0.033	8.036 ± 0.028***	7.156 ± 0.017	7.129 ± 0.021
R2	7.059 ± 0.102	7.952 ± 0.06***	7.037 ± 0.044	8.052 ± 0.072***	6.747 ± 0.149	7.621 ± 0.151***	6.908 ± 0.098	6.704 ± 0.072
R3	7.088 ± 0.034	8.061 ± 0.034***	7.127 ± 0.051	8.005 ± 0.088***	7.007 ± 0.033	7.965 ± 0.055***	7.001 ± 0.019	6.989 ± 0.025

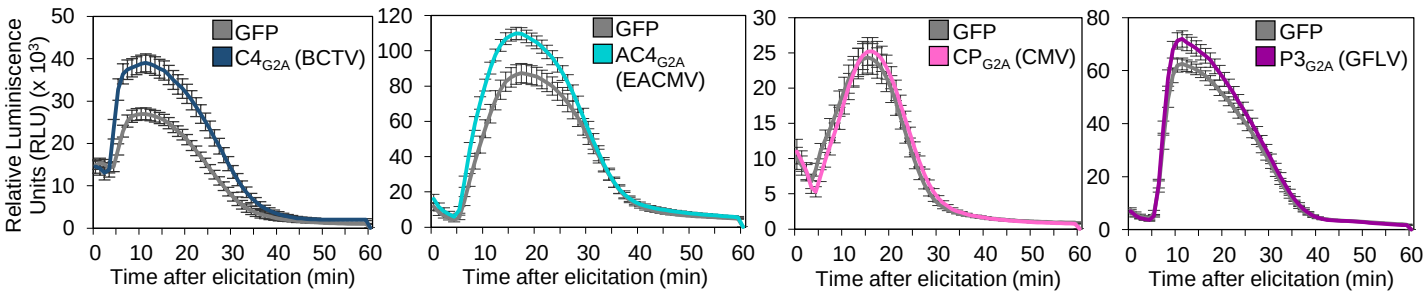

A

Ralstonia solanacearum GMI1000					
Transcript_id	**Gene name**	**Description**	**AA**	**myr**	**cTP (AA)**
Q8XRE0	*RSp0914*	LRR-gala family type III effector protein (GALA1)	661	yes	39
Q8XTS6	*RSp0028*	LRR-gala family type III effector protein (GALA3)	603	yes	58

B

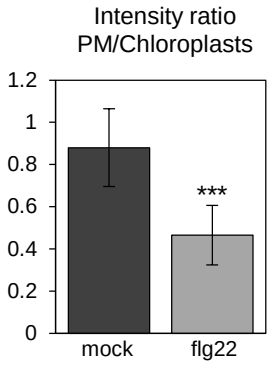

C

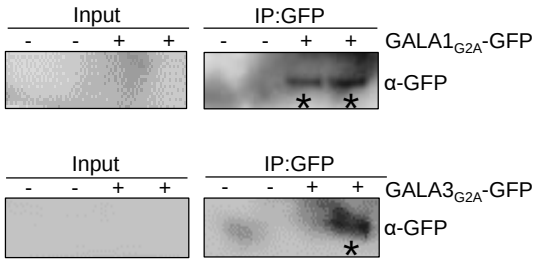

E

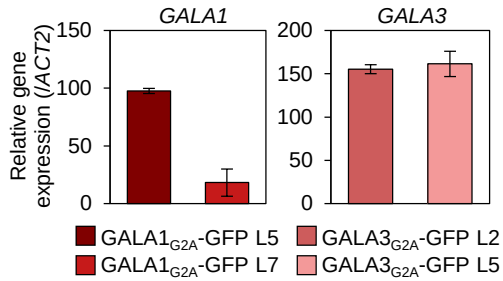

D

	Total luminescence ± SE (x10^4)					
	EV	**GALA1$_{G2A}$**	**EV**	**GALA3$_{G2A}$**	**EV**	**GUS**
R1	32.840 ± 4.518	20.434 ± 1.254****	30.102 ± 5.778	16.640 ± 2.014***	55.724 ± 19.385	46.944 ± 14.336
R2	38.644 ± 7.959	18.472 ± 1.159****	23.756 ± 2.284	17.838 ± 1.646***	21.776 ± 4.414	34.418 ± 9.276
R3	112.576 ± 23.158	49.260 ± 10.499****	103.916 ± 30.522	37.532 ± 7.888****	69.060 ± 8.960	77.337 ± 8.762

F

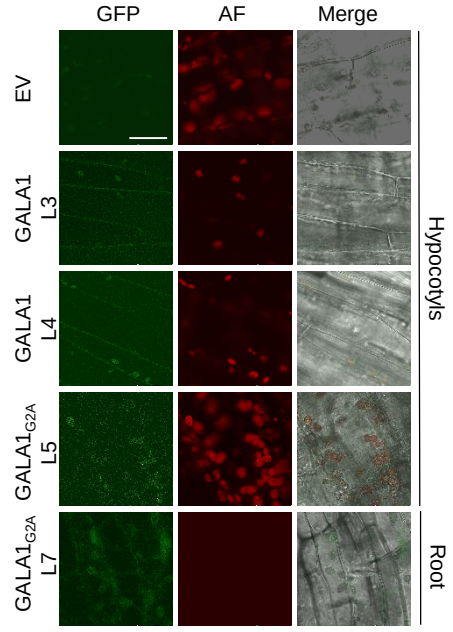

G

	log (cfu/FW (g)) ± SE				
	EV	**GALA1$_{G2A}$ L5**	**GALA1$_{G2A}$ L7**	**GALA3$_{G2A}$ L2**	**GALA3$_{G2A}$ L5**
R1	8.623 ± 0.152	9.083 ± 0.076*	8.566 ± 0.114	9.031 ± 0.113*	8.934 ± 0.094*
R2	6.892 ± 0.284	8.105 ± 0.126**	8.091 ± 0.129**	8.001 ± 0.111**	7.592 ± 0.106**
R3	7.332 ± 0.178	7.601 ± 0.113**	7.713 ± 0.118**	7.109 ± 0.088	7.294 ± 0.11
R4	6.231 ± 0.133	7.123 ± 0.218**	6.359 ± 0.148	6.332 ± 0.151	6.708 ± 0.163***

H

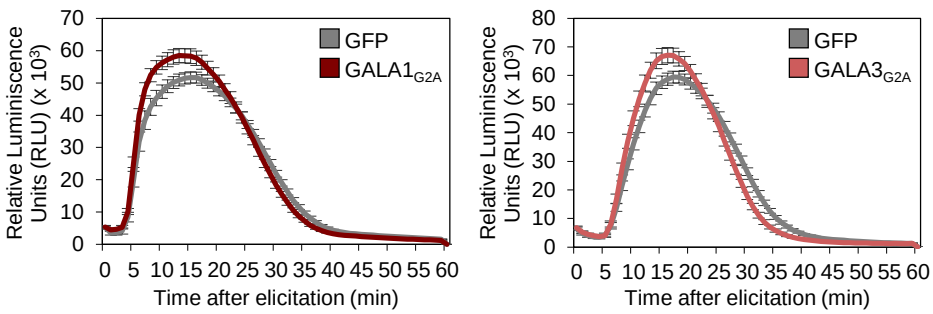

A

Arabidopsis thaliana

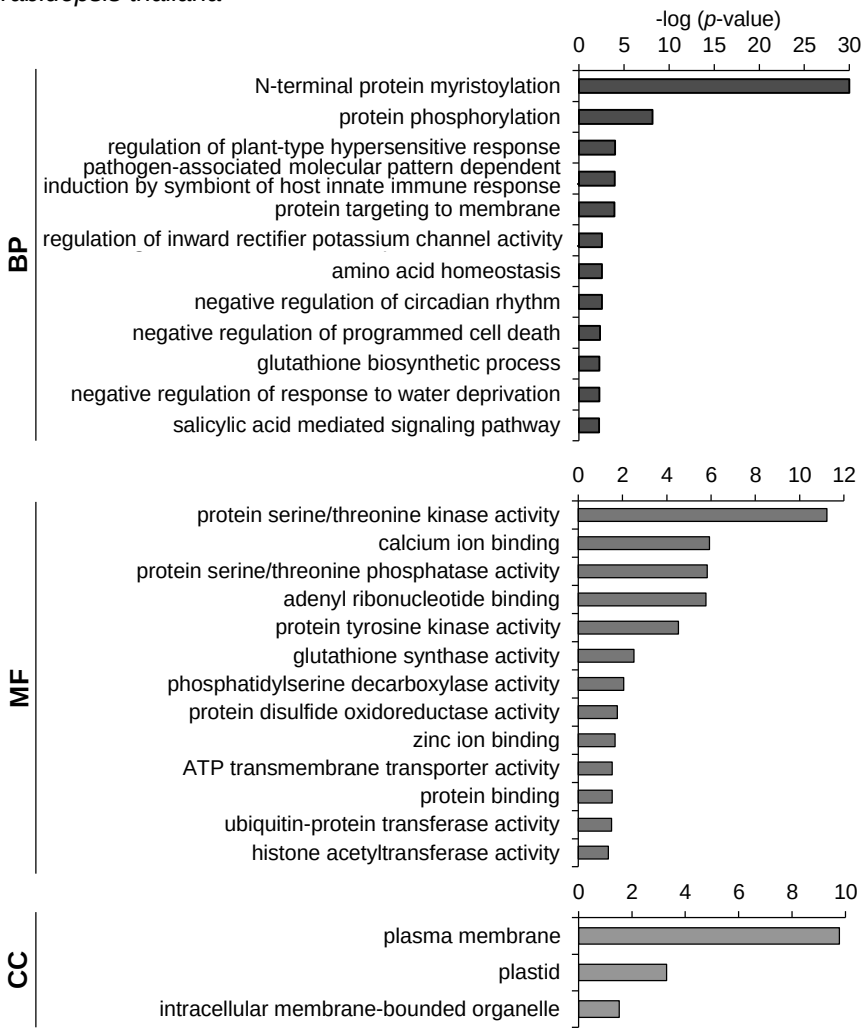

B

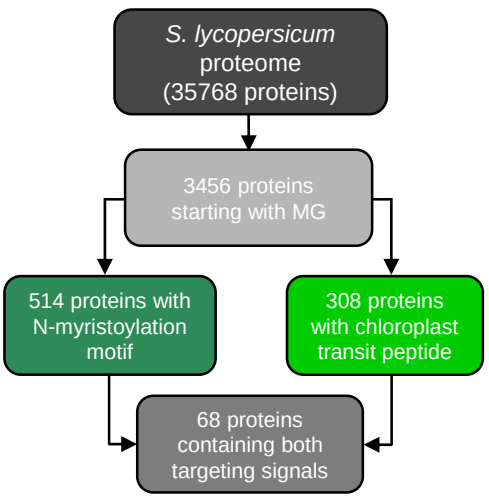

C

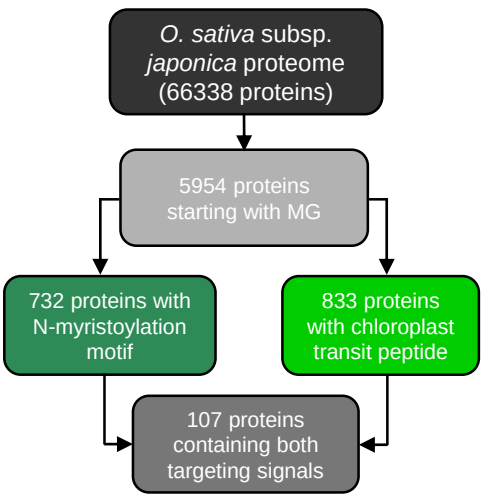

D

Solanum lycopersicum

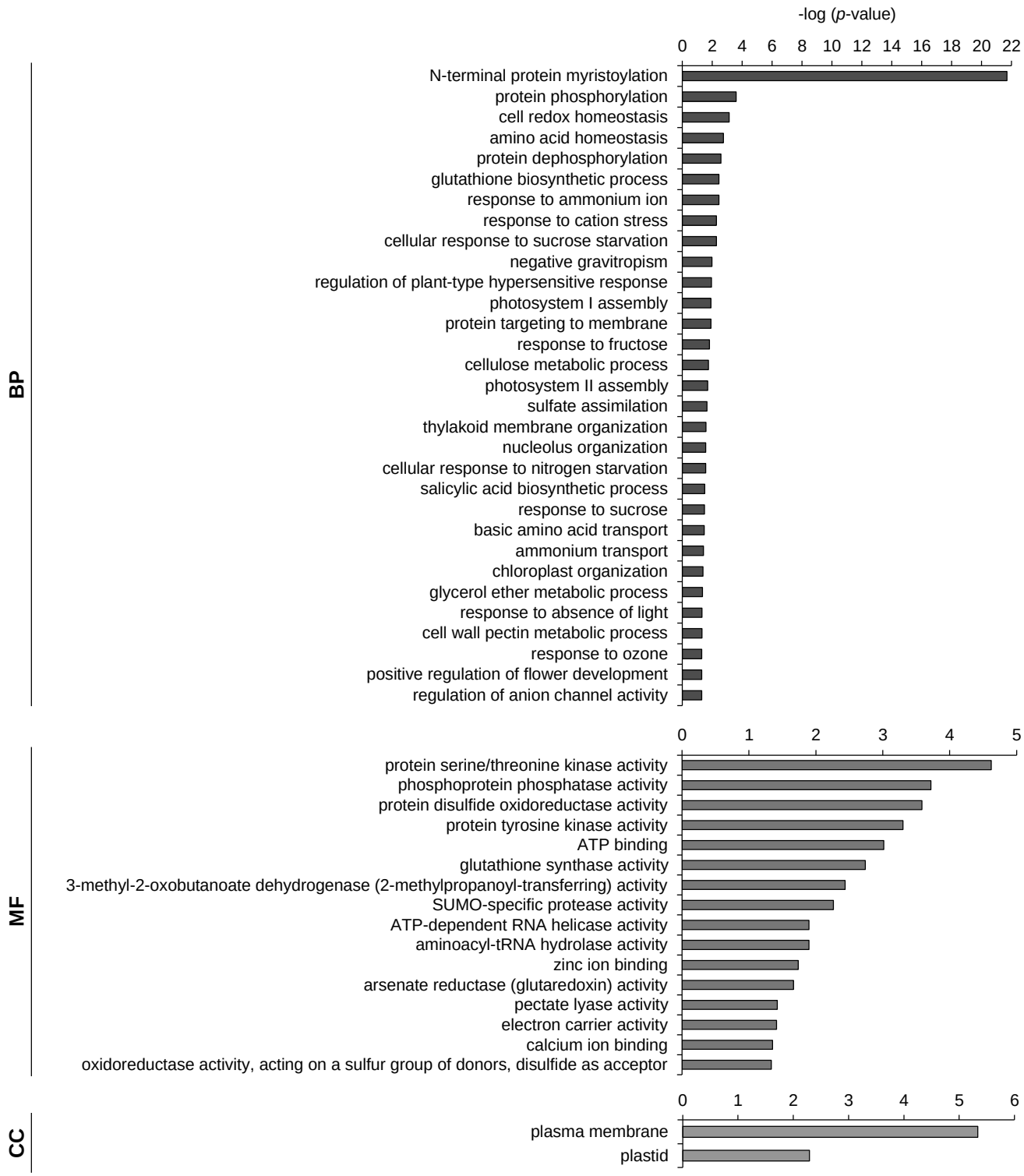

E

Oryza sativa subsp. *japonica*

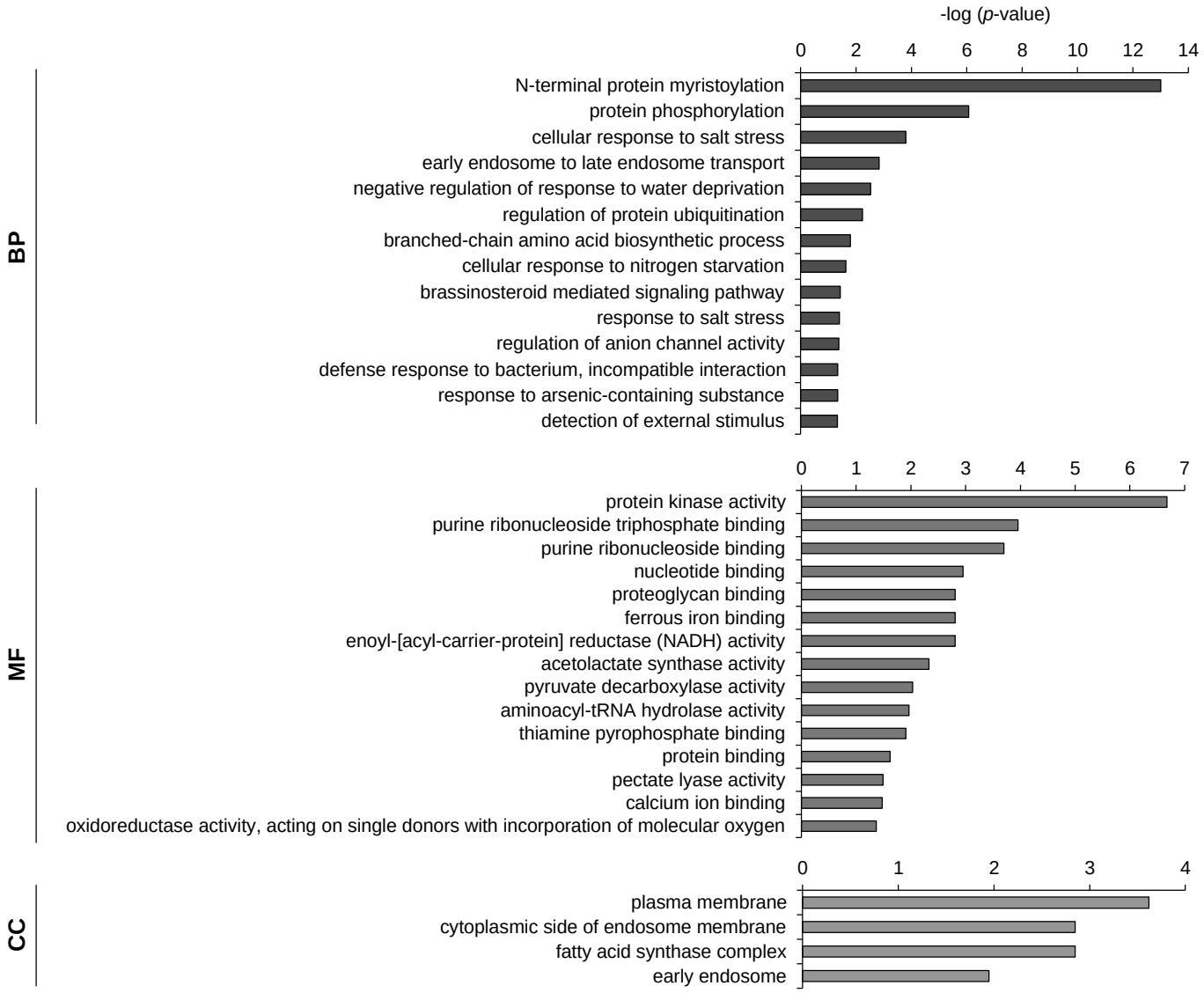

F

Chlamydomonas reinhardtii

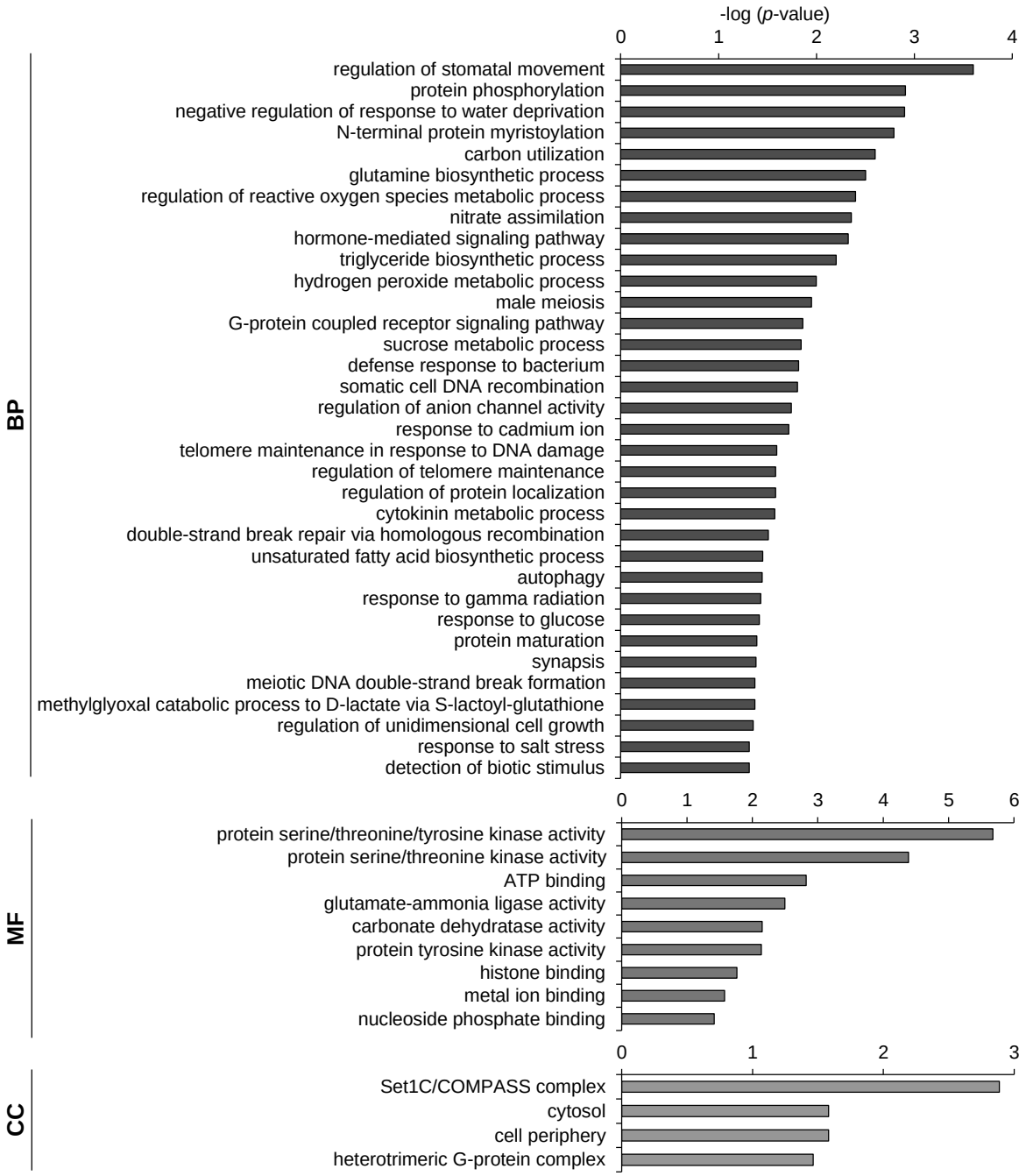

G

Marchantia polymorpha

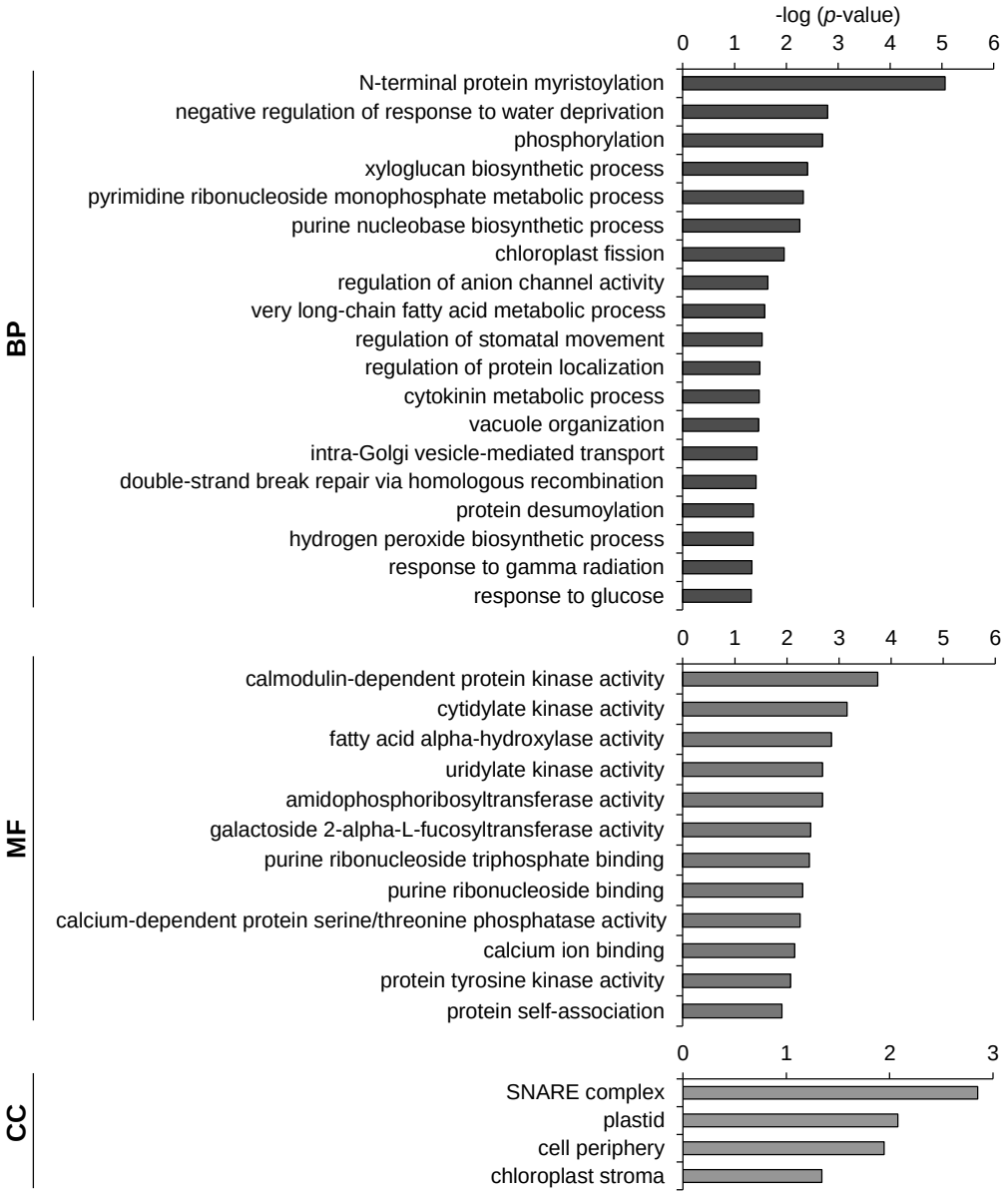

H

Physcomitrella patens

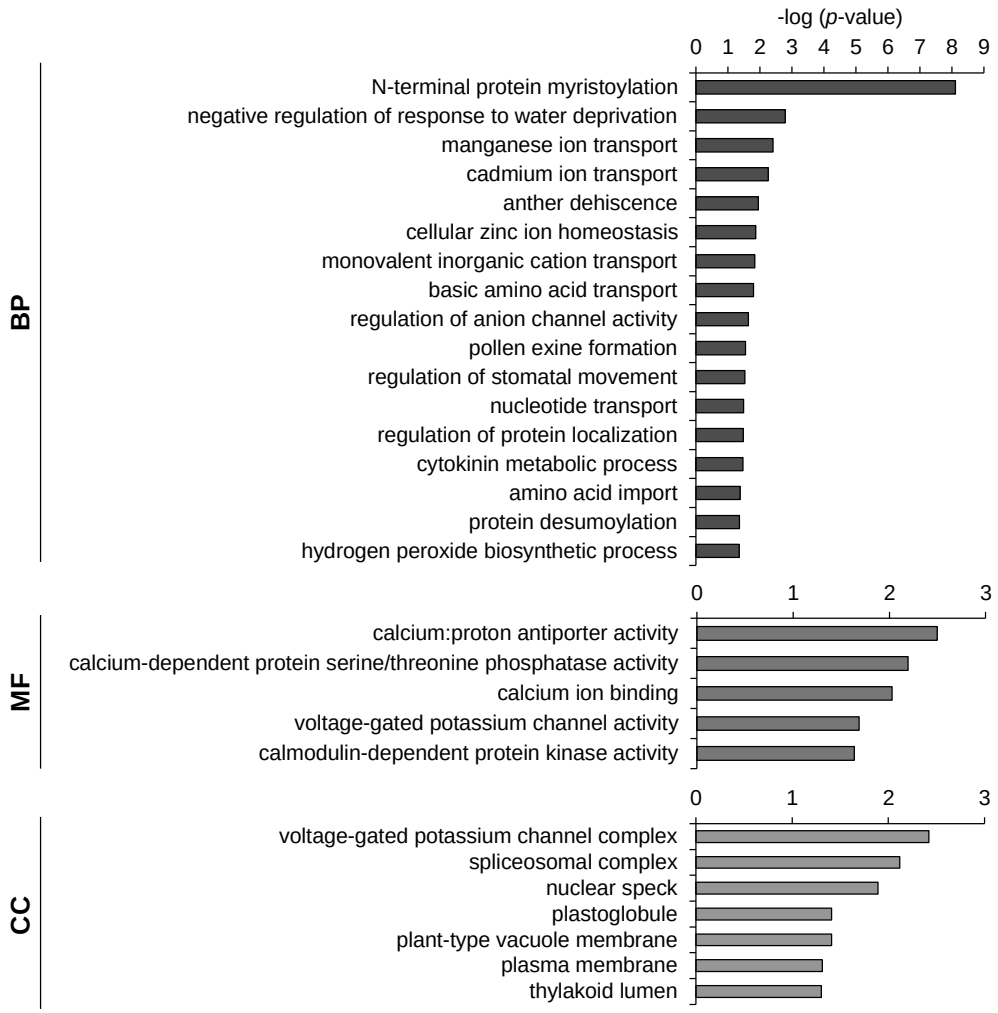

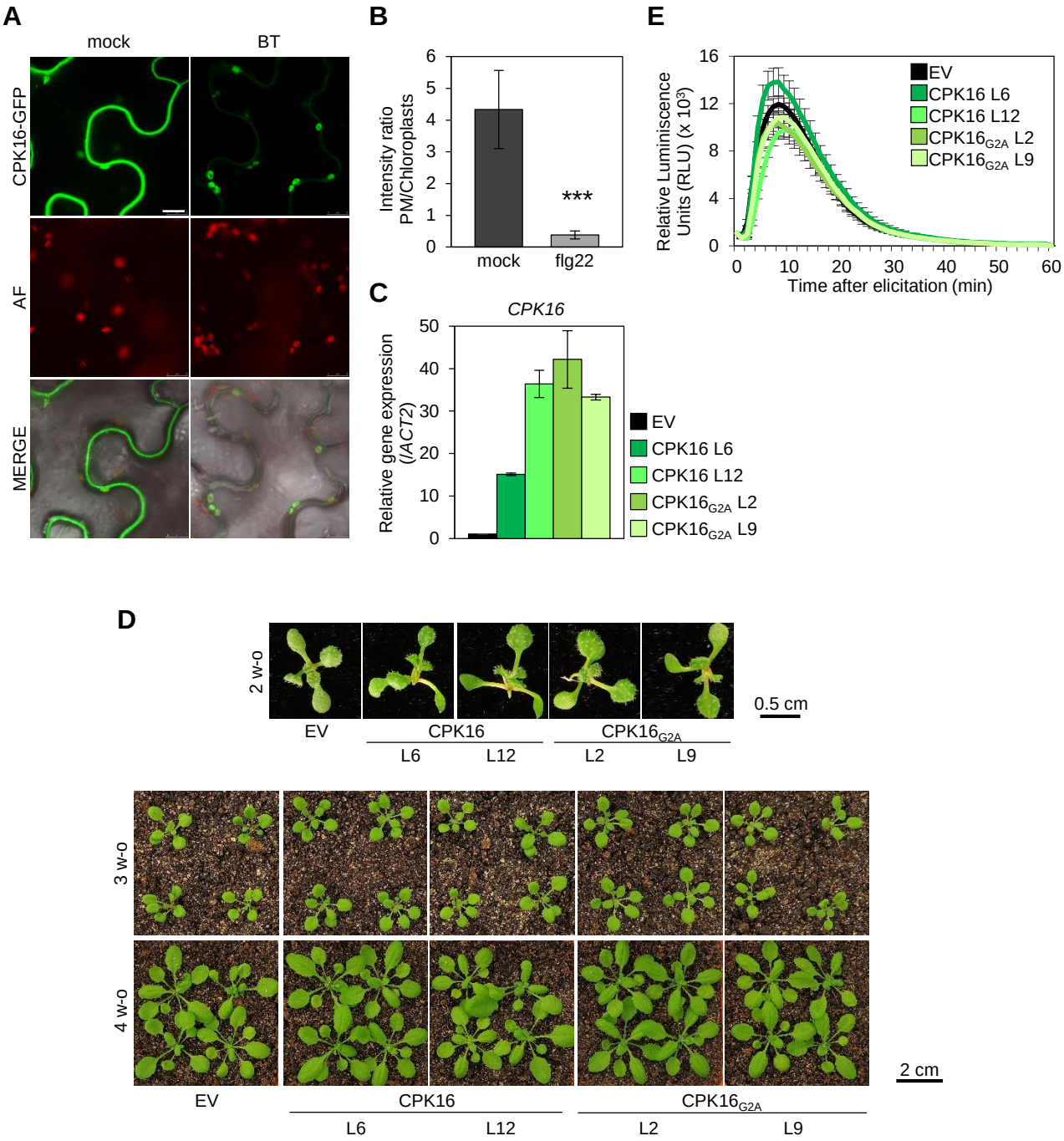

F

	Total luminescence ± SE (x10^4)					
	EV	**CPK16**	**EV**	**CPK16$_{G2A}$**	**EV**	**GUS**
R1	50.172 ± 6.442	79.444 ± 11.089****	44.112 ± 8.267	53.006 ± 8.111	55.724 ± 19.385	46.944 ± 14.336
R2	85.995 ± 16.614	125.572 ± 30.771*	106.774 ± 14.077	115.980 ± 20.191	69.060 ± 8.961	77.337 ± 8.762
R3	11.972 ± 1.707	19.391 ± 6.107*	13.688 ± 1.807	12.630 ± 1.861	14.700 ± 2.277	12.333 ± 2.813

G

	log (cfu/FW (g)) ± SE				
	EV	**CPK16 L6**	**CPK16 L12**	**CPK16$_{G2A}$ L2**	**CPK16$_{G2A}$ L9**
R1	8.053 ± 0.070	8.037 ± 0.096	8.126 ± 0.053***	7.322 ± 0.058***	7.407 ± 0.072***
R2	7.510 ± 0.129	7.575 ± 0.112	6.829 ± 0.060***	7.651 ± 0.100*	6.789 ± 0.092***
R3	6.990 ± 0.059	6.776 ± 0.008*	6.668 ± 0.115**	6.591 ± 0.147**	5.691 ± 0.181***
R4	6.669 ± 0.1512	6.248 ± 0.085***	6.291 ± 0.098***	6.294 ± 0.104***	5.983 ± 0.125***